Republic of Iraq

Ministry of Higher Education

And Scientific Research

University of Kerbala

College of Science

Department of Physics

Efficiency of Thermal Camera under Bad Weather and Moving Target Conditions in Holy Karbala City

A Thesis

Submitted to Council of the College of Science, University of Kerbala in Partial Fulfillment of the Requirements for the Degree of Master of Science in Physics

By

Ahmed Fadhil Abdul Raheem

BSc. 2009

Supervisors

Prof. Dr. Fadhil K. Fuliful **Assist. Prof. Dr. Azhr A. Raheem**

2021 A.D **1443 A.H**

بِسْمِ اللَّهِ الرَّحْمَٰنِ الرَّحِيمِ

{نَرْفَعُ دَرَجَاتٍ مَّن نَّشَاءُ وَفَوْقَ كُلِّ ذِي عِلْمٍ عَلِيمٌ}

صدق الله العلي العظيم

سورة يوسف

الآية (٧٦)

Supervisors Certificate

We certify that the preparation of this thesis, entitled "**Efficiency of Thermal Camera under Bad Weather and Moving Target Conditions in Holy Karbala City** ", has been prepared under our supervision by " **Ahmed Fadhil Abdul Raheem**" at the Department of Physics, College of Science, the University of Kerbala in partial fulfillment of the requirements for the degree of Master of Science in Physics.

Signature:

Name: Fadhil K. Fuliful

Title: Prof. Dr.

Address: Department of Physics College of Science, University of Kerbala

Date: \ \ 2021

Signature:

Name: Azhr A. Raheem

Title: Assist. Prof. Dr.

Address: Department of Physics College of Science, University of Kerbala

Date: \ \2021

In view of the available recommendations, I forward the thesis for debate by the examination committee.

Signature:

Name: **Dr. Rajaa A. Madlool**

Title: Professor

Head of Physics Department, College of Science, University of Kerbala

Date: \ \ 2021

Examination Committee Certification

We certify that we have read this thesis entitled " **Efficiency of Thermal Camera under Bad Weather and Moving Target Conditions in Holy Karbala City** " as the examining committee, examined the student " **Ahmed Fadhil Abdul Raheem** " on its contents, and that in our opinion, it is adequate for the partial fulfillment of the requirements for the Degree of Master in Science of Physics.

Signature:
Name: **Dr. Ali H. Abdul Muneim**
Title: **professor**
Address: Department of Laser and optoelectronics Engineering ,University of Technology
Date: \ \ 2021
(Chairman)

Signature:
Name: **Dr. Rajaa A. Madlool**
Title: **professor**
Address: Department of physics,college science/University of Kerbala
Date: \ \ 2021
(Member)

Signature:
Name: **Dr. Talib M.Abbas**
Title: **professor**
Address: College of Education for Pure Sciences ,University of Babylon
Date: \ \ 2021
(Member)

Signature:
Name: **Dr. Fadhil K. Fuliful**
Title: **professor.**
Address: Department of physics,college science/University of Kerbala
Date: \ \ 2021
(Supervisor)

Signature:
Name: **Dr. Azhr A. Raheem**
Title: **Assist. Prof. Dr.**
Address: Department of physics,
college of science/University of Kerbala
Date: \ \ 2021
(Supervisor)

Signature:
Name: **Dr.Jasem Hanoon Hashim Al-Awadi**
Title: **Assist. Professor**

Dean of the college of science/ University of Kerbala

of science Date: / / 2021

Dedication

To the one who separated us by her body, but her soul is still fluttering in the sky of my life

My mother

To the seed of benevolence, sacrifice, and altruism,

My dear father

To the highest symbol of loyalty and companion of my life

My dear wife,

To whom I hope to see their bright future

My sons

To whom was my permanently support during my life

My brothers my sisters

To who encourage and support me

My Friends

Ahmed

Acknowledgment

First of all, I thank God for helping me to finalize this thesis ،and best prayers and peace on his best messenger Mohammed, his pure descendants, and his noble companions. I would like to express my sincere appreciation and deep gratitude to my supervisors, Prof. Dr. Fadhil Khaddam Fuliful and Assist. Prof. Dr. Azhr Abdulzahraa Raheem, for suggesting the topic of this thesis, guiding, advising, and continuous encouragement throughout the research. My thanks go to all the staff members of the department of the physics University of Kerbala. I also extend my sincere thanks and great gratitude to the Ministry of the Interior represented by Minister Othman Al-Ghanmi and to the Holy Karbala Police Command and especially Major General Ahmed Ali Zwaini. In addition, I would also like to extend my thanks and appreciation to the Karbala Operations Command represented by Major General Ali Al-Hashemi. As well as, my thanks and appreciation is extended to the Directorate of Controls and External Roads represented by Mr. Brigadier General Hussein Al-Numina. Eventually, to all my brother officers in the Holy Karbala Police Command, I am pleased to give them my great thanks.

Ahmed

Abstract

Thermal imaging cameras are widely used in military applications for their night vision capabilities at different observation ranges. The efficiency of the thermal camera depends on the image quality or detecting and recognizing the target. In this work, a mathematical model that programed in Mathcad to verify the efficiency of the thermal camera (PT-602CZ HD) when the object is in motion at different speeds. The intensity distribution in thermal images is calculated by using the transfer function. Bar Spread Function (BSF) solved at two cases with and without linear motion of the object. The values of the linear motion factor of the object were calculated with different velocities (40,60,80.100, and 120) Km/h. The intensity distributing of the thermal image evaluated for different ranges (150 to 4500) m. The results show that the target can be detected and distinguished in the ranges (150, 300,500) m but the target detects only in the ranges (750) m. If the range of the moving target is larger than 750m the detection also occurs but at a different resolution, if the range is reached 2500 m and more the thermal imaging is impossible for this type of thermal camera. Compare the theoretical results of intensity degraded of the thermal image with the images of moving objects captured practically by the thermal camera at 40 Km/h velocity of the object in the Ain Al-Tamer area for the holy Karbala city. Detection of a target is influenced by the case of the weather conditions. Atmospheric transmission of the infrared band at (5, 10) μm is evaluated at different Visibility (200,300,400,500,600,700,800) m with the presence of fog at different ranges (200,300,400,500,600,700,800) m in the same area of study, and the effective range is investigated. Experimentally, thermal images are captured by the thermal camera at various ranges (200,300,400,500) m at visibility 400 m. The transmission of infrared radiation is affected by atmospheric conditions such as fog and the transmission depends on the concentration of particles suspended in the atmosphere. Both range and fog are a strong impact on thermal images captured by the thermal camera. The atmospheric transition of 10 μm under foggy conditions is

better than 5 μm. Therefore, the detection and recognizing of the object by the thermal camera with 10 μm is a favorite. The theoretical results agree with the experimental thermal images were taken in this case and the same area. Also, the detection of a target is influenced by air pollution such as dust (ambient particulate matter PM_{10}). Calculation of the visibility (V) range with ambient particulate matter PM_{10} is performed. Atmospheric Transmission of the Infrared Radiations (ATIR) with 10 μm is evaluated at different concentrations of particulate matter PM_{10} (10, 20, 30, 40, 50) $\mu g/m^3$ recorded by Iraq Meteorological Organization and Seismology in Ain Al-Tamer area for the holy Karbala city, Iraq. The results show that the PM_{10} concentration significant affects the resolution power of images in thermal imaging. The PM_{10} concentration in the study area has a slight influence on the thermal image.

List of Contents

List of Symbols

Symbol	Description	Units
λ	Wavelength	μm
I_S	Signal Current	Amber
I_N	Noise Current	Amber
$T_{(\omega)}$	Optical Contrast Transmission Function	
$\theta(\omega)$	Phase Side Transferal Function	
S	Spatial Frequency	Hz
$D(s)$	Optical Transfer Function	
H(u,v)	Transfer Function of Optical System	
G(u,v)	Spectrum of Image	
F(u,v)	Spectrum of Object	
I_{max}	Maximum Intensity	
I_{min}	Minimal Intensity	
(u, v), (u', v')	Reduced coordinates of the point in the object and image planes	
B (u, v)	Object intensity distribution at (u, v) in the object plane	
$B'(u', v')$	Image intensity distribution at (u', v') in the image plane	
(O, O´)	Origin points of the object and image	
(E, E´)	Entrance and exit pupils of the optical system	

(OE)	The radius of the reference sphere in the object space	
Z	Frequency of the plane	
α	The angle of the light beam in the plane of the object with the optical axis	
α´	The angle of the light beam in the plane of the object with the optical axis	
h	Height of the intersection of the ray with the reference field in the object space	mm
h´	Height of the intersection of the ray with the reference field in the image space	mm
(a, b) , (a', b)	Actual Cartesian coordinates on the entrance and exit pupils	
(X,Y)	Fractional coordinates of points on the entrance and exit pupil of image forming system	
(r , r′)	Respective radii of entrance and exit pupils	mm
(ζ, η) , (ζ´, η´)	Actual Cartesian co-ordinates	
F(x,y)	Pupil function	
a	Area of the output pupil	
$\tau(x, y)$	Function permeability	
k	Wavenumber	
H(z´-z):	The complex amplitude of line object image.	
T(z)	The complex amplitude of bar object image.	

T(z')	Spectrum in the image plane.	
$t(x,y)$	Bar spectrum	
B(z')	The intensity of the bar image or the bar spread function	
N	Normalized Factor	
L	Linear Motion Factor	
t_e	Snapshot Time	sec
$F^{\neq}$	Optical System Focal Number	mm
v_i	Image animation speed	m\sec
f	Focal length	mm
R	Distant of a target from the camera	m
v_0	Speed of the image movement	m\sec
V	Visibility	m
q	Exponent	
C	Concentration of particles	$\mu g/m^3$
τ_S	Attenuation Factor	
A	Absorption of IR	
T	Transition	

List of Abbreviations

Symbols	Meaning
IR	Infrared Radiation
NWIR	Near-wavelength infrared
SWIR	Short- wavelength IR
MWIR	Medium- wavelength IR
LWIR	Long- wavelength IR
FLWIR	Far long-wavelength IR
e	Emissivity
NDTT	Non-Destructive Thermal Testing
SNR	Signal-to-Noise Ratio
FPA	Focal Plane Array
TDI	Time Delay Integration
TIC	Thermal Imaging Cameras
IR F P A	IR Focal Plane Array
E M	Electromagnetic
UAVs	Unmanned Aerial Vehicles
fps	Frames per second

MTI	Moving Target Identification
IMU	Inertial Measurement Unit
RGBD	Red-Green-Blue-Depth
RCNN	Region-based Convolutional Neural Network
OTF	Optical Transfer Function
FT	Fourier Transform
MTF	Modulation Transfer Function
p s f	Point Spread Function
LSF	Line Spread Function
BSF	Bar Spread Function
PM_{10}	Particle Matter
FLIR	Forward-Looking Infrared
ADDE	Advanced Digital Detail Enhancement
ATIR	Atmospheric Transmission of the Infrared Radiations

List of figures

Chapter One

Introduction and Literature Review

1.1 Introduction

Astronomer Sir Frederick William Herschel discovered infrared radiation (IR) in 1800. The temperature of sunlight colors can be measured when it passes through a glass prism to produce spectra [1]. The temperature increased from the red to the violet colors in the visible part of the spectrum. Infrared radiation lies between the visible and microwave portions of the electromagnetic spectrum. The source of IR is heat or thermal radiation emitted from objects with a temperature above the absolute zero degrees of (-273.15) c^o [2].

A conventional camera works in the range of visible light, with wavelengths (400 to 700) nm approximately but a thermal camera is designed to detect the radiation with wavelengths up to 14 μm. The part of the electromagnetic spectrum in this range is referred to as IR. The infrared portion of the electromagnetic spectrum is usually divided into several spectral regions, named for their relation to the visible spectrum (see table 1-1).

Table 1-1: Infrared Imaging Spectra [3].

Sub-region	Wavelength (μm)
Near -wave infrared (NWIR)	0.75–1.4
Short wavelength IR (SWIR)	1.4–3
Medium wavelength IR (MWIR)	3–8
Long wavelength IR (LWIR)	8–15
Far long wavelength IR (FLWIR)	15-1000

The MWIR waveband is used commonly in the thermal imaging industry. The waveband 5–8 μm is virtually unusable for thermal imagers because this range has high absorption by the atmosphere [3]. The response of various IR detectors plays important role in determining the thermal imagers industry based on the IR

spectrum. All thermal cameras work at MWIR (3-5) μm and LWIR (8-12) μm as shown in figure 1-1.

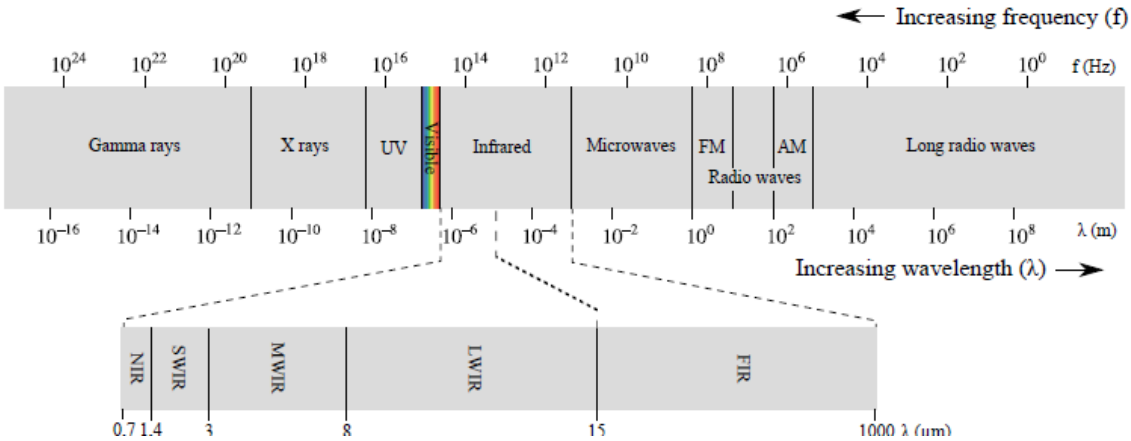

Figure 1-1: Electromagnetic spectrum [3, 4]

A special lens is used to focus the thermal radiation emitted by the objects when their temperature is above zero Kelvin. The infrared-detector elements scene the focused radiation and create electric impulses, the impulses sent to a signal-processing unit. The translating waves from the elements are converted into data in order to appear on display. The information scents by the signal-processing unit to the display and appears in different colors depend on the intensity of the infrared emission. Germanium is usually used for this purpose because the glass has a low transmittance for thermal radiation, Germanium is a grey-white metalloid and is always transparent to IR radiation, but it is reflective to visible light. Since germanium is expensive, then the size of the lens becomes even more significant. Another parameter that affects the image quality of thermal imaging is the camera lens characteristics. The optical system has an f-number of the lens which represented the ratio of the focal length to the diameter of the entrance pupil. Therefore, a higher f-number indicates that the price of the lens is low but a smaller amount of radiation reaches the detector [35].

1.2 IR Sources

Every object with a temperature above zero Kelvin degrees is an IR source and used for different purposes. The human body radiates a long-wavelength IR source of

about 10 μm. Another common IR source is blackbody radiation, which is a body or object that does not reflect radiation from its environment, so that, its only output is the thermal radiation from its temperature. Blackbody sources are primarily considered for calibration purposes, as it is characterized by high accuracy and emissivity. The black body is a cavity that usually takes the form of a uniformly heated or cooled. The inside surface of the cavity has high emissivity. The aim of using the cavity is to increase the effective emission [4, 5]**.**

1.3 Thermal Imaging

The amount of radiation and its distribution radiation is depended primarily on the temperature of the body. According to Wien's Displacement Law, the peak value of the intensity of the spectrum shifts to smaller wavelengths as the temperature is increased [6].

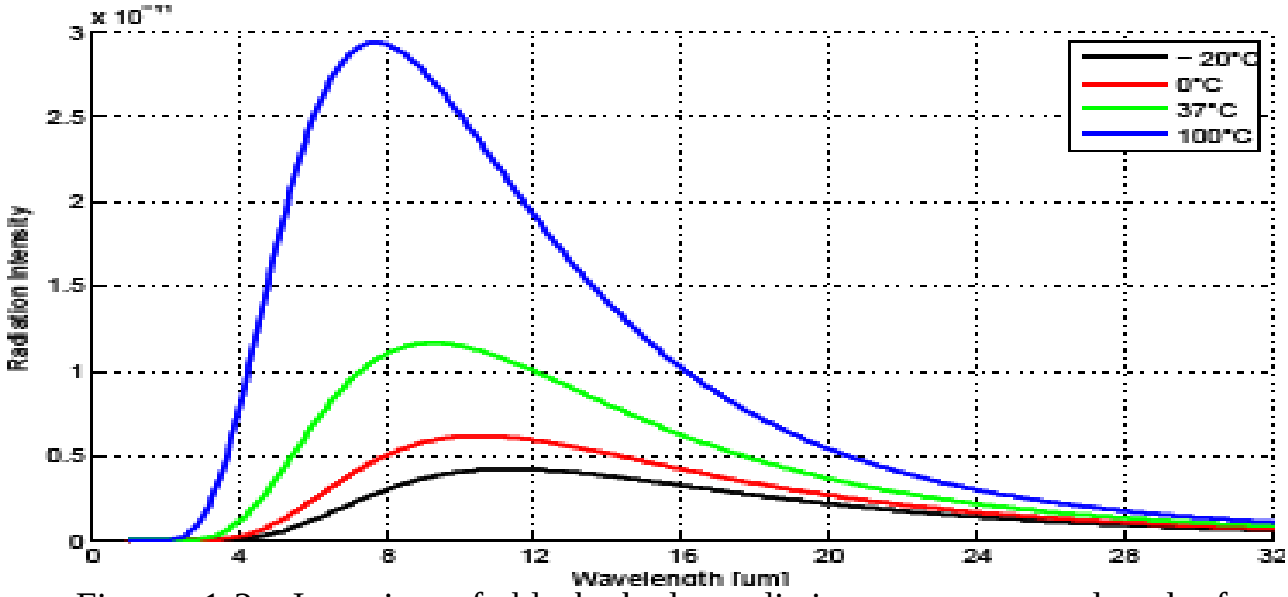

Figure 1-2: Intensity of black body radiation versus wavelength four temperatures [3].

Wayne's displacement law is

$\lambda_{max} = \frac{b}{T}$ 1-1. $\lambda_{max} = wavelength\ peak$, b=constant of proportionality, T=absolute temperature

All objects and organisms generate some amount of heat. Heat is a form of light is invisible to the human eye and is also known as thermal IR radiation. The thermal camera serves as a heat sensor that detects temperature differences between objects and the surrounding environment. Rather than a picture of light, the thermal image is a visual capture of heat. The object emits more heat produces a thermal image with high brightness. Thermal images are a good tool to give the most information on temperature differences in a scene. The difference was helpful crest the contrast in image and gray scale obtained. The dark areas indicate colder temperatures and light areas warmer ones. Color plates can be used to enhance different shades in the image. Thermal cameras can be applied in various applications such as detecting people and objects in complete darkness, or other challenging conditions such as smoke-filled, dusty environments and incidents in low-light environments [7].

Thermal cameras are also used inside a building after business hours or in emergency situations like rooms filling with smoke, High-security buildings, airports, nuclear power, plants pipelines, and sensitive sections of railways. A major aim in the development of thermal imagers is to develop military applications, where they are can to see through the smoke, mist and distinguish the targets at above ambient temperatures and when their background is achieved [8, 9].

The ability of the material surface to emit thermal radiation is called emissivity (e). All materials have more or less emissivity, which depends on their properties; the amount of thermal radiation depends on the object emissivity [10].

When reflected the light the human eye sees images, the fact is by different objects. No light means any reflection, and the eye is “blind” under such circumstances. On the other hand, thermal images are not dependent on visible light, created by operating in the thermal IR spectrum. The works perfectly well even in total darkness since the ambient light level does not matter [11].

In general infrared detectors are used to detect an image, and measure thermal radiation patterns from objects whose temperature is above zero Kelvin. These

detectors had extensively developed since the 1940's when the sulfide (PbS) was the first practical IR detector with sensitivity to infrared wavelengths up to ~3 μm [13].

Since infrared detectors produce a wide range of military and civilian applications, it is difficult to determine the spectral range in which a given detector must operate to achieve optimum performance [14].

Manufacturers often offer multi-band detectors that can to operate in both the medium and long wave infrared bands, but they are expensive requirements that need to be done. The performance of detectors received serious attention for the first time in the early 1970s by [15].

1.4 Thermal Imagers

Thermal imagers are employed to generate images when the objects emitted thermal radiation, it can be classified into different groups.

The first group is due to a method of creation of the two-dimensional image of the observed scenery. This leads to dividing into two distinct groups: thermal cameras and thermal imaging scanners.

The second group is due to the application area, it can be divided into two groups: surveillance thermal imagers and measurement thermal imagers.

The third group is due to a spectral band, it can be divided into two groups: mid-wave infrared (MWIR) and long-wave infrared (LWIR), in other cases, the short wave infrared (SWIR) also depended.

The Fourth group is due to the manufacture of IR detectors, it can be classified into three generations as shown in figure (1-3).

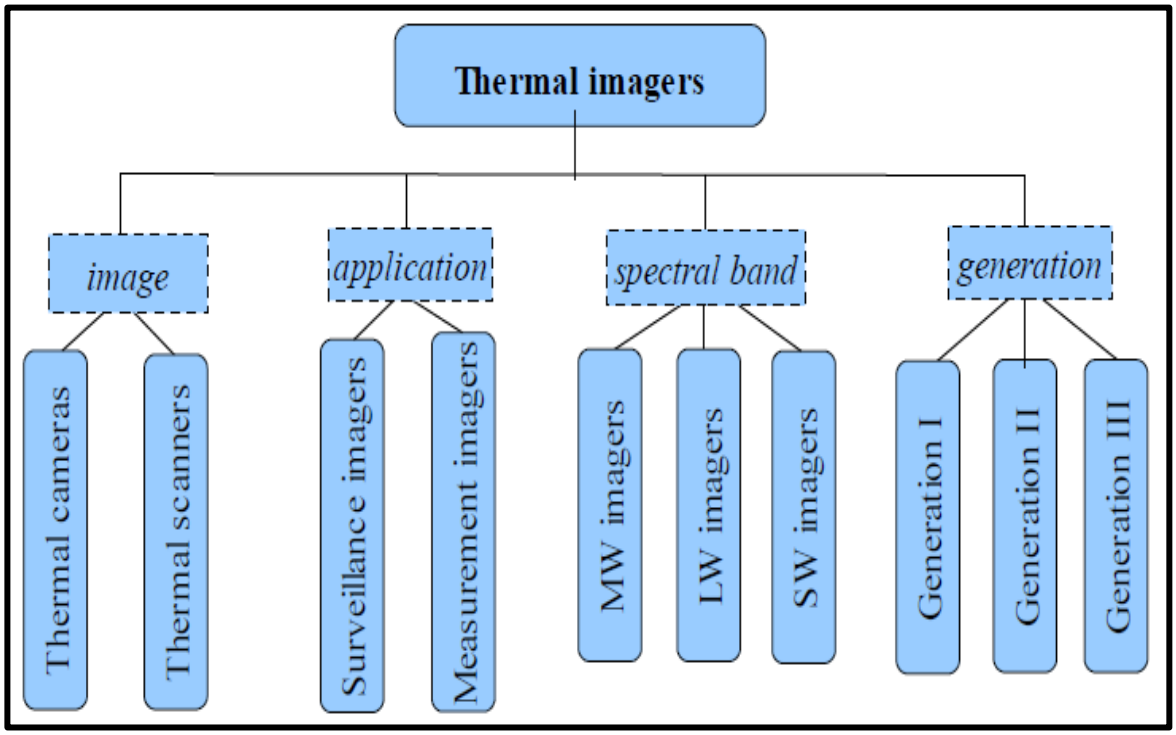

Figure 1-3: shows the classification of thermal imagers [18].

1.4.1 Thermal Cameras versus Thermal Scanners

The thermal imaging system used a thermal camera to enable us to create a thermal image in two-dimensional, the observed scene affects by the weather or objects are movable or stationary.

A thermal imaging scanner provides a thermal image two-dimensional only when the scanner moves. Imaging thermal scanners are almost exclusively airborne systems used for reconnaissance applications because a very wide field of view (standard 120º) obtained in contrast to the thermal cameras give a field of view not wider than about 30º [19, 20].

Thermal cameras represent 99% of all existing thermal imagers systems approximately, because of the difference in the design of these two types of thermal imaging systems and narrow specialized market, the imaging thermal scanners are very expensive systems [19, 21].

1.4.2 Surveillance and Measurement Thermal Cameras

In general thermal imagers can be divided into two basic groups: thermal measurement cameras and thermal surveillance cameras due to their applications.

The thermal surveillance cameras are mostly used in military applications to observation of a battlefield in darkness or difficult atmospheric conditions. The surveillance thermal cameras are performed by creating the relative temperature distribution of the terrestrial scenery observed.

Some cameras belong to thermal measurement cameras are used for civilian applications such as industry and science. The applications occur for non-contact measurement of temperature distributions on the surface of the tested objects. In comparison, the image quality of the measurement systems is less than the image quality of the observation thermal cameras. The efficiency of thermal cameras used in military surveillance depends on the image quality which is the most important criterion for efficiency. The situation is more complicated in the case of commercial measurement by thermal cameras.

Measurement thermal cameras can be divided into two groups due to their applications, the first require only relative temperature measurement, and the second requires absolute temperature measurement. Their criteria are different for the assessment of camera suitability for these two groups of applications. If the camera is used in applications to obtain relative temperature measurement only, the quality of the thermal image of the tested object is usually the most important criterion like in the situation the surveillance thermal cameras. But if the thermal measurement camera is used in applications when an absolute temperature measurement is needed, then the temperature accuracy of measurement is the most important criterion [19, 22].

1.4.3 Spectral Band

There are two types of "atmospheric windows" in the range of IR a 3-5 μm and an 8-12 μm.

There are two types of "atmospheric windows" of IR radiation a 3-5 μm and 8-12 μm. The thermal imaging systems can be classified due to these windows. The most important atmosphere transmission in the infrared radiation occurs in the MWIR range of 3 to 5 μm and the LWIR range of 8-12 μm [12]. The analysis of imaging systems operating achieved in medium and long waves in terrestrial situations. It was shown that the MWIR has a good performance compared to LWIR in most situations. But the performance in the MW band was found to degrade more rapidly compared to performance in the LW band for cooler targets [16].

For spectral ranges, there are different emissive characteristics of targets in the MW (3–5) μm and LW (8–12) μm, which contributed to achieve dual-band detection and the spectral recognition of a target [17].Thermal imaging systems can be divided into two main types of MWIR systems using a 3-5 μm and LWIR systems using an 8-12 μm spectral range of SWIR systems used in the 1-3 μm. The MWIR and LWIR spectral bands are significantly different indicate the temperature contrast of the target, background, and atmosphere and its transmission under various weather conditions. MWIR band prefers higher contrast, superior performance in clear weather, higher transmittance at high humidity, and higher accuracy due to smaller optical diffraction. LWIR bands are better performance in fog and dust conditions. The LWIR range has a higher sensitivity for cold objects, while the MWIR range may be more suitable for hotter objects such as engines, power generators, and combustion gases. Some detectors may operate at higher temperatures, then cooling to 77 K is generally required, and larger openings for accuracy when operating at the diffraction limit [23,24]. Appropriate materials and different filters must be used to reach the requirements of high transmittance AND a careful selection of various bands, this system leads to an increase in the weight of the additional lens group. Also, there is a reduction in the amount of incident light so that the signal-to-noise ratio $SNR = \frac{S}{N}$……1.2.

Therefore a thin-film layer must be used on the surfaces of the lens. Dispersion caused by the lens should be corrected to maintain the image quality SNR= $\frac{I_S}{I_N}$ where $I_S$is the signal current and I_N is the noise current [25–27].

1.4.4 Generations of Thermal Imagers

IR detector technology contributed to the design of the thermal imagers, according to the number of elements which detector contained, three distinct generations of thermal imagers were designed:

The first generation of thermal imagers contains a single element detector, or detectors have few elements (usually PbSe, InSb, or HgCdTe). A mechanical scanner with a two-dimensional is usually used to generate a two-dimensional image. They operate in an 8-12-μm spectral range, the f-number is F/2-F/4, and it's characterized by a temperature resolution of about 0.2 K. The first-generation thermal cameras were introduced as military equipment in the 1970s, and in the 1980s. Although of these systems are still in military services, spare parts also were available for many years. The common module HgCdTe arrays is that employs 60, 120, or 180 pixels.

The second generation of thermal imagers is presently the majority of all military thermal cameras, usually containing 94*4 pixels. The two-dimensional scanner was simplified to use in the vertical direction, to include the interlace motion only. The temperature resolution of these detectors improved about to 0.1 K. The characteristics are smaller weight, size and improving reliability. 1980s, modern army forces started to use second-generation thermal cameras. The new version is the Fire Protection Accreditation Scheme, which is employed single chip fully integrated with readout electronic, which becomes an attractive solution for many observation applications. Thermal cameras of these systems are considered HgCdTe that work at both ranges 3–5-μm and 8–10.5-μm.

The third generation of thermal imagers contains two-dimensional arrays with several columns of elements. The scanning process of these thermal imagers occurred in one direction and performs a Time Delay Integration (TDI) of the signal to improve the signal-to-noise ratio. Thermal imagers designed in 2D array detectors cooled Focal Plane Arrays (FPA) based on InSb, HgCdTe, or non-cooled FPA based on micro-bolometer or pyro electric/ferroelectric technology. They have at least 640*512 pixels. The opt-mechanical scanner was eliminated and the only task is to focus the IR image on the matrix of sensitive elements .The temperature resolution of these detectors improved about 0.05 K. Thermal cameras of these systems are considered HgCdTe that work a ranged 8–14-μm. I became commercially available at the end of the 1990s [18].

1.5 Attenuation of Thermal Radiation

Absorption of IR radiations happens due to CO_2 and H_2O. The variations of the wavelengths with the certain transmission of IR radiation are depicted in figures 1-3. The water vapor has continuum absorption to the IR radiation in 5 to 8 μm ranges, where the cameras are insensitive here. Similar is the case for radiations above 14 μm [12].

There are many processes such as absorption, scattering, and transmission affected on the propagation of radiation. These phenomena cause attenuation of propagating optical radiation ,and the turbulence distorts of the image of the emitting objects [23]. The concentration of H_2O depends significantly on high, season, geographic location, time of day, and is subjected to large fluctuations. The amount of H_2O in the air decreases speedily with high. H_2O and CO_2 are responsible for most of the absorption in the IR region at sea level [28].

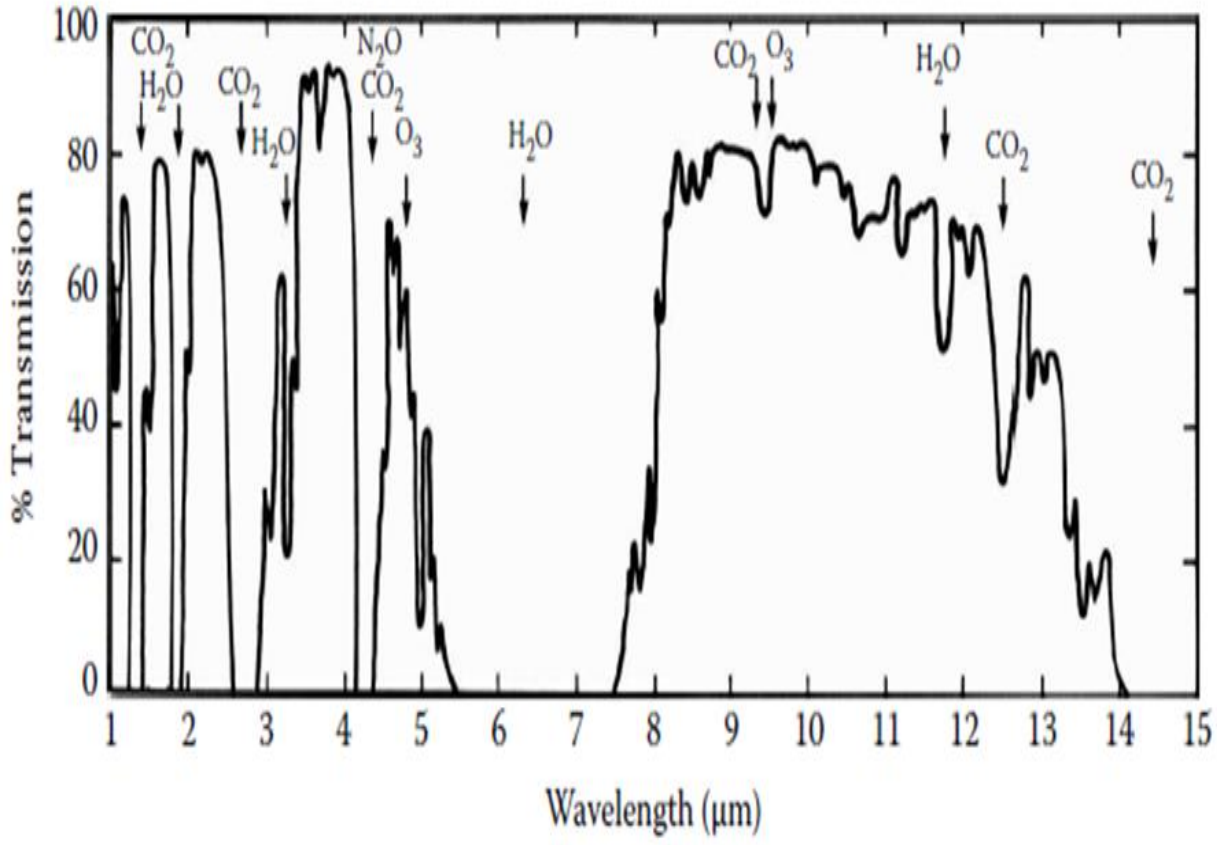

Figure 1- 4: The transmission of IR through the atmosphere [28].

For the atmosphere absorption, ozone, nitrous oxide, carbon monoxide, and methane are less important in IR absorption [29]. Water vapor and ozone in the atmosphere thermal infrared radiation is called the atmosphere effect [30].

1.6 Thermal Cameras

A thermal imaging camera responds to the intensity of IR radiation and converts it to a visible image [31].

Thermal cameras have historical significance, mainly for military applications. Image quality, power resolution, decreasing price and size during new years are characteristic opened of up new application areas of the thermal camera. In recent years, they have been widely used for civilian applications and for military applications because of their advantages due to their ability to see in total darkness [32].

The first commercial thermal imaging camera was sold in 1965 to check high-voltage power lines. Thermal imaging technology has greatly developed in the last years. It becomes compact and is similar to a digital photo camera. It produces in real-time, high-resolution, and clear images, making it a widely important tool in various applications and detecting objects that are generally invisible to the naked human eye in specific conditions [33]. The importance of Thermal Imaging Cameras (TIC) displays image quality to the firefighters to able them to perform a hazard recognition task. Test subjects were employed to identify a fire hazard by observing infrared images. The interactions between contrast, spatial resolution, brightness, and noise in an image have a more significant effect on human perception than anyone variable by itself [34].

1-6-1 Components of Thermal Imaging Camera

Any optical system creates an image of any external object by using thermal radiation with a specific wavelength. The optical system consists of the following parts.

1. The detector elements convert the thermal radiation into electrical signals relational to the intensity.
2. Scanning systems are required to scan the thermal image in even designs through the detector elements, although it is more topical. Imaging devices may not require this, as they use large detector arrays that can to cover completely the photographer's field of view.
3. The electronic processor can process the detector output in conjunction with the data from the scanning mechanism, and it can be transformed into a video signal.
4. Image viewer generates a visual image from a video signal [36].

All part of image forming is shown in figure 1-5.

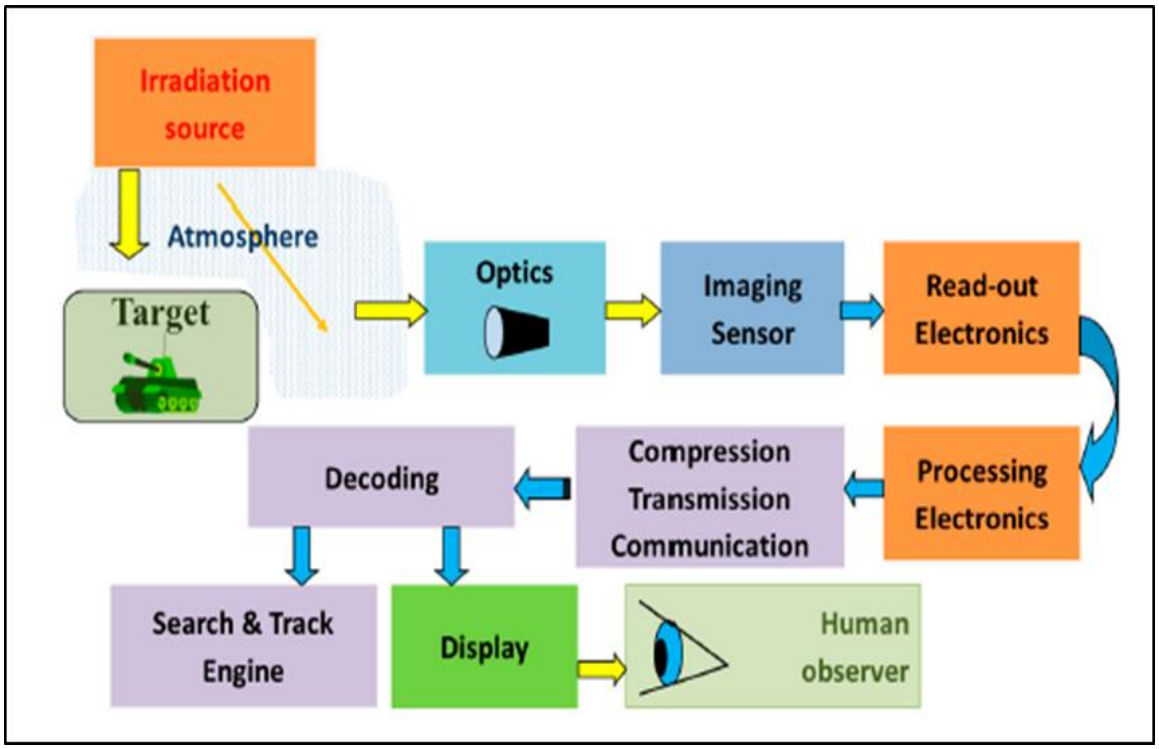

Figure 1-5: Image forming chain [37].

1.7 Thermal Camera Applications

The temperature can be used to detect specific objects and can also provide information about them. It is very important to employ temperature in various applications. This is clear in the applications of thermal imaging systems.

Thermal imaging systems have many applications such as in the food industry as well as in agriculture. Portable systems are used in the food industry that works in real-time and measure temperature without contact [38].

Because thermal cameras see through the smoke, it is useful for detecting fires and is commonly used by firefighters to find persons and to localize the base of the fire. The camera works by detecting places heats than the surrounding [39]. Heat losses in buildings also can be detected using a thermal camera. Heat loss is detected by thermal image map through the automatic methods from 3D models for visualization [40]. Also, Thermal imaging systems are used to provide skin temperature distributions to know details of physiological processes due to blood

perfusion. Thermal cameras with high resolution are used to observe of temperature in variations the medical field [41].

Recently, the smartphone has a small thermal camera to create new applications not yet imagined. In addition, thermal cameras are used in sports to obtain a visual image of the heat in your muscles [42]. Another application of thermal cameras is searching for persons independently of daylight using cameras carried by Unmanned Aerial Vehicles UAVs, helicopters, or rescue robots [43]. Also detection, tracking, and behavior analysis of persons and vehicles to detect of intrusion and suspicious behavior [44].

IR cameras are used as scanning devices or a 2-D IR focal plane array. In the case of using a scanning device, a solid sample is briefly exposed to a time-variant heat source and the surface temperature of the specimen results is measured instantaneously with an IR camera. A part of the incident radiation is absorbed in the sample surface and converted into heat to get a that heat pulse is into the material. The thermal wave suffers attenuated and disturbance into the material after it propagates, and any subsurface is scatter by defects it. The surface temperature in the area directly above the defect is increased by scattering a portion of the thermal wave. IR thermal scanning device maps the sample surface temperature to reveal the subsurface defect. If it used as a 2-D IR focal plane array (IRFPA) all elements are captured simultaneously for each detector in the array. Nowadays, IRFPA is the most important technology because it is faster, has better resolution, and has no moving parts as compared to scanning devices [19].

Detectors that are used in thermal cameras can be classified into aphoton and thermal detectors. In Photon detectors, the EM radiations are directly absorbed and converted into electronic energy that is distributed in a semi-conductor due to free charge carriered concentration. In thermal detectors, the absorbed EM radiations transform into thermal energy and cause an increase in the temperature of the detector. The electrical output of the thermal detector is generated by a relative change in some of the physical properties of the object [12].

1.7.1 Thermal Imaging in Military Applications

The technique of finding specific or anomalous objects by images or videos is called detection. The background in the scene is divided into two parts, first is the background subtraction, also known as change detection which is a possible way to perform anomaly detection. It is the technique of learning a background model and classifying all samples not belonging to the background as foreground, or anomalies. The greatest challenge for to background subtractions is probably the gray areas when deciding whether a region belongs to the foreground or not [6].

The second is to distinguish adaptive link filters which are used for many applications, especially in optical detection and tracking. Its performance is wonderful despite its great simplicity and its super speed of 20.8 frames per second(fps) [45].

1.8 Object Detection in the Infrared Images

The goal of object detection is to provide their exact position. Object detection is to determine where objects are located in a given image (object localization) and which group each object belongs to (object classification). As different objects may appear in any position of the image and have different aspect ratios. A classifier is needed to distinguish a target object from all the other groups and to make the representations more ordered, semantic, and informative for visual recognition [46].

Tracking methods of objects are affected by the type of the application. Some of those methods depend on the object division model, motion model, and probabilistic model. Video is a method of tracking but it is a difficult problem in computer vision because of many different and varying situations such as variations illumination, change in scene, and a varying number of targets that need to be resolved. Optical flow is one of the most algorithms used to identify the local feature of a target, this process occurs between two frames, the target intensity remains suitable and the target moves slowly [47, 48].

In addition, tracking can be defined as determining the path of an object over time. The path is represented either by the object location or as the whole region that the object induces in each observation [49].

Detection and tracking are often described as two problems separately. However, tracking depends on detection and the task of detection can either be done separately or jointly in case of separately achieved detection. Tracking was reduced to establish correspondence between detections. If detection makes jointly, an initial detection is needed in order to consider the object model. The tracking method performs by repeated specific detection. The initial detection is determined manually or automatically.

In the second case, a framework is required to initialize a new instance of the tracker [50]. Tracking must be short or long-term, single or multi-sensor, as well as single or multi-object. Short-term tracking is defined as short periods of time, for example, a couple of minutes maximum also that there is no requirement of re-identification of targets [51].

1.8.1 Long Range Object Detection

Imager range represents the effective distance between the interest object and the imager. A specifying object can be detected when the surveillance task perception norms depend on Moving Target Identification (MTI). This task has wide and important applications nowadays. Range imager is a very important parameter that every user wants to know, it depends on imager design parameters, scene, and tracing path properties. The thermal imager range is estimated only when all influencing factors are known for a selected target, the determination of all factors is not always possible or they could be estimated with poor accuracy. Also, there is no universal theoretical model that is applied to follow the data available in the field. Recently various complex models are developed for thermal imager analysis. That is used in

the technology of planning and development phase. Moreover, in some specific conditions, they cannot guarantee accurate results in field conditions [44, 52].

1.8.2 Short Range Object Detection

Imager range is investigated by using theoretical models that backing the ability to check range performance. Estimated of all factors is performed approximately. Thus choosing the suitable range of object detection is due to the selected visual perception standards. The measured radiance and the polarization of the radiance depend on the temperature of the target and the reflection of the surrounding area about the target [52, 53].

Many variables must be known to determine the thermal camera range, including:

- Atmospheric conditions.
- Type of lens.
- Type of thermal imaging camera.
- The geometrical factors of the object.

In summary, the efficiency of detecting a target by a thermal camera is not easy. This task depends on many parameters such as environmental conditions and system variables, which briefly describe as the state of the target likes the static vehicle or motion vehicle, the background likes hot desert or cold and snow and the atmospheric conditions like clear skies or fog and rain. In addition, it considered the specification of the camera which it chooses due to the applications [3].

1.9 Literature Review

Many studies and researches have been performed and published in the field of thermal imaging systems. Here, numerous of these studies, which have a relation with the present work, will be presented.

J. Shi et *al.* in 2012 employed an obstacle detection system dependent on thermal vision is the purpose of enhancing the realization of pilots during taxiing in bad weather conditions. Detection of the objects and estimation of the obstacle distance were achieved by employed two infrared cameras. The distance is estimated by stereo vision technology. A warning is recorded when the distance becomes less than the safe distance predefined. The proposed system is an on-board system that does not depend on airports or other airplanes. The type of obstacle was choosing by the temperature of the object. The results suggested that the stereo vision system developed the ability of detection and the estimation of the distance [54].

Y. Iwasaki *et al*. during 2013 detected the position and speed of the movement vehicles under adverse environmental conditions in snow and dense fog. This detection was achieved by using thermal images with the Viola-Jones detector. Based on the thermal energy reflection of the tires and the accuracy of detection was (92.8%) [55].

E. Bernard *et al*. in 2013 introduced a study to determine the modifications of thermal imaging according to bad weather conditions. The propagation of light through rainfall was considered in this model. The rainfall affects the properties of a solid target such as the reflectance or the temperature of the surface. The developed models with validity ranges were dependent to get the fast computation of synthesized images under waste weather conditions [56].

N. Goyette *et al*. in 2014 suggested an efficient algorithm for detecting moving targets in infrared images using the spatiotemporal information presented. Spatial information was obtained using the common spatial frequency distribution. The method was validated experimentally to generate data consisting of a variety of moving targets. The experimental results showed that a high scale value for the proposed algorithm was investigated [57].

K. Lenac *et al*. in 2015 presented an algorithm for moving object detection. This algorithm allowed the detection of moving objects in thermal images of low quality without imposing restrictions on the temperature and/or shape of the object. The main

assumption required for good performance of the algorithm was that the transversal movement of the vehicle was not produced a significant change in the optical flow of the static objects [58].

Y. Cao *et al* in 2016 analyzed the characteristics of infrared moving targets. Target Detection algorithm based on the local clustering segmentation that was proposed. This novel algorithm used a local gray scale clustering to accomplish target detection. The mean shift tracking algorithm was also improved to solve the problem of missed targets caused by error convergence. A kernel-based mean shift target tracking algorithm based on detection updates was also proposed. This tracking algorithm used the interaction between detection and tracking to correct the tracking errors in real-time and to realize robust target tracking in complex scenes [59].

R. Usamentiaga and D. F. García in 2017 proposed a model for both real movements and vibrations of the target, which are treated equally. The three key steps of the proposed procedure were image rectification, motion estimation, and motion compensation. The result was a sensor for the temperature of moving material that can also be used to measure the speed of the target. Different experiments were carried out to validate the proposed method in laboratory and real environments [60].

L. Maddalena and A. Petrosino in 2018 proposed an algorithm, that the vehicle transversal movement has not affected the optical flow of the static objects. The algorithm got a good efficiency for detecting moving objects like humans in urban environments by using an inertial measurement unit (IMU) sensor and a thermal camera. The method used was the Red-Green-Blue-Depth RGBD camera to record the data of moving objects by involving the background subtraction method [61].

Z. Tong *et al*. in 2018 developed a method used to estimate and determine the background rotational motion due to an optical flow field. A small moving target was detected by selecting the Shi–Tomasi angular points. The background rotation with the scattered optical flow field of a complete image was considered [62].

J. Crone and U. H. Sjoblom in 2019 introduced a study to improve the IR technology in adverse weather conditions. The project was divided into two parts,

first was concerning the transmittance of IR radiation through different states of the atmosphere. The second part was to create a simplified imaging IR simulator [63].

Mate Kris *et al*. in 2020 introduced image and data processing technologies that improved intelligent inspection systems capable of extracting hidden information. Image segmentation techniques, data mining, and machine learning methods have been applied by proposing innovative models suitable for accurately monitoring processes. The proposed models for industrial process engineering can be adopted that include quality, production performance indicators, safety systems, resource management, and smart activity scheduling. The various networks capable of transmitting data and thermal diagrams were described through a discussion of system integration into automated systems [64].

Y. Han and D. Hu in 2020 presented the traffic surveillance systems that were employed to detect, account, and classify vehicles to get gathering traffic statistics and achieving better traffic control in intelligent transportation systems. Using thermal cameras led to a good detection of images in daylight because of good visibility. It often struggles when the visibility of the scene is impaired by insufficient illumination or bad weather conditions such as fog, snow, haze, and rain. Therefore, the work focused on designing a dual input faster region-based convolutional neural network (RCNN) in order to make full use of the color and thermal images to detect traffic objects in bad weather [65].

F. Leira *et al* in 2021 introduced object detection, identification and tracking of unmanned aerial vehicles (UAVs). The system can be implemented on any UAV platform using machine vision to automatically detect objects in a camera image stream file combined with the UAV's navigation data, which is on board. It uses a tracking algorithm that uses a Kalman filter and a constant velocity motion model showing that the system is able to automatically detect and track the position and speed of the boat [93].

S Thermovision et *al* in 2021 proposed an algorithm that allows automatic detection of thermal hazards using a smartphone-type device and a mobile thermal

camera. The algorithm operates in two stages. First, it analyzes the environment of the disabled person for areas of very high or very high temperature. If they are detected, they indicate by voice messages the appearance of such an object in the field of view of the camera [94].

1-10 The Aim of Work

This work aims to study the efficiency of the thermal camera in detecting and recognition the targets under specific conditions (bad weather and moving objects) in the Ain-Altamur region- in the holy city of Karbala Province-Iraq.

In the present work, the following steps are performed

1- Calculate the transfer function of the bar spread function, which is used as a tool for determining the performance of the thermal imager at different parameters, ranges, object velocities, the concentration of fog, and concentration of particulate matter PM_{10}.

2- Thermal images are captured by the thermal camera (PT-602CZ HD) of moving objects at various ranges and at various concentrations of fog to compare with the theoretical results in the same area of the study.

Chapter Two

Theoretical Part

2-1 Introduction

Recently, optical imaging of objects distinguished with a camera in the infrared range of the electromagnetic spectrum has achieved wide attention in researches. The quality of the thermal image depends on the information collected from the object by the optical system. Infrared images are mainly detected with noise due to different reasons, such as noise caused by the movement of objects or detecting images with bad environmental conditions. Due to these noises, getting images with a high resolution is a requirement and represent a challenging issue. In particular, detection of the moving objects against a night- background with a high resolution represents a very important issue for the night vision purpose [3]. The thermal camera is widely used in military applications to detect objects in dark environment conditions. In optical imaging systems, there are many valuable criteria to antsy for the performance image quality. Transfer Functions such as point spread function (PSF), optical transfer function (OTF), and bar spread function (BSF), provide information about the source (objects) . These functions are mathematically calculations that describe the amplitude and intensity of the image; thus, they serve the goal of optical design. Such functions are studied explicitly to enhance the intensity profile and resolution of the detected images [66].

2-2 Optical Transfer Function (OTF)

The quality of optical systems can be estimated by many methods such as Optical Transfer Function (OTF). It is an objective, accurate, quantitative evaluable parameter and represents an interest function to define the performance of the imaging system optical [67]. The OTF is defined as the ability of the optical system to transfer the frequencies of the object to the image level [68]. OTF is widely used in optical design because it can be measured directly. Since the modern optical theory explained that optical systems are linear spatial filters, and this concept leads to

imaging quality. It can be estimated by the ratio of the spectrum between object and image [69]. The OTF can be expressed as:

$$D(s) = T_{(\omega)} exp^{i\theta(\omega)} \qquad 2\text{-}1$$

Where:

$T_{(\omega)}$ = Optical contrast transmission function

$\theta(\omega)$ = Phase side transferal function

S=Spatial frequency

The specific target analysis is described in figure (2-1), where FT is the abbreviation of Fourier Transform. Transfer Function of optical system H (u, v) is defined as Optical Transfer Function OTF (u, v). So getting the OTF of an optical system due to the principle of the figure (2-1) from the formula:

$$\mathrm{OTF}(\mathrm{u},\mathrm{v}) = \frac{G(u,v)}{F(u,v)} \qquad 2\text{-}2$$

Moreover, OTF was derived from the Point Spread Function of the optical system PSF(x, y) by the Fourier Transform method.

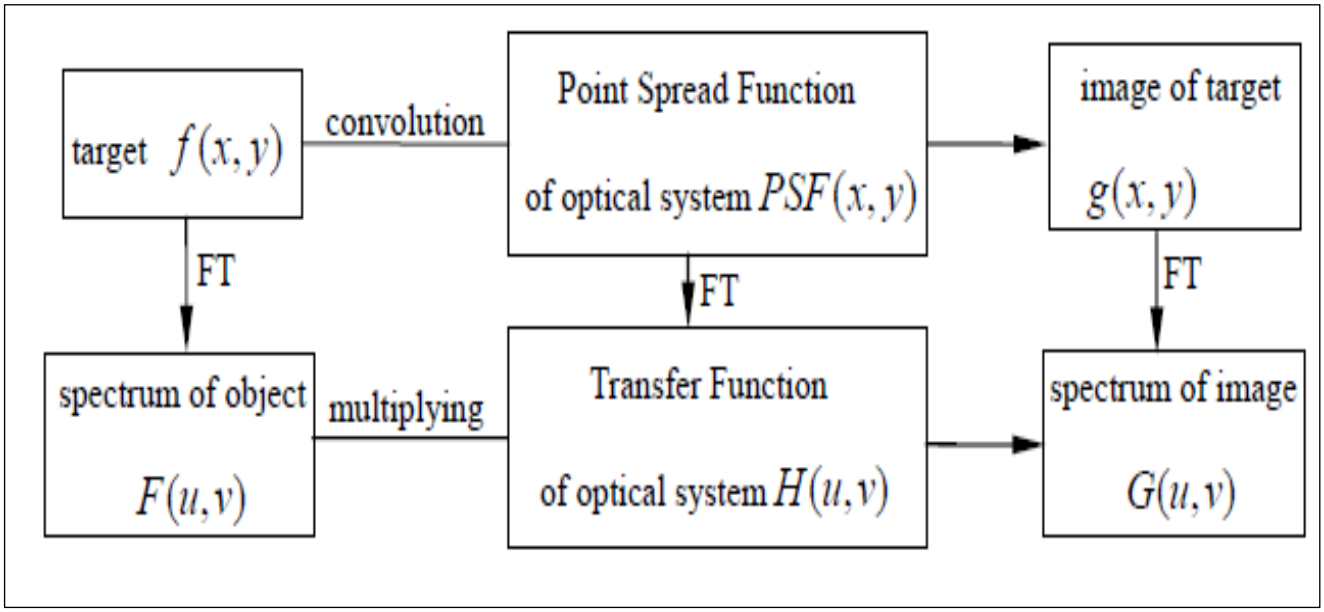

Figure 2-1: The principle of a specific target analysis[69, 70].

2-3 Modulation Transfer Function (MTF)

The system is defined by diffractions or has symmetric aberrations, the optical transfer function is real and there is no phase change. In this case, the performance of the optical system and the image quality can be predicted from knowing the curves of the optical transfer function and the phase modification function. The phase modification function is found from a function identified as the modulation transfer function (MTF). This function can be identified by measuring the ability of the optical system to transfer contrast from the object plane to the image plane at a specific resolution [71]. The image quality of an optical system can be estimated from the determination of MTF. Where the limit of the analysis of the transferred frequencies is limited to the value of the spatial frequency at which the optical contrast transmission function falls to zero [72]. The MTF is defined as the ratio of image modulation to that of the original object and can be expressed as [73] :

$$MTF = \frac{I_{max} - I_{min}}{I_{max} + I_{min}} \qquad 2\text{-}3$$

Here:

I_{max} =The maximum intensity, and I_{min}= Minimal intensity.

2-4 Fourier Theory

Linear transform methods such as the Fourier transform are widely used in solving problems in science and engineering. The Fourier transform (FT) is employed in linear systems analysis. Particularly, Fourier analysis is used in every aspect of the subject ranging from solving linear differential equations to develop computer models, the processing and analysis of data [74]. The FT, in essence, decomposes or separates a waveform or function into sinusoids of simulations using the mathematical technique. That's means, a Fourier series decomposes a signal into components that vibrate at integer frequencies [75]. By contrast, the FT decomposes a signal defined on an infinite time interval into a frequency component, where can be any real (or even complex number). The time and frequency domains are alternative ways of representing signals, thus, the FT is the mathematical relationship between these two representations [75]. The Fourier transform of a two-dimensional signal can be expressed [76]:

$$F(u,v) = \int_{-\infty}^{\infty}\int_{-\infty}^{\infty} f(x,y)e^{-2\pi i(ux+vy)}dxdy \qquad 2\text{-}4$$

The inverse FT of the intensity of PSF in the (u, v) dimensions is given by [76]:

$$f(x,y) = \int_{-\infty}^{\infty}\int_{-\infty}^{\infty} F(u,v)e^{2\pi i(ux+vy)}dxdy \qquad 2\text{-}5$$

Real objects contain continuous distributions of image intensity while image sensors contain separate pixels, so that, all image processing is performed using separate matrices. [76].

2-5 The Convolution Theorem

Convolution is a mathematical way of combining two signals to form a third signal. This theory is the most important technique in Digital Signal Processing. Using the strategy of impulse decomposition, systems are described by a signal called

the impulse response. Convolution is important because it relates the three signals of interest: the input signal, the output signal, and the impulse response. In many cases, G (u´, v´) is not known explicitly, therefore, using the condition of shift-invariance is necessary. For example, in the object plane, the diffraction image of a point located at (u, v) is given by $(u' - u, v' - v)$. The convolution of the object intensity distribution and the point spread function gives the resultant intensity $B'(u', v')$ at a point (u', v') in the image plane as given:

$$B(u', v') = \iint_{-\infty}^{+\infty} B(u, v) G(u' - u, v' - v) du dv \qquad 2\text{-}6$$

Where:

B (u, v): is the object intensity distribution at (u, v) in the object plane [9, 10].

Figure 2-2 shows the convolution of two functions. A convolution is presented as the amount of overlap of one function (g) as it is shifted over to another function (f). It is therefore the first and second functions are "blends" and can be expressed mathematically as $f * g$.

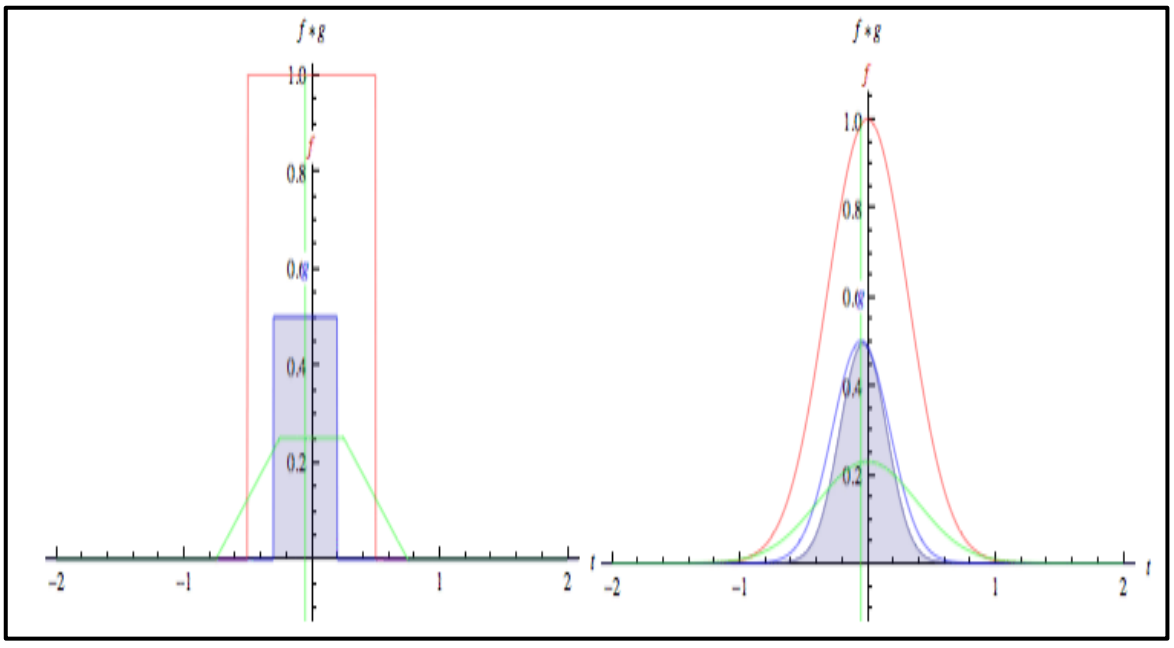

Figure 2-2: The convolution of the two functions g (t) (Green) and f(t) (red) [77, 78].

2-6 Pupil function

A pupil is a hole located in the optical system and determines the array of light that entering to this system. The pupil function technique limits the amount of transmitted light through an optical imaging system such as a camera, microscope, or the human eye [79]. Since the defects caused by an aberration in the optical system have a direct consequence on the pupil function, therefore, the pupil function is considered as one of the preferred tools to study the performance of the optical imaging systems [80]. Moreover, pupil function represents by a complex function that describes the relative change in amplitude and phase of the transmitted wave [80].

To study the complex amplitude in the image plane of the point source, a schematic representation of an image forming in the optical system with incoherent illumination is depicted in figure 2-3.

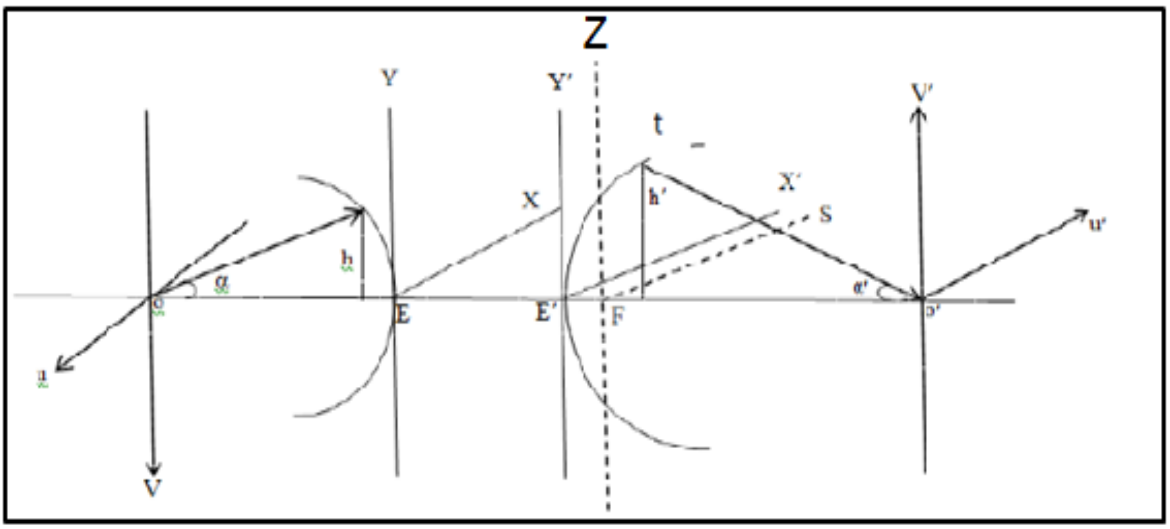

Figure 2-3: Schematic representation of an optical system for imaging an incoherently illuminated object [73].

Considering a wave propagate through the optical systems to form an image of a point source. The point in the object plane will form in the image plane as a diffraction pattern. From figure (2-3), the object and image planes are represented by the coordinates (u, v) and (u´, v´), respectively. This coordinate is indicated

concerning the origin points of the object and image at O and O´, respectively. The entrance and exit pupils of the optical system are shown on the axis (E) and (E´). The radius of the reference sphere in the object space is represented as (OE). A ray of light comes from the point (O) in the object plane, making an angle (α) with the optical axis. This ray intersects with the reference sphere in the object space at a height of (h). To form the image, the ray converges from (O) to (O´) in the image plane make an angle (α´) with the optical axis. The converged ray intersects with the reference sphere in the image space at a height (h´). The advantage of transferring the actual coordinates into these dimensionless diffraction variables is that it takes care of the problem of magnification produced in the final image. The fractional coordinates of points on the entrance and exit pupil of image forming system are defined as:

$$X = \frac{a}{r} = \frac{a'}{r'} \qquad Y = \frac{b}{r} = \frac{b'}{r'} \qquad \text{2-7}$$

Where: (a, b) and (a', b') are the actual Cartesian coordinates on the entrance and exit pupils, respectively, r and r′ are the respective radii of entrance and exit pupils, respectively.

The advantage of this transformation is that normal infinite limits of integration in the Fourier transform will be reduced to finite limits. A system with circular symmetry will be considered throughout this work within the aperture limit $x^2+y^2=1$. Thus, any part of the wave front which lies outside the circle of unit radius is not transmitted by the optical system. The reduced coordinates (u, v) and (u', v') of the point in the object and image planes are defined as:

$$u = \frac{2\pi}{\lambda}(n \sin\alpha)\zeta \qquad \text{v} = \frac{2\pi}{\lambda}(n \sin\alpha)\eta \qquad \text{2-8}$$

$$u' = \frac{2\pi}{\lambda}(n' \sin\alpha')\zeta' \qquad v' = \frac{2\pi}{\lambda}(n' sin\alpha')\eta'$$

Where: (ζ, η) and (ζ′, η′) are the actual Cartesian co-ordinates, $\frac{2\pi}{\lambda}$ is the propagation constant factor of the illuminating beam, $n \sin\alpha$ represents the numerical aperture at the objective of the optical system, n and n' are the refractive indices of the object and image space, respectively.

It is assumed that the wave front results from the disturbance at (O) which lies in the object reference sphere has a unit amplitude and zero phases.

2-7 Spread Functions

Spread functions are a tool to find the intensity distribution in the image plane detected by the camera and sensors. These functions are very important to determine the image quality and efficiency of the optical system. The type of these functions depending's on the shape of detected objects and the shape of the optical system aperture. Therefore, many formulas of these functions are derived to be suitable to the investigated cases.

2-7-1 Point Spread Function

The image formed by a point source is not a point due to aberration and diffraction [81]. The image becomes expanded to a large size, and this means that the intensity distribution in the image plane of the point object is the Point Spread function [82]. The complex amplitude in the image plane of a point source located at the origin (0, 0) in the object plane is given by [83]:

$$F(u', v') = \frac{1}{a} \iint_{-\infty}^{+\infty} f(x, y). e^{i2\pi(u'x+v'y)} dxdy \qquad 2\text{-}9$$

Where f(x, y) is the pupil function which is finite within the circular aperture, and thus it is equal to zero outside this circle. Consequently, the limits -∞ to +∞ in the

integral are restricted by the finite extent of the limiting aperture, (a) is the area of the output pupil.

The intensity of the image profile is calculated by multiplying the function $F(u', v')$ with the complex conjugate $F^*(u', v')$ as follows:[83].

$$G(u', v') = F(u', v').\ F^*(u', v') \qquad 2\text{-}10$$

The image intensity of a point source located at the point (0, 0) in the object plane is given by:

$$G(u', v') = |F(u', v')|^2 \qquad 2\text{-}11$$

Equation 2-11 represents the point spread function[83].

2-7-2 Line Spread Function

The line spread function (LSF), which is mathematically derived from PSF, represents a good model to be measured instead of PSF. The (LSF) is defined as the intensity distribution in the image plane when a linear object illuminated the imaging system.

The image of a line object formed by a lens with a circular aperture can be considered as an infinite number of points along a line. Thus, the (LSF) can be expressed for incoherent line source placed at the coordinates (u', v') in the image plane as [83]:

$$L(u', v') = \int_{v'} G(u', v')dv' \qquad 2\text{-}12$$

From eq. (2-11), then we get:

$$L(u', v') = \int_{v'} G|F(u', v')|^2 dv' \qquad 2\text{-}13$$

By substituting eq. 2-9 in eq. 2-13, we get:

$$L(u',v') = \int_{v'} \left| \int_{y} \int_{x} f(x,y) e^{i2\pi(u'x+v'y)} dxdy \right|^2 dv' \quad 2\text{-}14$$

The intensity of point image can be described by multiplying the amplitude function and its complex form as expressed in Eq.2-10, thus:

$$L(u',v') = \quad 2\text{-}15$$
$$\int_{v'} \int_{y} \int_{x} \int_{y_1} \int_{x_1} f(x,y) f(x_1,y_1)^* e^{i2\pi(u'x+v'y)} . e^{-i2\pi(u'x_1+v'y_1)} dx_1 dy_1 dxdy\, ydv'$$

Eq.2-14 can also be written as:

$$L(u',v') = \int_{v'} \int_{y} \int_{x} \int_{y_1} \int_{x_1} f(x,y) f(x_1,y_1)^* e^{i2\pi u'x} . e^{-i2\pi u'x_1} . e^{i2\pi v'y} . \quad 2\text{-}16$$
$$e^{-i2\pi v'y_1} dx_1 dy_1 dxdydv'$$

Or:

$$L(u',v') \quad 2\text{-}17$$
$$= \int_{y} \int_{x} \int_{y1} \int_{x1} f(x,y) f(x_1,y_1)^* e^{i2\pi u'x} . e^{-i2\pi u'x_1} dx_1 dy_1 dxdy . \int_{v'} e^{i2\pi v'(y-y1)} dv'$$

From the properties of Dirac function, we can get [84]:

$$\int_{v'} e^{i2\pi v'(y-y1)} dv' = \delta(y-y1) \quad 2\text{-}18$$

Eq.2-17 can express as:

$$L(u') = \quad 2\text{-}19$$
$$\int_{y} \int_{x} \int_{x_1} f(x,y)\, e^{i2\pi u'x} . e^{-i2\pi u'x1} dx_1 dxdy \int_{y_1} f(x_1,y_1)^* \delta(y-y_1)\, dy_1$$

The convolution of the complexes form of the pupil function $f(x_1,y_1)^*$ with the Dirac function is given by the relationship [85]:

$$\int_{y_1} \delta(y - y_1).f(x_1, y_1)^* \, dy_1 = f(x_1, y)^* \qquad 2\text{-}20$$

Then, eq.2-19 is expressed as:

$$\mathrm{L}(u') \qquad 2\text{-}21$$
$$= \int_y \int_x \int_{x1} f(x, y).f(x_1, y)^*.e^{i2\pi u' x}.e^{-i2\pi u' x1} \, dx_1 dx dy$$

By assuming that $z = 2\pi u'$, eq.2-21 becomes:

$$L(z) = \int_y \left| \int_x f(x, y) e^{izx} dx \int_{x_1} f(x_1, y)^* e^{izx_1} dx_1 \right| dy \qquad 2\text{-}22$$

Or:

$$L(z) = N \int_y \left| \int_x f(x, y) e^{izx} dx \right|^2 dy \qquad 2\text{-}23$$

Where: N is the normalization factor that makes the central intensity of LSF equal to one when z = 0 for an aberration-free system. The amount of this factor depends on the shape and area of the entrance pupil.

Equation 2-22 represents the linear spread function (LSF). The pupil function in the last equation can be written as [86]:

$$f(x, y) = \tau(x, y) e^{-ikw(x,y)} \qquad 2\text{-}24$$

Where: $\tau(x, y)$ is the function permeability which represents the distribution of the real amplitude at the pupil, and it is equal to (1) of the uniform symmetric aperture, k: is the wavenumber and is equal to ($2\pi/\lambda$), λ: the wavelength of the transmitted light.

2-7-3 Bar Spread Function

In this research, the efficiency of thermal images detected in the infrared range is studied. To reach this purpose, the bar spread function BSF was investigated. This function offers information about the image that formed for the detected object. The bar object represents an ideal example of distinction and discovering vehicles, in the military. The bar object consists of a group of lines. Using the convolution theorem, complex amplitude of the bar objects image can be achieved. Subsequently, the complex amplitude of the image of a bar object can be written as [87]:

$$T(z') = \int_{-\infty}^{\infty} T(z).H(z'-z)dz \qquad 2\text{-}25$$

Where:

H (z´-z): is the complex amplitude of line object image.

T (z): is the complex amplitude of bar object image.

T (z'): is the spectrum in the image plane.

The complex amplitude of line object image is given by [87]:

$$H(z'-z) = \int_{y}\int_{x} f(x,y).e^{i(z'-z)x}.e^{-i(z'-z)y}\,dxdy \qquad 2\text{-}26$$

Where (x, y): is the coordinates of the exit pupil.

By substituting eq. 2-26 into eq. 2-25 we get:

$$T(z') = \int_{y}\int_{x} f(x,y).e^{iz'(x-y)}dxdy \int_{-\infty}^{\infty} T(z).e^{-iz(x-y)}dz \qquad 2\text{-}27$$

Where:

$$\int_{-\infty}^{\infty} T(z).e^{-iz(x-y)}dz = t(x,y) \qquad 2\text{-}28$$

Here: $t(x,y)$: is the Bar spectrum (entrance pupil of the optical system).

In the case of the bar, the width of the bar object is (2d), and then the complex amplitude is given by the following conditions:

T(Z) = 1 When $|Z| \leq d$

T(Z) = 0 When $|Z| > d$

Then, equation 2-28 becomes:

$$t(x,y) = \int_{-d}^{d} e^{-iz(x-y)} dz = 2\frac{\sin(x-y)d}{(x-y)} \qquad 2\text{-}29$$

By substituting the value of $t(x,y)$ from eq. 2-29 into the eq.2-27 we get:

$$T(z') = 2\int_{x}\int_{y} f(x,y).e^{iz`(x-y)}\frac{\sin(x-y)d}{(x-y)}dxdy \qquad 2\text{-}30$$

According to eq.2-24, the bar spread function can be expressed as:

$$T(z') = 2\int_{x}\int_{y} e^{iz'(x-y)+kw(x,y)}\frac{\sin(x-y)d}{(x-y)}dxdy \qquad 2\text{-}31$$

Or

$$T(z') = \int_x \int_y \cos(z'(x-y) + kw(x,y))\frac{\sin(x-y)d}{(x-y)}dxdy \qquad 2\text{-}32$$

If $w(x,y)$=0 for an ideal system, the last equation becomes:

$$T(z') = cos(z'(x-y)\frac{\sin(x-y)d}{(x-y)}dxdy \qquad 2\text{-}33$$

Since:

$B(z') = |T(z')|^2$, then:

$$B(z') = N\left[cos(z'(x-y)\ \frac{\sin(x-y)d}{(x-y)}dxdy\right]^2 \qquad 2\text{-}34$$

Whereas B (z'): represents the intensity of the bar image or the bar spread function.

Here: (N): is the normalized factor whose value is equal to ($\frac{1}{\pi^2}$) [88].

2-8 Different Parameters Effect on the Quality of the Thermal Imaging

2-8-1 The Effect of Linear Motion on the Thermal Imaging

The efficiency of the thermal camera depends on the image quality or detecting and recognizing the target. When objects are in motion at different speeds, the intensity distribution in the thermal imager will affected. The linear motion occurs as a disturbance in the source which can be noted in the imaging of the detected objects. As well, the distance between the thermal camera and targets affects the quality of the detected images. In both cases, the target detection in addition to tracking single and multiple moving objects are affected in a thermal video sequence. The best achievement of possible detection at different ranges and speeds provides instruction of the camera limitation in thermal imaging at various conditions. This can perform by studying the intensity distribution of BSF at different ranges and different linear motions of the detected objects. The influence of object motion on the intensity distribution in the image formed by the thermal camera is investigated in this research. By including the part of a linear motion in the bar spread function BSF, the intensity distribution of the detected images is determined and thus, the quality of detected images is determined. The linear motion factor (L) can represent as[88] :

$$L = \frac{t_e v_i}{\lambda F^{\neq}} \qquad 2\text{-}35$$

The parameters of (L) factor were initiated for moving targets at different speeds depending on the information available on the operated thermal camera. Thus, the parameters of eq. 2-35 can define as:

t_e : Is the snapshot time and for the thermal camera equal to $t_e = \frac{1}{25}\ sec.$

$F^{\neq}$: Is optical system focal number, which for the used thermal camera equal to 18.

λ: The wavelength of the incident rays. The wavelength which is detected for the used thermal camera is $\lambda = 10\mu m$.

v_i : is the image motion and can be found from the following relationship:

$\frac{v_0}{v_i} = \frac{R}{f}$ or $v_i = \frac{f v_0}{R}$

Where:

f: is the lens focal length of the thermal camera and it is equal to 36 mm.

R: is the distant of target from camera was set to:

R= (150 to 4500) m.

v_0: is the speed of the object's motion and was determined for a moving target at (40 km/h).

A- The Bar Spread Function with The Linear Motion Factor (L)

By inserting the linear motion in the BSF equation, via including the term τ(x, y) in eq. 2.24 as the linear motion, the equation of BSF becomes:

$$B(z`) = \frac{1}{\pi^2}\left[\int_x \int_y \cos(\acute{z}(x - y))\frac{\sin(x-y)d}{(x-y)}dxdy\right]^2 \frac{\sin(\pi L(x-y))}{\pi L(x-y)} \quad 2\text{-}36$$

Where:

L: is the linear motion factor and can be defined from eq. 2-35 [88].

B- The Bar Spread Function with The Range Factor (R)

$$B(z`) \qquad 2\text{-}37$$

$$= \frac{1}{\pi^2}\left[\int_x \int_y \cos(\acute{z}(x,y))\frac{\sin(x-y)d}{(x-y)}dxdy\right]^2 \frac{\sin(\pi R(x-y))}{\pi R(x-y)}$$

Where: R is the distance between the camera and the target.

2-8-2 The Effect of Attenuation Factor on the Thermal Imaging

The efficiency of a thermal imager is considered as the main objection developing target detection in military applications under bad weather conditions [89]. The effects of weather conditions (dust, fog, rain, snow) on the thermal images appear as degrade in the image intensity by several means that limit the range of the imager. The radiation propagates through the atmosphere suffers many phenomena such as absorption and scattering. Since the transmittance is estimated by using the Beer-Lambert law [37]. As a result, the total radiation that arrives at the camera is decreased. Rainfall affects the quality of images when the light is propagated through it. The rainfall changes the properties of the target such as reflectance or temperature of the surface. Detecting movement vehicles under adverse environmental conditions in dense fog were achieved by using thermal images and compared with the calculated results. An empirical expression used to calculate atmospheric attenuation as a function of wavelength and fog concentration is given by [90].

$$\tau_{S=exp\left[\left(\frac{-3.91}{V}\right)\left(\frac{\lambda}{0.55}\right)^{-q}\times R\right]} \qquad 2\text{-}38$$

Where:

λ: is the wavelength of IR, R: is the propagation range, V: is the visibility, and q is the exponent depends on the size distribution of scattering particles or the visibility. The value of q can determine as:

when the visibility range is 0.5(km) <V<1(km), the value of q=0.5, and if V is V<0.5 (km), the value of q is zero.

The visibility values (800, 700, 600, 500, 400, 300, 200) m are determined from the meteorological station in Ain al-Tamer area, Karbala city at the same time of images capture by the thermal camera (PT-602CZ HD).

2-8-3 The Effect of Different Concentrations of particulate matter PM_{10} on Thermal Imaging

In many cases, thermal imaging detects the target but not distinguished it due to various factors that influence the performance of the optical system such as ambient PM_{10}. This is a problem in the IR atmosphere transition of the radiation. In this part of the work, a study of the efficiency of the thermal imaging that detected and recognized under specific conditions (different concentrations of particulate matter PM_{10}) in the Ain Al-Tamer area of the holy city of Karbala. Mathematical calculations are used to simulate the intensity distribution in the thermal imaging of the target at different concentrations. The atmosphere transitions of infrared at wavelengths of 10 μm with different visibility ranges are calculated by considering an empirical expression of transmittance equation (2-38). The selection of the study area is considered according to many military operations that occur from time to time by terrorists; therefore, thermal imaging has a significant role in surveillance cameras in case of bad weather conditions such as dust storms. So that, providing information that is employed to monitor military targets in bad weather conditions is very important in this area of Karbala city.

Including the effect of particle concentrations are performed by inserting the absorption factor (A) into the intensity equation 2-34, thus:

$$B(z`) = \frac{1}{\pi^2}\left[\int_x \int_y \cos(\acute{z}(x-y))\frac{\sin(x-y)d}{(x-y)}dxdy\right]^2 \frac{\sin(\pi A(x-y))}{\pi A(x-y)} \quad 2\text{-}39$$

Where: A is the absorption of IR with the wavelength of 10 μm at a range (R) equal to 1 Km.

An empirical expression equation (2-38) is used to calculate atmospheric attenuation of IR (τ_S) as a function of wavelength and concentration of PM_{10}.
The values of (V) are determined by equation (2-38) [88] due to the concentration of the particulate matter PM_{10}, (10, 20, 30, 40, 50) μg/m^3, which are recorded by the meteorological station in Ain al-Tamer area, Karbala city.

$$V = 7080 \times C^{-0.8} \qquad 2\text{-}40$$

Where C is the concentration of particles [90].

Since the transmittance is estimated by using the Beer-Lambert law equal
$A = 2 - log10\%T$ [37]. 2-41
Where T is the transition, A is the absorption

Chapter Three

Properties of the Thermal Camera (FLIRPT-602CZ)

3-1 Introduction

The PT-602CZ HD is a pan/tilt thermal security camera for medium- to long-range includes a high- sensitivity thermal camera and a long-range daylight camera with an accuracy pan/tilt stand. Moreover, the PT-602CZ HD camera can be integrated into existing networks or used as a stand-alone unit. The thermal camera Properties used through the experimental work (forward-looking infrared) FLIR PT-602CZ HD, showed in figure (3-1) and figure (3-2), is a high-Performance Cooled Long-Wave Pan/Tilt Multi-Sensor thermal camera

Figure 3-1: The thermal camera Image PT-602CZ HD.

Figure 3-2: The thermal camera PT-602CZ HD which is used in the area of study.

3-2 PT-602CZ HD Thermal Camera

The PT-602CZ HD is a pan/tilt thermal security camera for medium- to long-range applications and can be used with the traditional analog video setting up or video networks. It includes a high- sensitivity thermal camera and a long-range daylight camera with an accuracy pan/tilt stand.

The PT-602CZ HD camera is equipped with a cooled detector mid-wave Infrared (MWIR) band employed. The pixel of thermal images is 640 * 512 and the product image is ultra-sharp. This detector helps the users to see the smallest detail and demand the best possible image quality.

The PT-602CZ HD has multiple sensors and is equipped with an ultra-cooled mid-wave detector that provides medium to long range detection in all weather conditions but without detection.

In addition, the thermal imaging camera presents continuous optical and electronic zoom. This zoom offers excellent situational awareness while also give the ability to zoom in at suspect activities, and has a closer look, once they are detected. Moreover, the PT-602CZ HD camera can be integrated into existing networks or used as a stand-alone unit.

Furthermore, the PT-602CZ HD thermal camera comes with a accuracy pan/tilt mechanism. It allows the user to rotate the camera 360° freely and to tilt it +90° or -90°. This property increases situational awareness. The Pan/Tilt has 128 preset positions and it is ideal when we want to scan an area continuously.

Besides, the PT-602CZ HD camera can be connected to a radar system by the integrator. If the radar detects an object, the PT-602CZ HD will turn in the right direction automatically and give a visual image so that we can instantly see what the blip on the radar screen means.

FLIR systems developed a powerful algorithm that helps to overcome the problem of determining the low contrast targets in high dynamic range scenes. Advanced Digital Detail Enhancement (ADDE) assures clear, properly contrasted thermal images. DDE provides a high-quality thermal image by delivering a high

contrast image even in extremely dynamic thermal scenes. also in any night- or daytime environmental conditions, as shown in figures (3-3) and (3-4).

Figure 3-3: The thermal image of a person in night conditions

Figure 3-4: The thermal image of a person in night conditions and the presence of fog

Not that all information in this chapter (including sections 3.2, 3.3, 3.4) has been taken from the catalog that supported by the company where the camera is produced

3-3 PT-602CZ HD Camera Characteristics

Thermal Camera parameters	**Camera Characteristic**
Array Format	640 x 512 pixels
Detector Type	Cooled Focal Plane array
Spectral Range	8~14μm
Effective Resolution	327,680
Field Of View	14x continuous optical zoom WFOV: 28° x 22.4° NFOV: 2° x 1.6°
Optical zoom	Continuously Adjustable
Focus Range	Autofocus or manual focus
Thermal Frame Rate	25 Hz
Lens diameter	2mm
focal length	36mm
Focal Number	18mm
Pan/Tilt Performance	
Pan Angle / Speed	Continuous 360°; to 60°/sec
Tilt Angle / Speed	+90° to -90°; to 30°/sec
Weight	18.5kg
Camera Size (L x W x H)	348* 467*326 (mm)
Input Voltage	24 VDC (21-30 VDC) 24 VAC (21-30 VAC)
Power Consumption	24 VAC: 70VA (max w/o heaters); 260 VA (max w/heaters) 24 VDC: 60 W (max w/o heaters); 203 W (max w/heaters)

3-4 Detection Range of PT-602CZ HD Thermal Cameras

Detection of actual object performance may vary depending on camera set-up, environmental conditions, user experience, and type of display use, and the range of the detection. All specifications are subject to change to get a high-quality thermal image. The actual range camera detection ranges from 3000 m to 3300 m.

3-5 Focal Length of PT-602CZ HD Thermal Camera

Each lens has a focal length, which means the distance between the external lens and the sensor inside the camera. So, the greater the distance between the lens and the sensor, the greater the approximation. Which is measured in millimeters (mm)? One of the fixed rules in the focal length is that the relationship between it and the angle of view is an inverse relationship. The focal length of the PT-602CZ HD Thermal Camera is 36 mm [91].

3-6 Focal Number of PT-602CZ HD Thermal Camera

Focal Number is the focal length divided by the diameter of the lens. All lenses have a maximum and a minimum aperture. Therefore the focal number of the PT-602CZ HD Thermal Camera is 18[92].

3-7 The Zoom of PT-602CZ HD Thermal Camera

The area of the image changes only by the zoom which was shown on the display and not the focal length of the lens. there are two types of zoom.

Digital zoom: - It is processing the image digitally from inside the camera itself, and the image is distended, not through the lens, as the zoom here is not real.

Optical Zoom: - Optical Zoom is done by using a series of lens elements, whereby glass elements are moved inside or outside the lens to zoom in or out. Optical zoom is considered the best type of approximation (zoom) because it gives real and clear results with the least possible losses in terms of accuracy.

3-8 Thermal Imaging in the Work Area

A-In The Presence of a Linear Motion Factor

During the experimental work, the 17-11-2020 at 8:00 PM is the date and time of using FLIR PT-602CZ HD thermal camera to capture thermal images of a moving target (vehicle) at a speed of 40 Km/h .In order to compare with the intensity distribution in the image which is calculated theoretically under the same conditions by using BSF method .Also, the intensity distribution of thermal images and experimental thermal images are investigated at different ranges, due to the importance of detection estimation and the ability to recognize a target at a given range in military applications. . The distribution of the intensity in the thermal image is calculated at different target speeds (40,60,80,100,120) Km / h and in practice, the thermal images of a moving target at different ranges and a speed of 40 Km / h are determined, only 40 Km/h speed of moving target considered in experimental part because of the nature of the earth in the area of the study.

B- In The Presence of the Fog Factor

The 19/12/2020 at 5:00 AM is the date and time of performing the second step of the experimental part, thermal images of the target (car) were captured by the PT-602CZ HD camera in the work area. The Ain Al-Tamer area at a specific concentration of fog. The vehicle is considered as a target at different ranges (200, 300, 400, 500, 600, 700, and 800) m in the case of 400 m visibility Also, the concentration of fog and the visibility range were considered from the meteorological station in the Ain Al-Tamer to calculate the theoretical results and compare with the thermal images captured by the thermal camera.

Chapter Four

Results and Discussion

4-1 Introduction

This chapter includes the results obtained from solving the equation of the bar spread function for the diffraction-limited optical system. Effects of different parameters have been taken into accounts, such as the linear motion of detected objects. The range between the camera and objects, and the attenuation of images caused by bad weather conditions like fog or dusty weather. All calculations were performed for infrared radiation of wavelengths (5-10) μm. The effects of such parameters (different ranges, speeds, and concentrations of particles) are included in the equation of BSF, as discussed in chapter two. In addition, the comparison with the experimental results (thermal images), which was obtained using the thermal camera (PT-602CZ HD) in the study area at different times and dates, was performed in detail this chapter.

4-2 The Influence of the Range Factor on the Thermal Image

The thermal imager is affected by many factors such as properties of the camera, environment conditions, range of detection, and characterization of the detected object. In this section. The intensity distribution of an object is calculated at different ranges by programing the BSF equation (2-37).using the Mathcad program. By including different. The effect of the range on the image quality is fulfilled. In order to apply this study on the thermal camera under investigation, the characterization of the thermal camera is also involved in the BSF equation.

Figure (4-1) illustrates the intensity distribution of the object images at different ranges. The range strongly affects the central peak intensity values. In addition, the distribution of intensity in the image area is changed. From the figure, it is clear that the intensity in the image plane at the range of approximately 0.5 Km (red curve) has similar behavior with the case when the object is very close to the thermal camera (R=0) (black curve). However, the peak intensity value of the BSF, when the object is at the range of 0.5 Km, has a reduction comparing to the case with a very close

distance between the thermal camera and the object. Likewise, the behavior of the intensity curve at R= 1 Km (green curve) still behaves the same intensity distribution. Therefore, we can judge from the previous three cases that the object is detected and recognized at the range of less than 1 Km. One can observe the decrease in the intensity value of the central peak when the range is (1.5 and 2) Km. As well as, the shapes of these curves (blue and cyan) are different and start to lose the shape and characteristic of the central peak intensity, which expresses the image quality. Thus. The object only can be detected at these ranges. In other cases, at ranges (2.5,3,3.5,4) Km, (pink, yellow, mossy, dark blue curves). In such cases, the intensity distribution appears as a surface and, there is no clear central peak of the intensity. According to that, the object cannot be detected and recognized at these ranges.

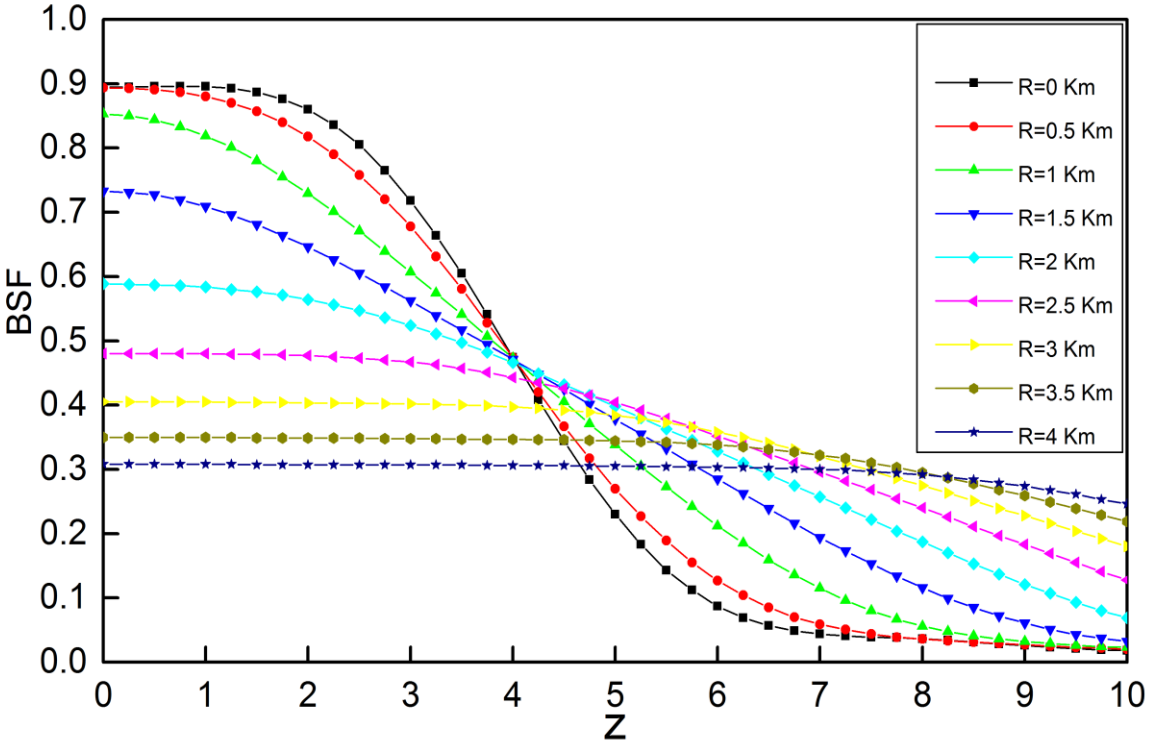

Figure 4-1: The intensity distribution in the thermal image at different ranges.

4-3 Effect of Linear Motion Factor on the Image

The effect of object motion on the intensity distribution of an image detected by the thermal camera (PT-602CZ HD) is determined by calculating the linear motion factor with different values on the detected objects. This can be performed by including the linear motion factor in the BSF equation (2-36). By solving the BSF equation using the Mathcad program and including the characteristics of a thermal camera are (PT-602CZ HD) in the BSF equation, the calculated intensity distribution of the thermal image is compared with the thermal image. Throughout experimental work, the thermal camera (PT-602CZ HD) was used on 17-11-2020 at 8:00 pm at the Kerbala city border to capture images at specific conditions. These conditions are taken as a reference to compare the detected images with the calculated intensity distribution at the same conditions.

The BSF linear motion effect is calculated for different values and presented in figures from (4-2) to (4-16). Since all the parameters, included in the BSF equation are constant only the image motion is affected Thus, the intensity distribution of the thermal image depends on object speed. The object speed are (0, 40, 60, 80, 100, and 120) Km/h. The intensity distribution of the thermal image is calculated at different ranges. (150 to 4500) m. In practical the thermal images are calculated for the moving target at different ranges and only velocity of 40 Km/h due to the nature of the earth at the place where the research fulfilled.

Figures (4-2) (a) and (b) show the intensity distribution of the thermal image with different speeds and the thermal image of a car target both of them are detected at a range of R=150 m, respectively. There is evidence that the reduction of intensity increased as the target speed the increased because of the increment in the image motion. The high-intensity values are (0.89, 0.86. 0.81, 0.73, 0.65) when the object speeds are (0, 40, 60, 80, 100, 120) Km/h, respectively. The thermal image in figure 4-2 (b) can be compared to the red curve in the central intensity of BSF in figure 4-2 (a). Moreover, the detection and recognization of a vehicle object are possible for the

thermal image of a vehicle object at a linear speed of 40 Km/hour. As a result, targets in this range (150 m) can be detected and distinguished by the thermal camera.

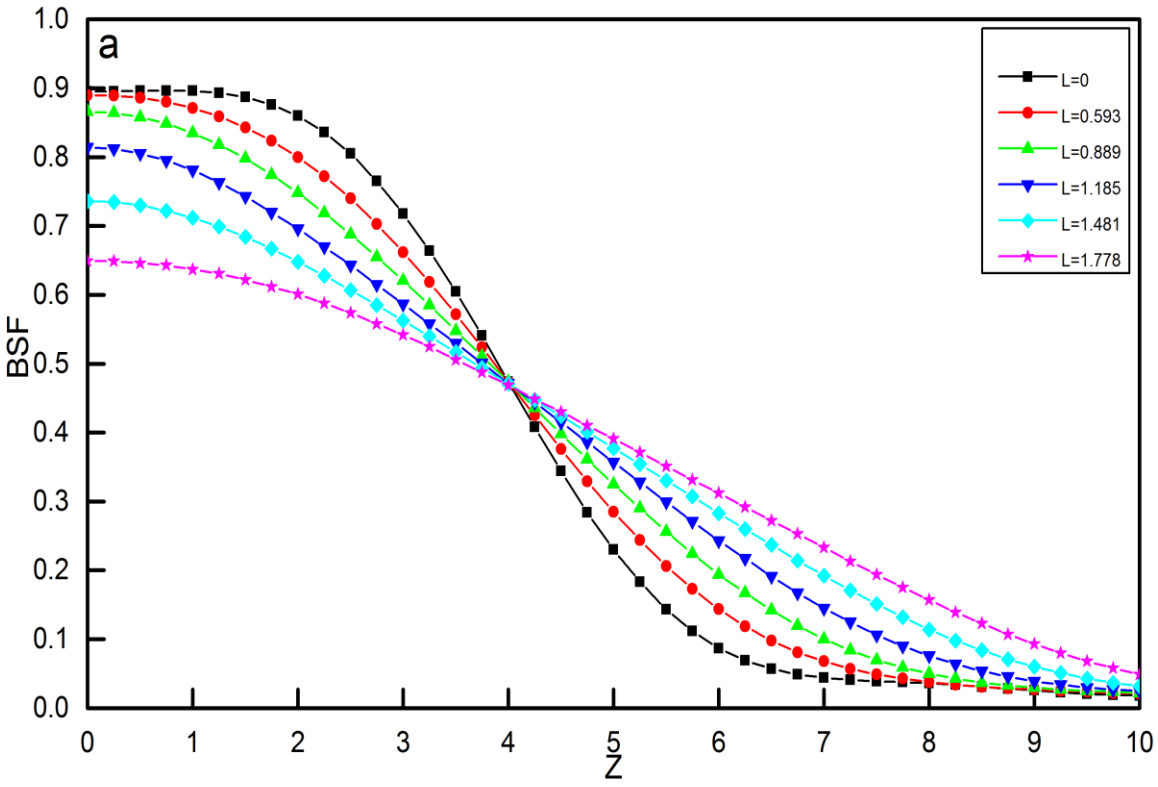

Figure 4-2: (a): The intensity distribution in the BSF at R= 150 m

Figure 4-2: (b):The thermal image of a car object at R =150 m.

In figure 4-3 (a and b), the results show the same behavior as in figure 4-2 (a and b) .But at low resolution. In this case, the intensity distribution in the central peak of BSF is changed .The linear motion effects become less on the intensity distribution. The detection and recognition of moving objects are still possible. This is concluded from comparing the detected thermal imager at the same range, as shown in figure 4-3 (b).

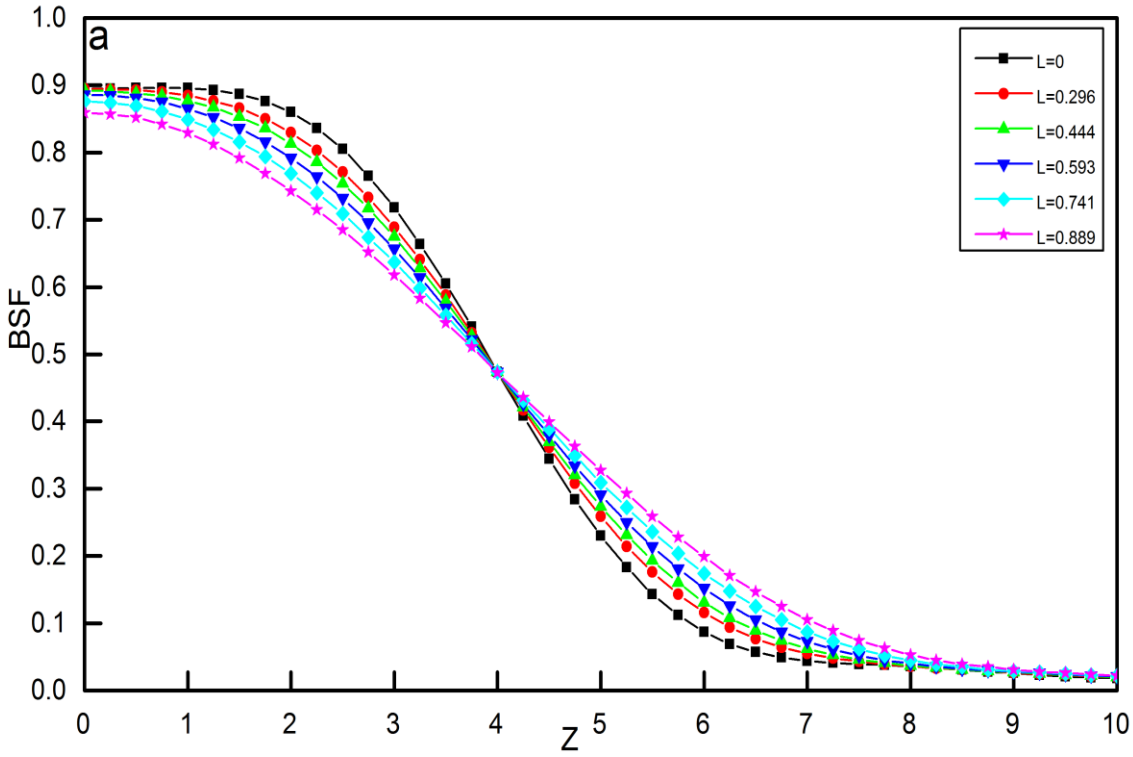

Figure 4- 3: (a): The intensity distribution in the BSF at R= 300 m, (b): The thermal image of a car object at R =300 m.

Figures 4-4 (a) and 4-5 (a) illustrate the image intensity distribution of Bar objects at the range of 500 m and 750 m, respectively. When the range of the target becomes more than 500 m, the values of image motion are decreased, and the value of the linear motion factor becomes small. Therefore, the intensity distribution in the image does not affect it. In such a case, only the distance between targets and the thermal camera has impacts on the clarification of the thermal image. Thus distribution shape of BSF leads to the conclusion that targets can only detecedt and not be recognized. This behavior results clearly in the thermal images captured by the thermal camera at the ranges 500 m and 750 m, respectively ,as shown in figures 4-4 (b) and 4-5 (b), respectively.

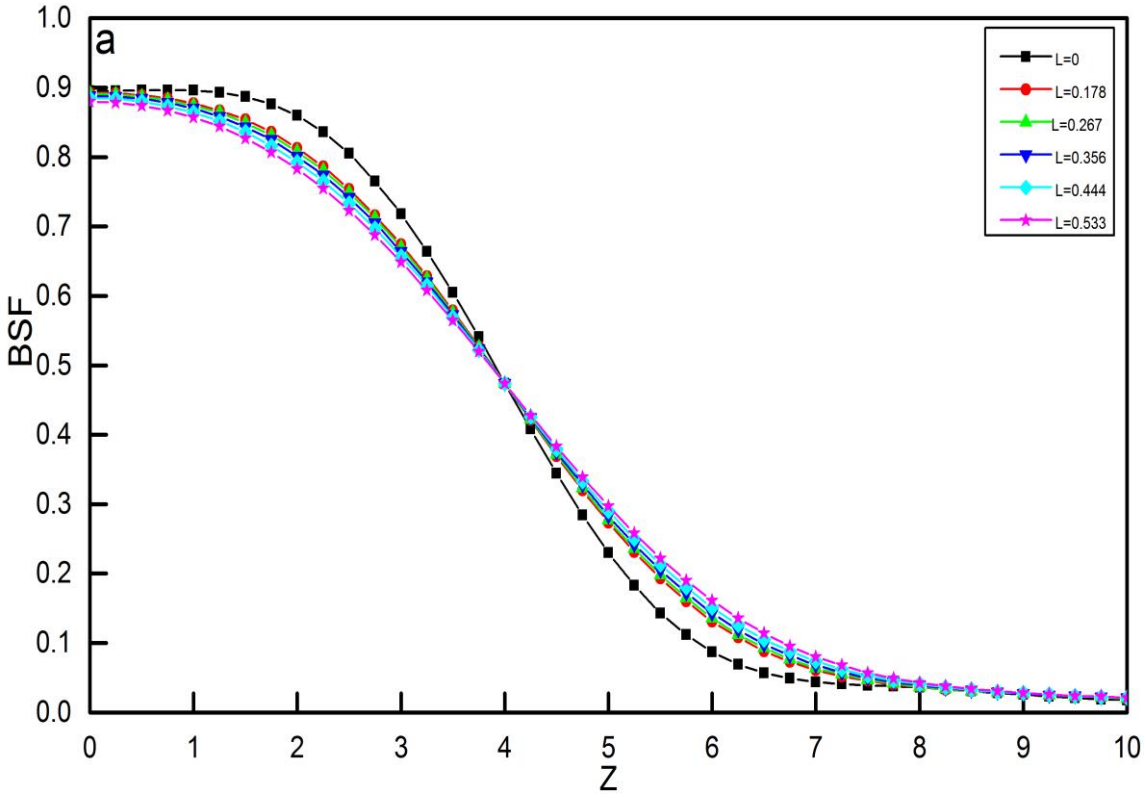

Figure 4- 4: (a): The intensity distribution in the BSF at R= 500 m, (b): The thermal image of a car object at R =500 m.

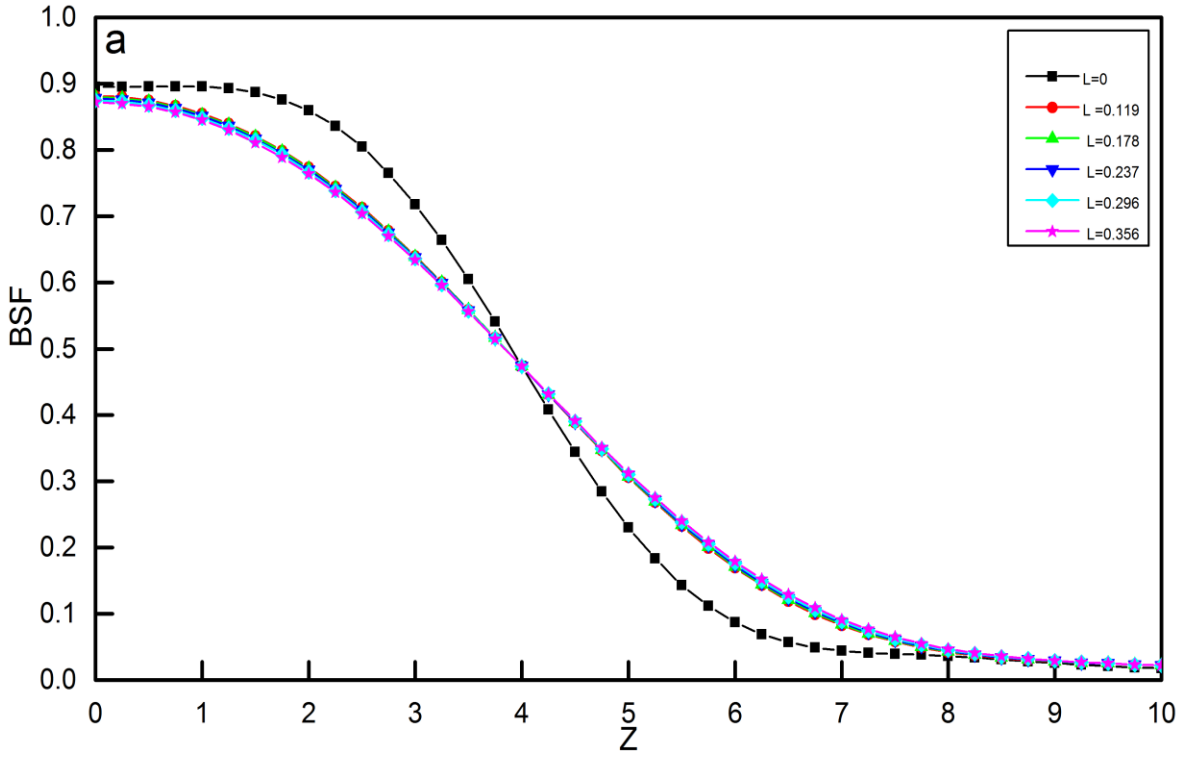

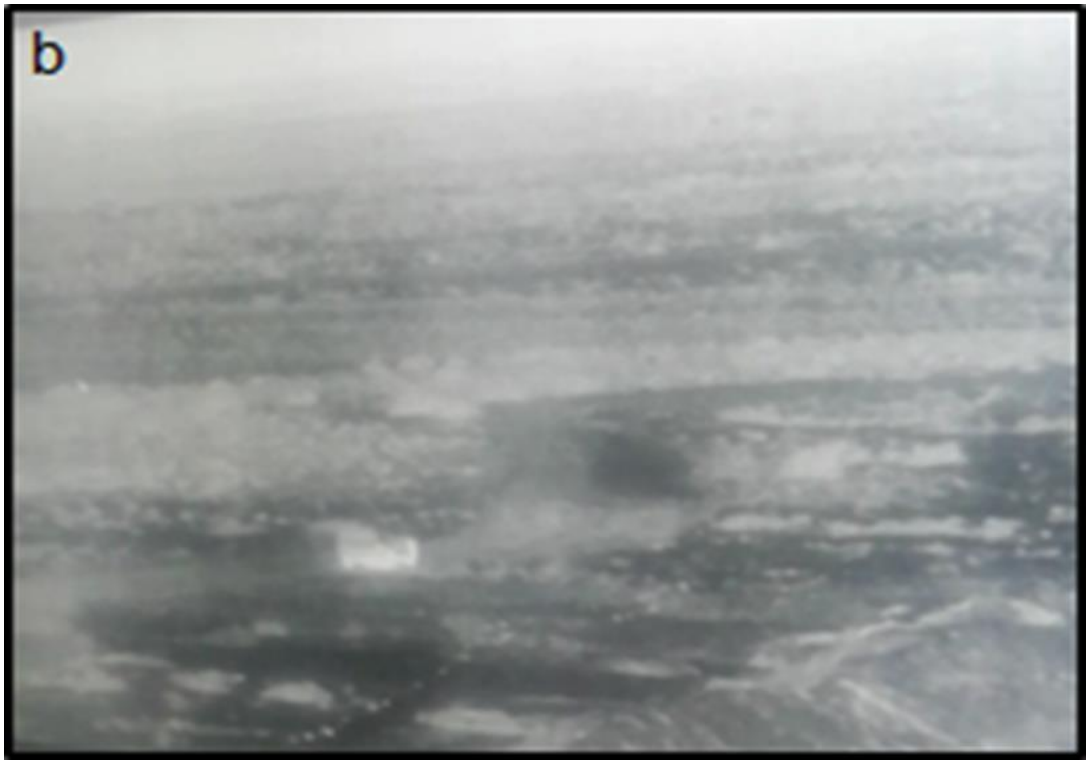

Figure 4- 5: (a): The intensity distribution in the BSF at R= 750 m, (b): The thermal image of a car object at R =750 m.

Figures 4- 6 (a, b) and 4- 7 (a, b) show the intensity distribution in the BSF and thermal images of vehicle objects captured by the thermal camera at the range of 1250 m and 1500 m, respectively. From the BSF curves, It's clear that the intensity distribution of the central peaks is distorted and becomes less value and wider. Such behavior leads to a decrease in the resolution and increases the distortion in the captured images. This is clear in the captured images that appearing blurring in both cases and thus, the target does not detect or recognize.

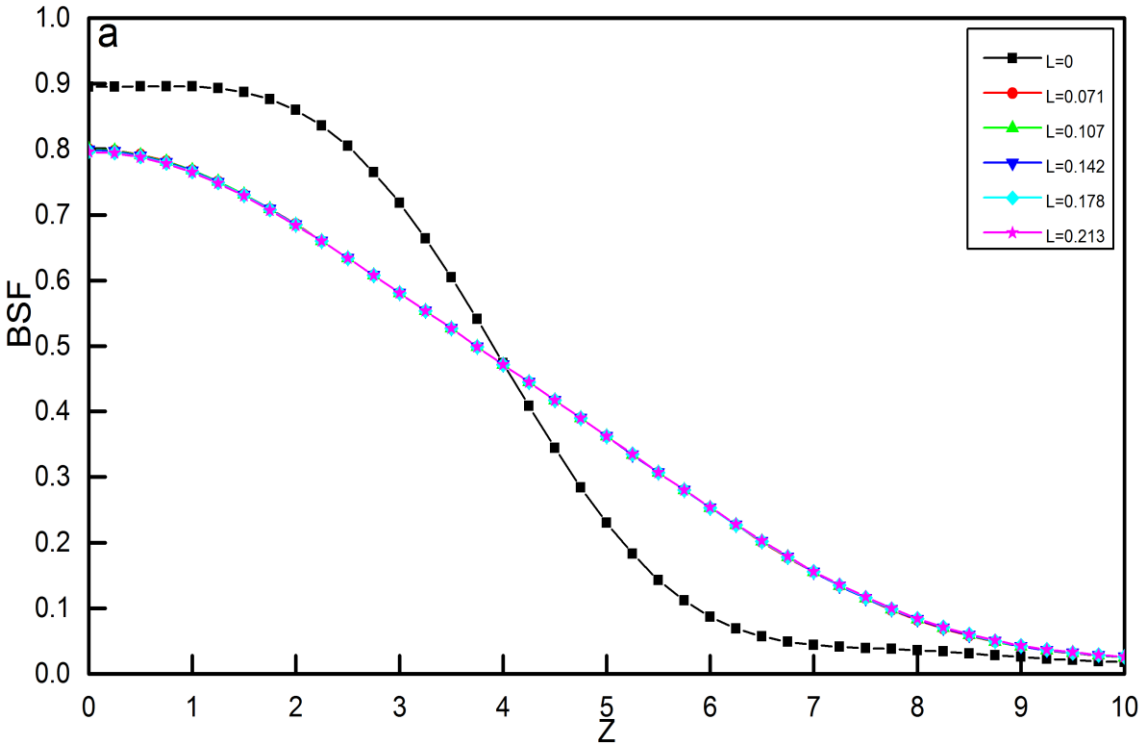

Figure 4-6: (a): The intensity distribution in the BSF at R= 1250 m, (b): The thermal image of a vehicle object at R =1250 m.

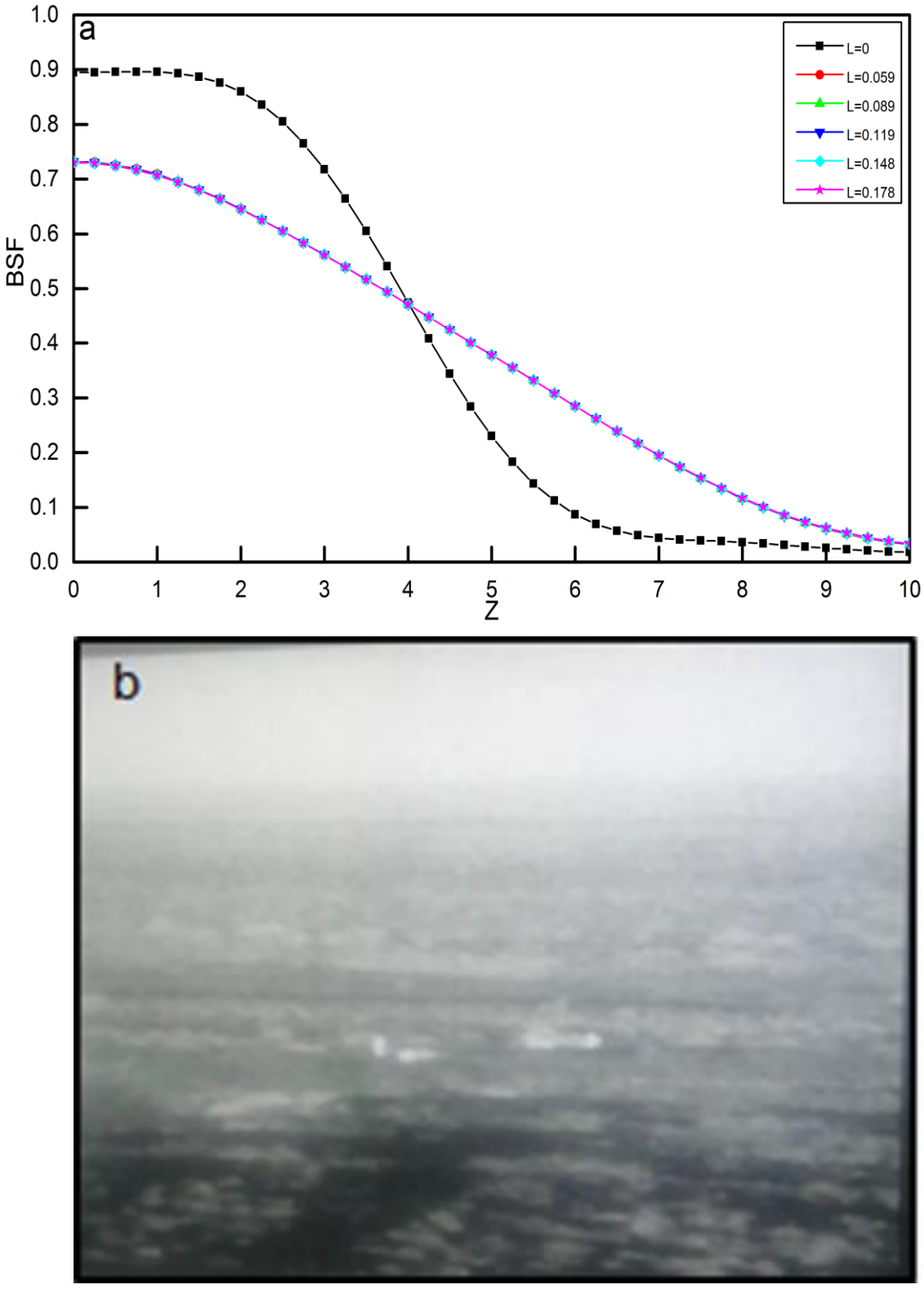

Figure 4- 7: (a): The intensity distribution in the BSF at R= 1500 m, (b): The thermal image of a car object at R =1500 m.

It is clear from figures (4-8, 4-9, 4-10) that the intensity distribution and the thermal images have the same behavior as shown in figures (4-6,4-7) but at low visibility due to the increase in the range to (2000, 2500, 3000) m, respectively. Due to the decrease of intensity in the central curves of BSF, as shown in figures (4-8, 4-9, 4-10) (a), the captured images become less resolution and more blurring, as shown in figures (4-8, 4-9, 4-10) (b).

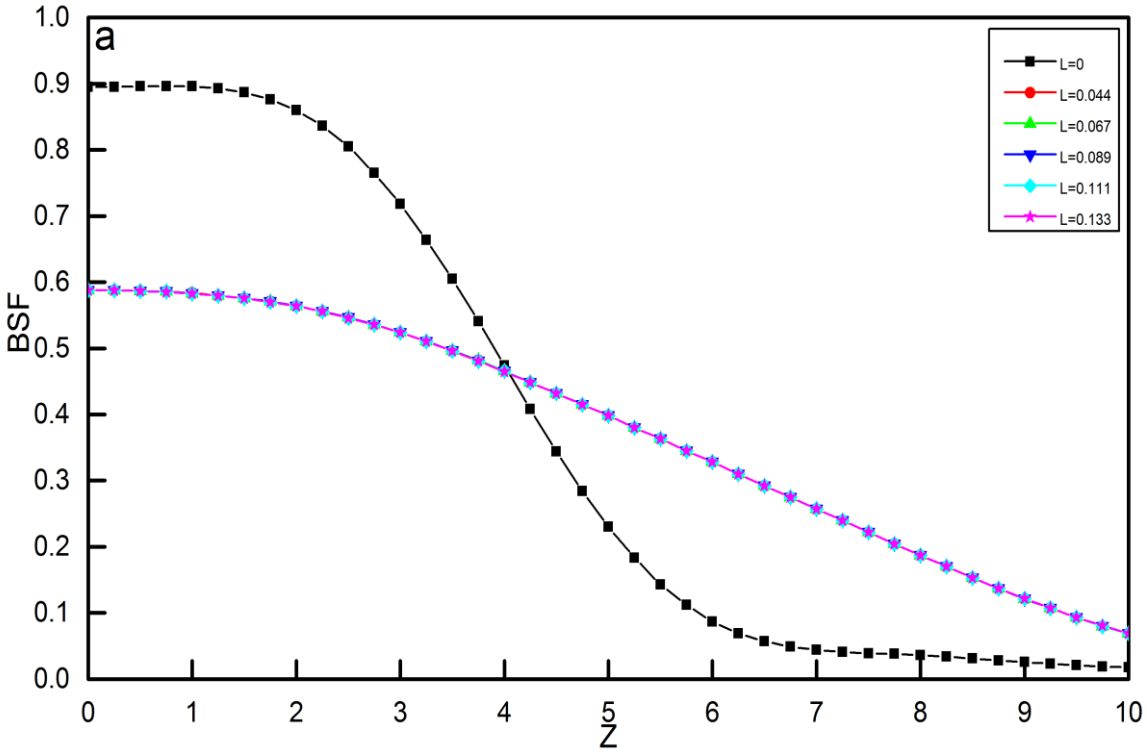

Figure: 4- 8: (a): The intensity distribution in the BSF at R= 2000 m, (b): The thermal image of a car object at R =2000 m.

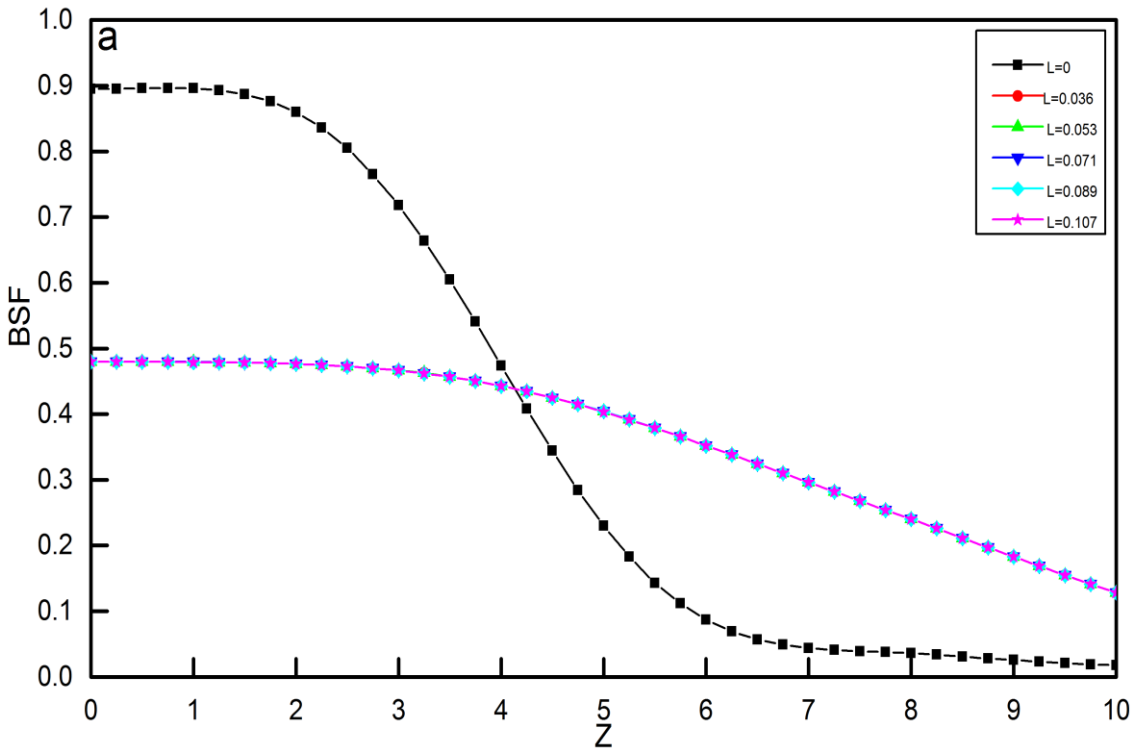

Figure 4-9: (a): The intensity distribution in the BSF at R= 2500 m, (b): The thermal image of a car object at R =2500 m.

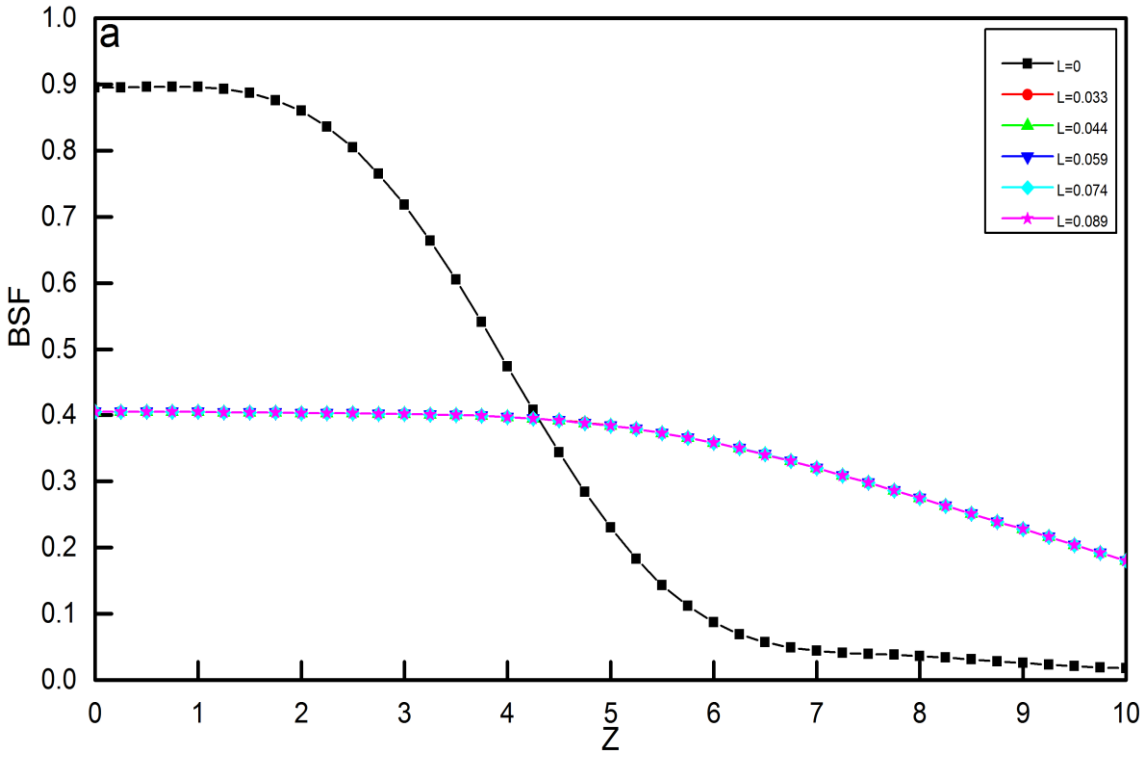

Figure 4- 10: (a): The intensity distribution in the BSF at R= 3000 m, (b): The thermal image of a vehicle at R =3000 m.

Figures (4-11, 4-12, 4-13, 4-14, 4-15) illustrated the intensity distribution in the BSF and the thermal image captured by the thermal camera (PT-602CZ HD) at the range of at (3500, 3750, 4000, 4250, 4500) m, respectively. It is clear from the curves of BSF, which are presented in the figures (4-11, 4-12, 4-13, 4-14, 4-15) (a), that the intensity of the central peaks has a low value and the width of the curve become larger. This implies that there is no clear objects that can be detected by the thermal camera can detect. Moreover, all images, which are shown in the figures (4-11, 4-12, 4-13, 4-14, 4-15) (b) vanish completely at long ranges. These results show that the thermal camera (PT-602CZ HD) has a short-range detection of approximately 3000 m. After this range, as shown in the figures (4-11, 4-12, 4-13, 4-14, 4-15) (b), the thermal camera (PT-602CZ HD) is useless for detecting moving objects. From all measured images by the thermal camera (PT-602CZ HD) and calculated from the equation of BSF, it is clear that there is a good agreement between the theoretical

results (intensity distribution in bar spread function) and the experimental results (thermal images). The value of the highest intensity of the central peak of BSF reaches 0.5. The thermal image becomes blurred and the target was not recognized. In addition, the intensity of the BSF is independent of the linear motion when the distance between the thermal camera and object is more than 500 m. Therefore, the effect of the linear motion at the long distances becomes very small and the detection of the objects depends completely on the distance between the thermal camera and the selected object.

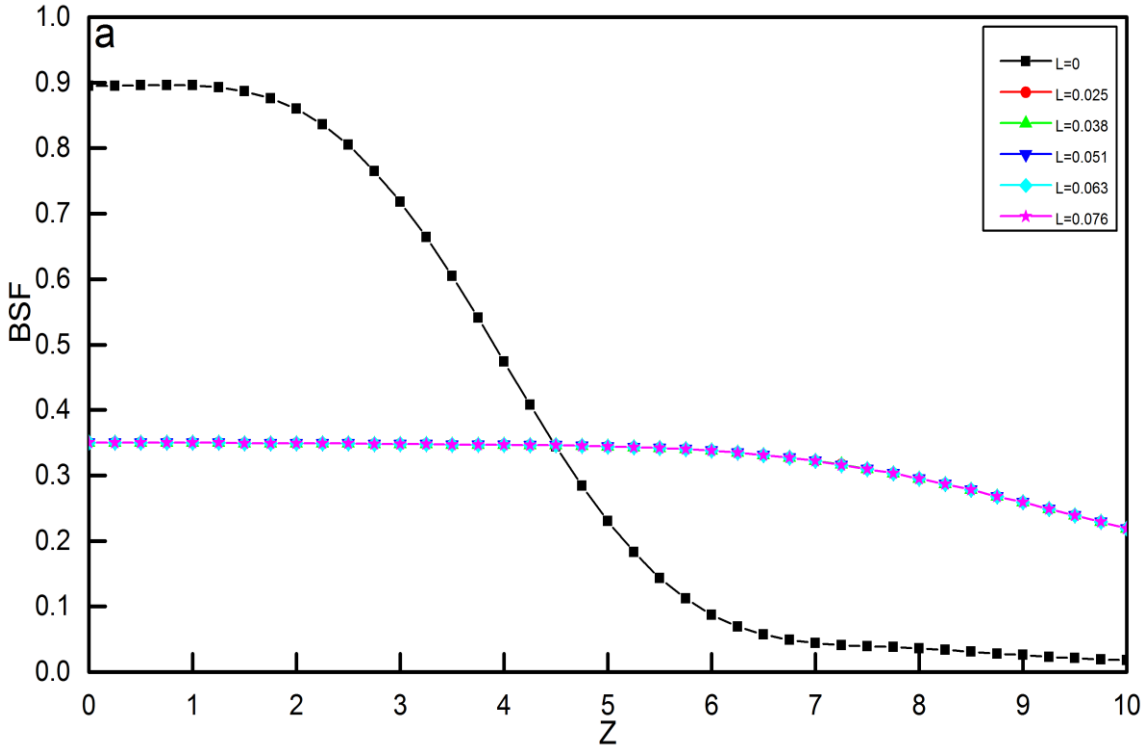

Figure 4-11: (a): The intensity distribution in BSF at R= 3500 m, (b): The thermal image of a car object at R =3500m.

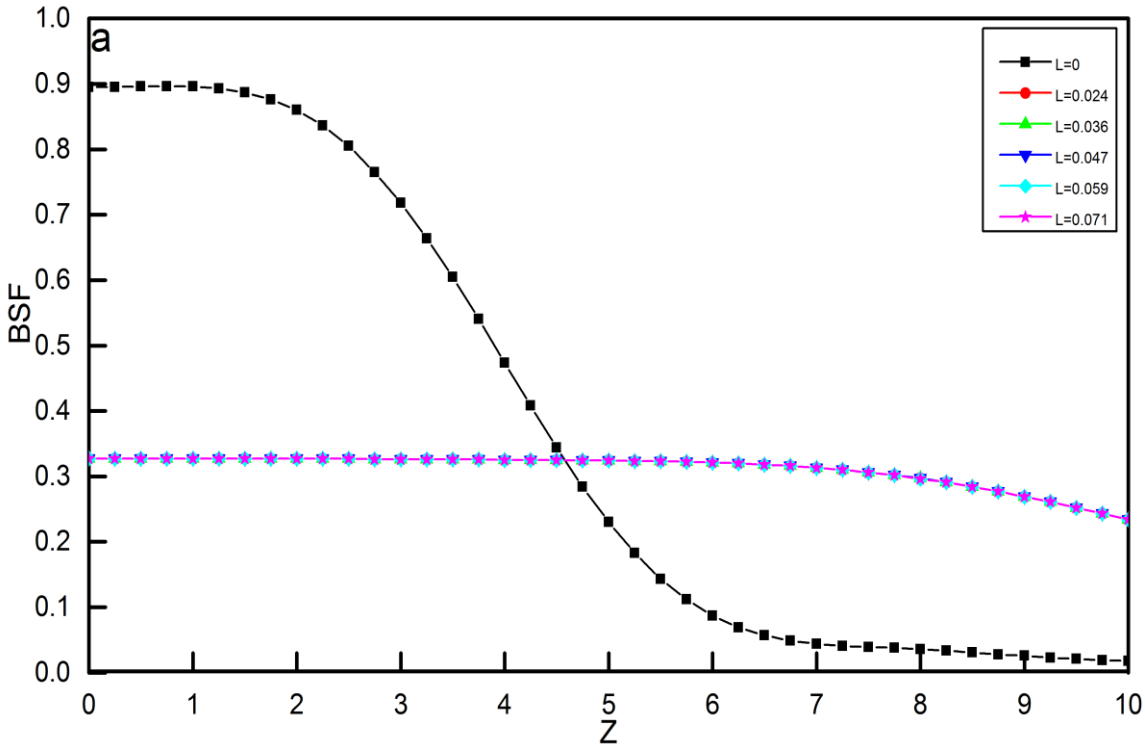

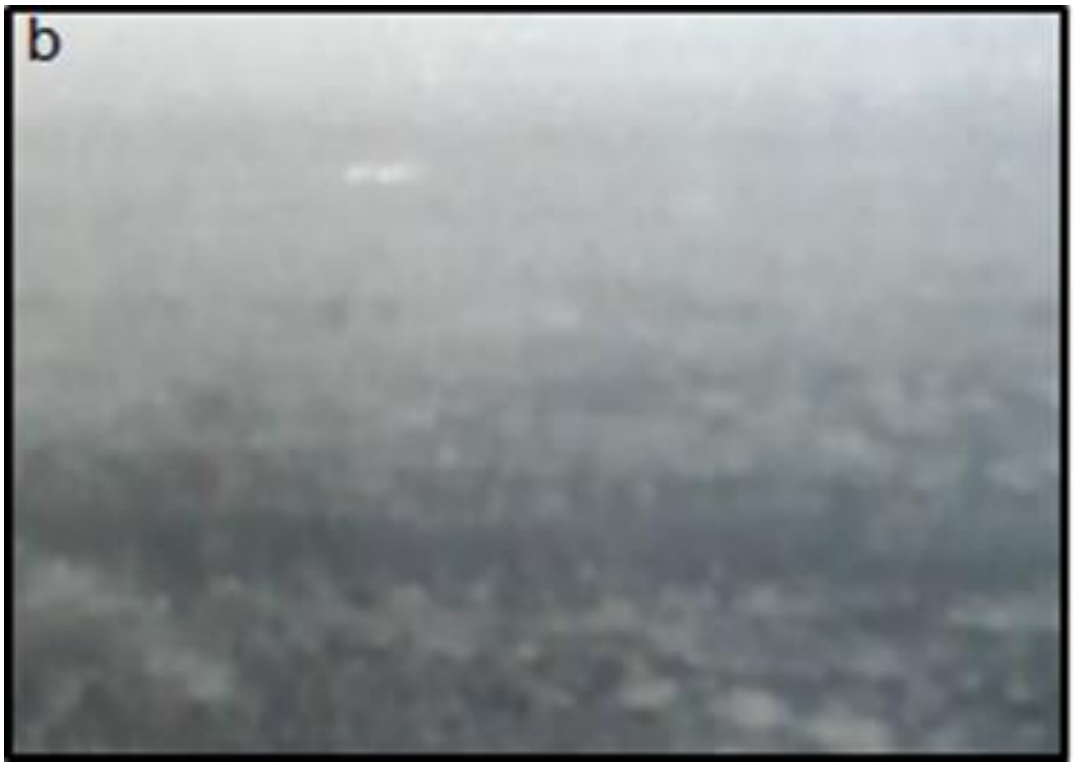

Figure 4-12: (a): The intensity distribution in the BSF at R=3750 m, (b): The thermal image of a car object at R=3750m.

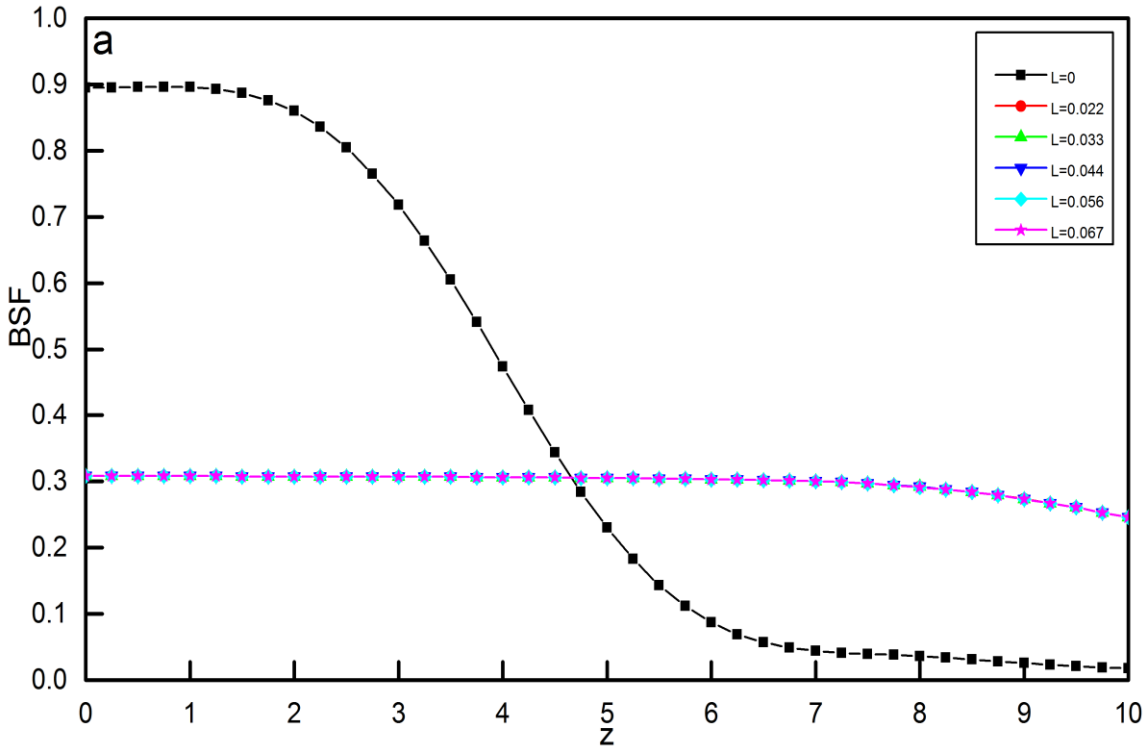

Figure 4-13: (a): The intensity distribution in the BSF at R= 4000 m, (b): The thermal image of a car object at R =4000 m.

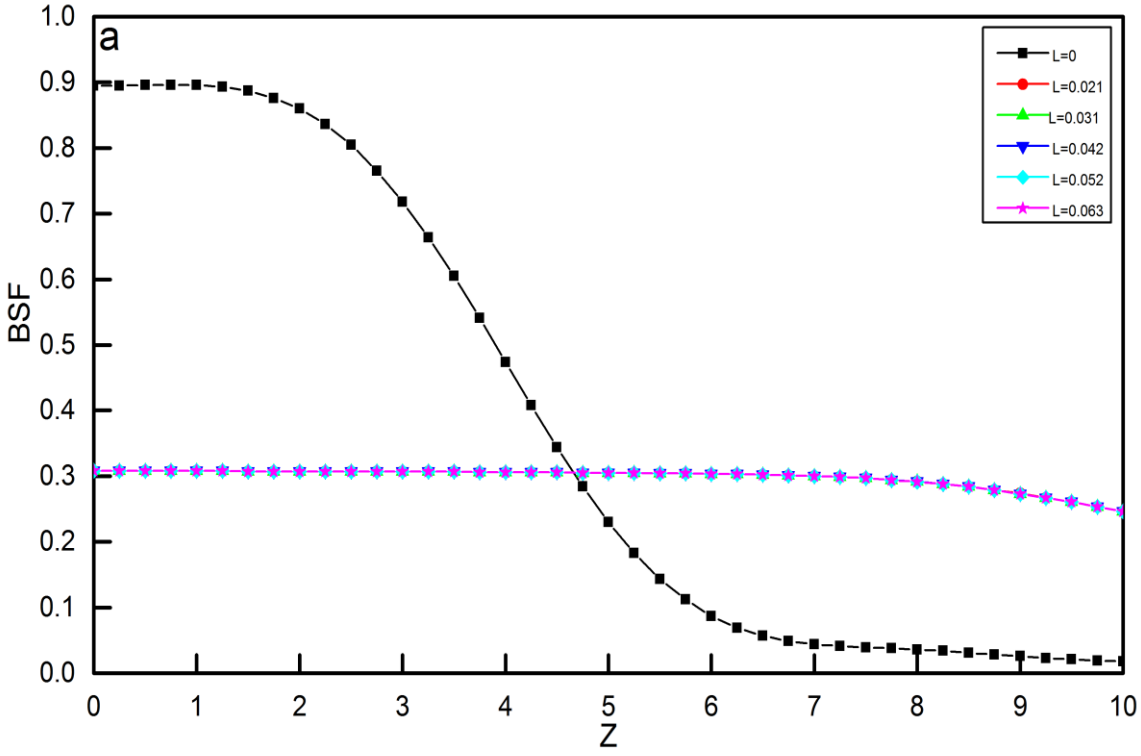

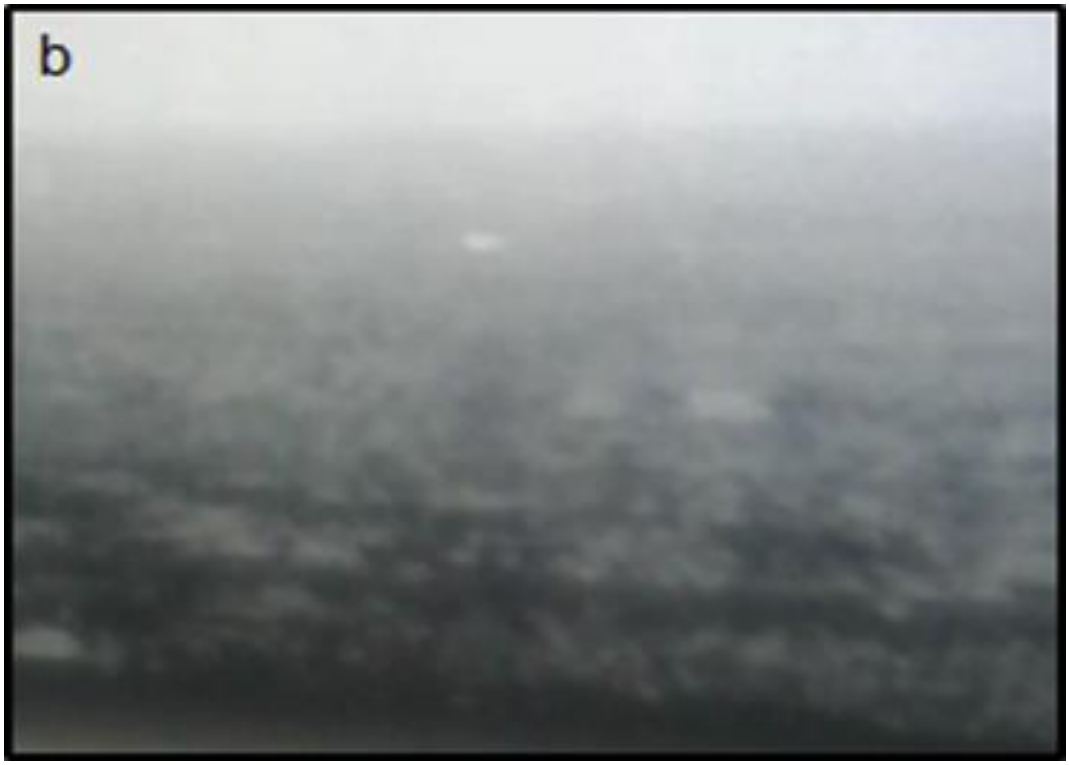

Figure 4-14: (a): The intensity distribution in the BSF at R= 4250 m, (b): The thermal image of a car object at R =4250 m.

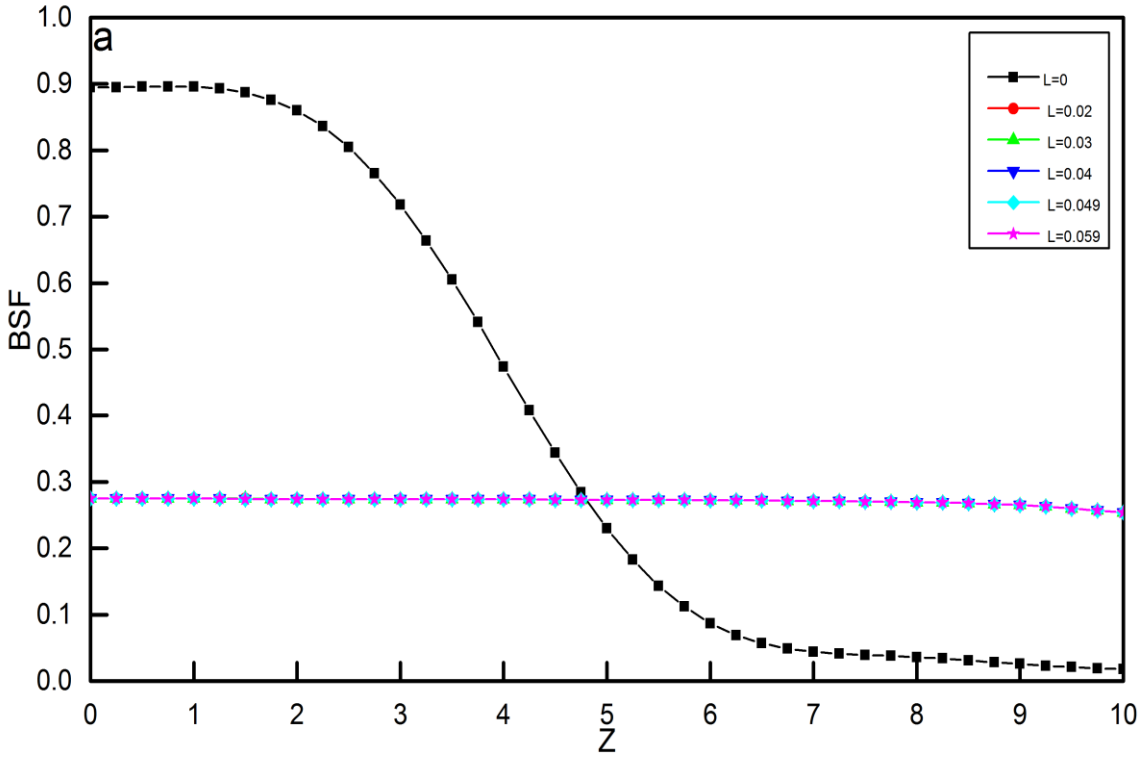

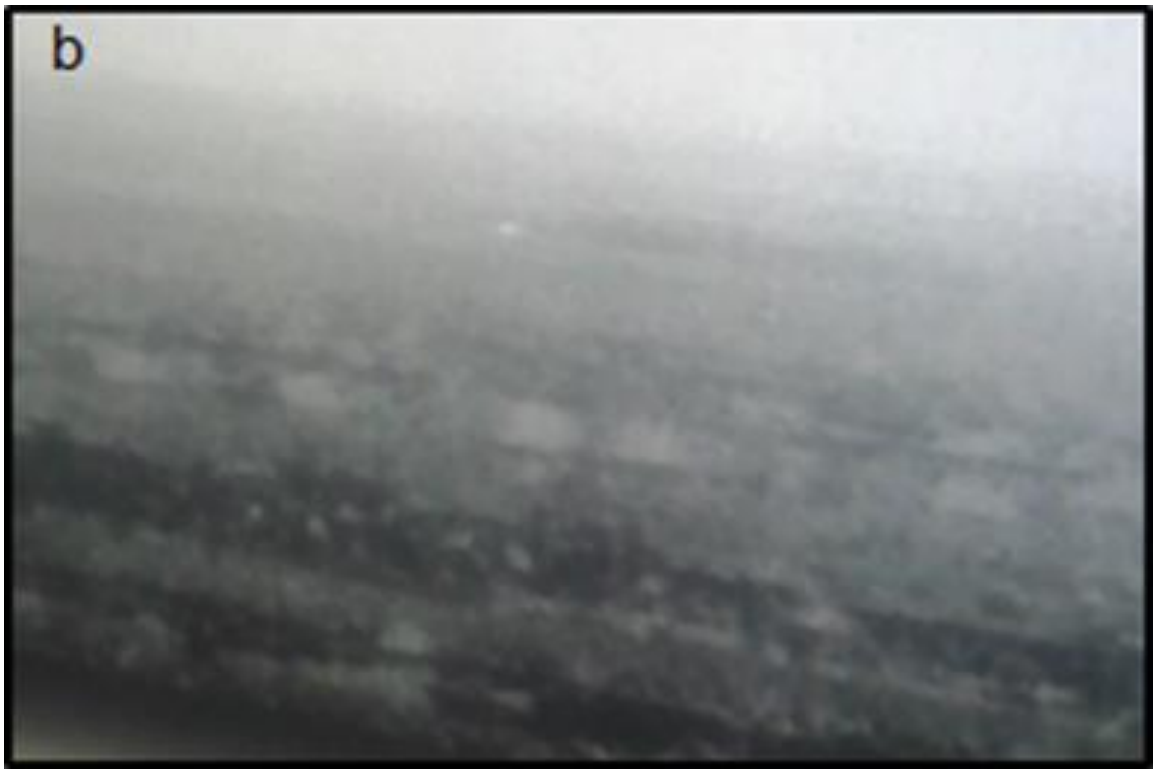

Figure 4-15: (a): The intensity distribution in the BSF at R= 4500 m, (b): The thermal image of a car object at R =4500 m.

4-4 The Effect of Attenuation on the Image

Bad weather influences the performance of the thermal camera, where the detection of the target is possible, but without distinguishing it. In this section, the efficiency of the thermal camera in detecting and recognizing targets is investigated via studying the atmospheric transmittance of IR in different values of visibility due to various fog concentrations. This work is applied in the Ain Al-Tamer area of the holy city of Karbala. The atmospheric effects are acquired by solving equation (2-38) to simulate the intensity distribution in the thermal image of the target at different ranges. The atmosphere transitions of infrared with wavelengths (5 and 10) μm with different visibility ranges are calculated by considering an empirical expression of transmittance. A thermal camera (PT-602CZ HD) is used to capture thermal images at various ranges (0.2,0.3,0.4,0.5) Km with 10 μm of focal length and a visibility range of 400 m in the same area of the study.

Figure 4-16 shows the transition of IR radiation (10 and 5) μm in the atmosphere in case visibility range is 200 m in the Ain Al-Tamer area. It is clear that the value of the transition approach is approximately zero because of the high fog of concentration and thus the visibility (V) is weak. Therefore, thermal imaging is impossible in this condition.

Figure (4-17) and (4-18) show the same behavior of atmosphere transition of IR radiation (10 and 5) μm that it is happening in fig (4-16). I these two cases, one can observe that the transition increased slowly due to the increase of visibility ranges to (300 and 400) m, respectively.

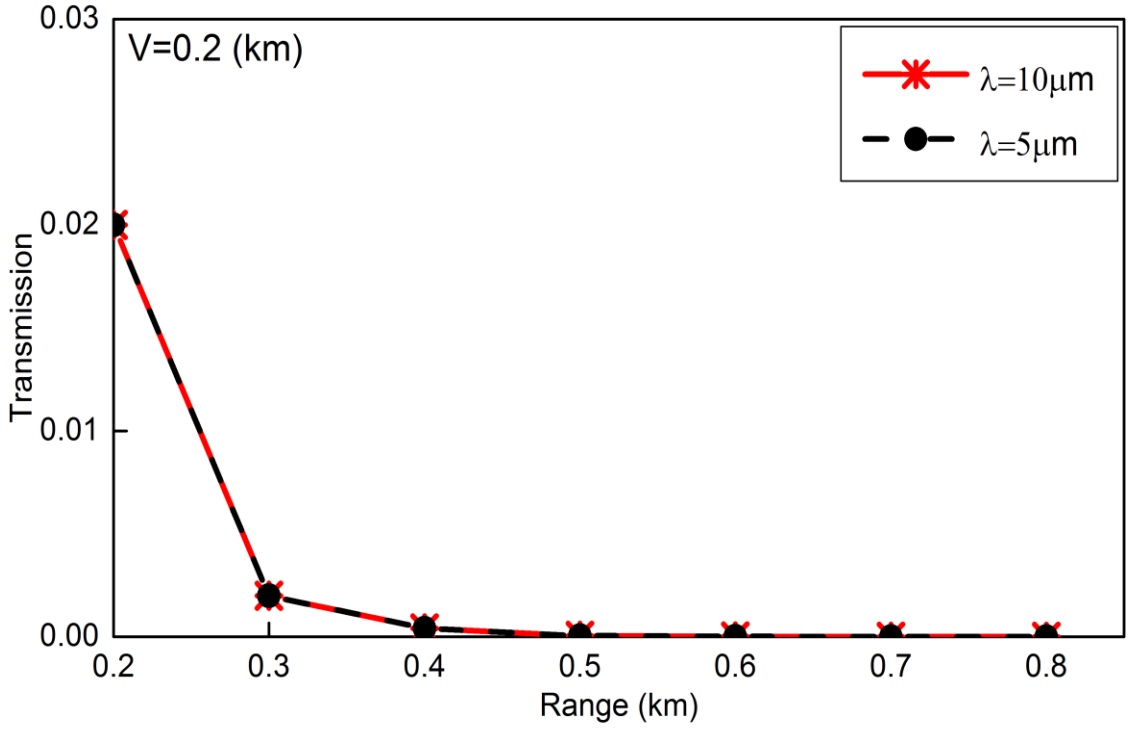

Figure 4-16: The atmosphere transition of IR radiation at V = 0.2 Km.

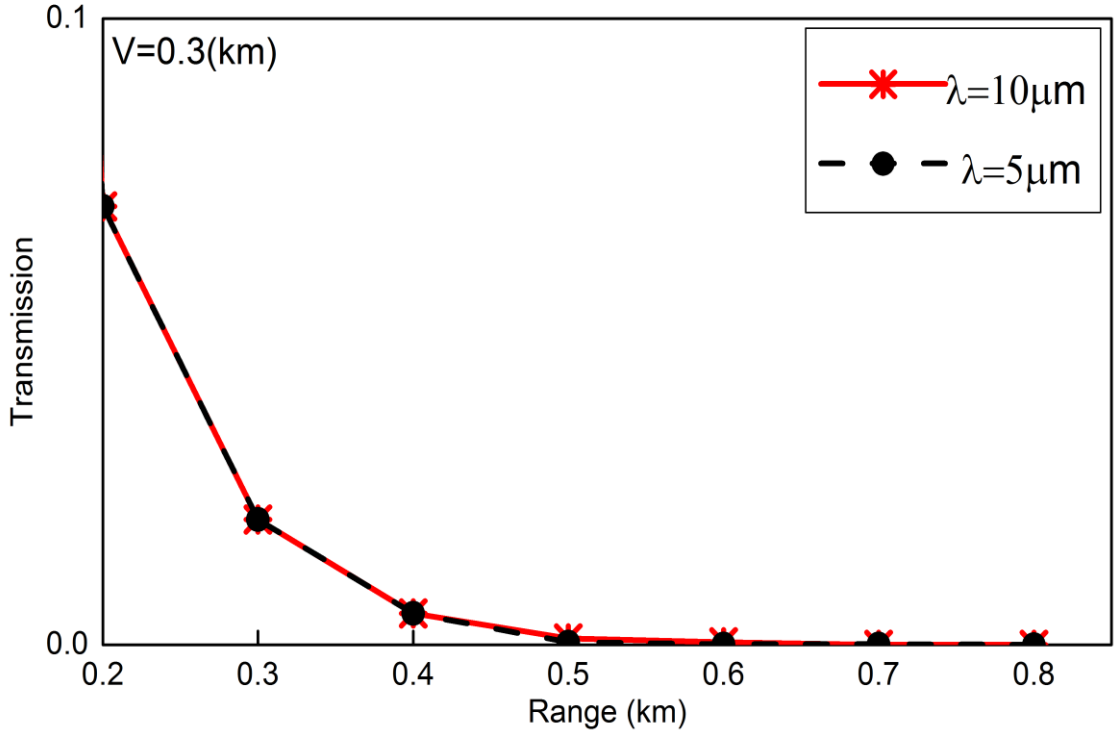

Figure 4-17: The atmosphere transition of IR radiation at V = 0.3 Km.

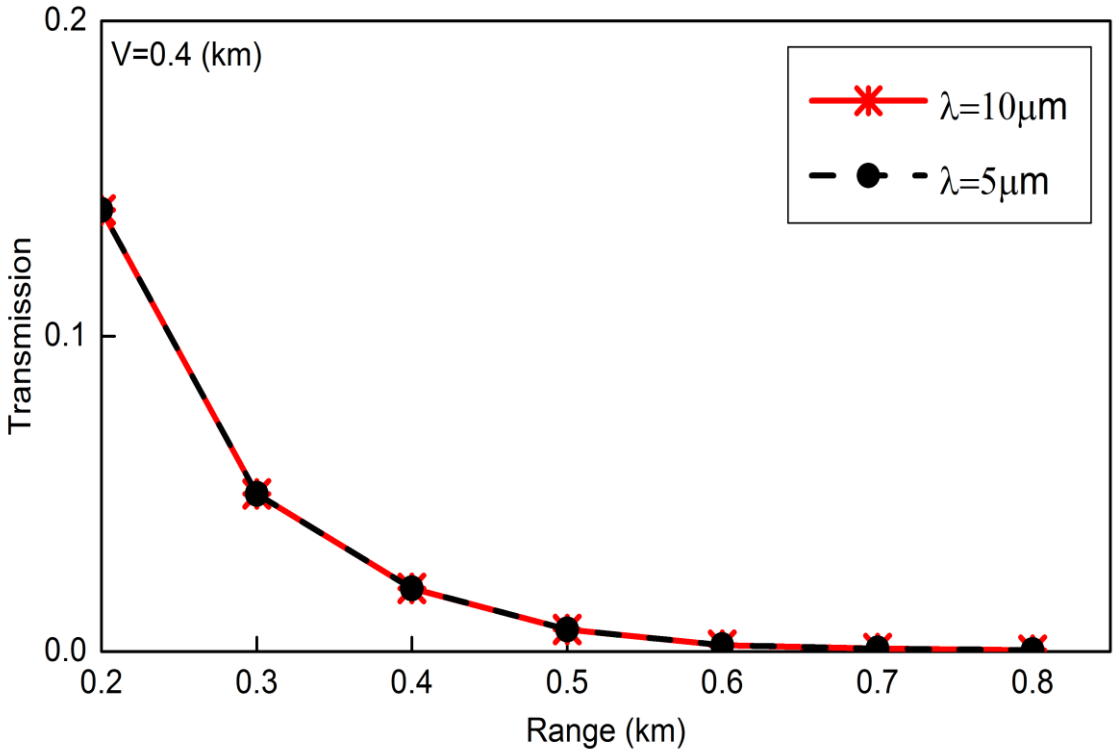

Figure 4-18: The atmosphere transition of IR radiation at V = 0.4 Km.

Figure (4-16, 4-17, 4-18) show the atmosphere transition of IR (5 and10) μm as increase V (200, 300, 400,) m. It is clear that the transition has a small value (0.1-0.2).This value does not present a good condition to make an image by a thermal camera. Since the detection and recognition of targets depend on IR emitted from targets and its transmission through the atmosphere. Therefore, the detection and recognizing of the object is impossible for the previous cases.

In figures (4-19, 4-20, 4-21, 4-22), the atmosphere transition of IR radiation (5 and 10) μm is increased as V increased due to the reduction in fog concentration. The transition has large values (0.7-0.8) for 10 μm at close range (the distance of the object from the camera), while the values of the transition decrease at the far range. The thermal image is clear at near range (0.2-0.4) but it is a blur in far range (0.5-0.8).

From the results obtained in this section, one can consider that the object can be detected at the near range although there is an absorption of IR radiation which is caused by fog. The atmosphere transition of 5 μm IR radiation is similar to the

atmosphere transition of 10 μm in the behavior but it has less values. The atmosphere transition at 10 μm is better than 5 μm under these conditions because high transitions are obtained.

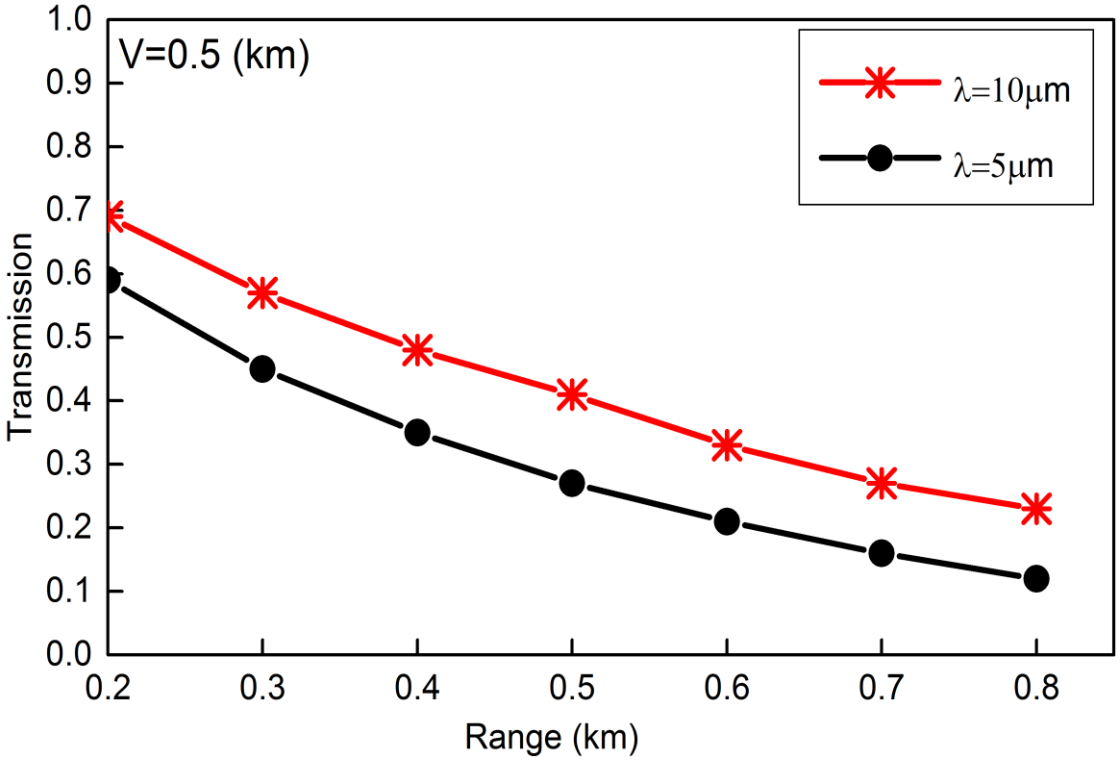

Figure 4-19: The atmosphere transition of IR radiation at V = 0.5 Km.

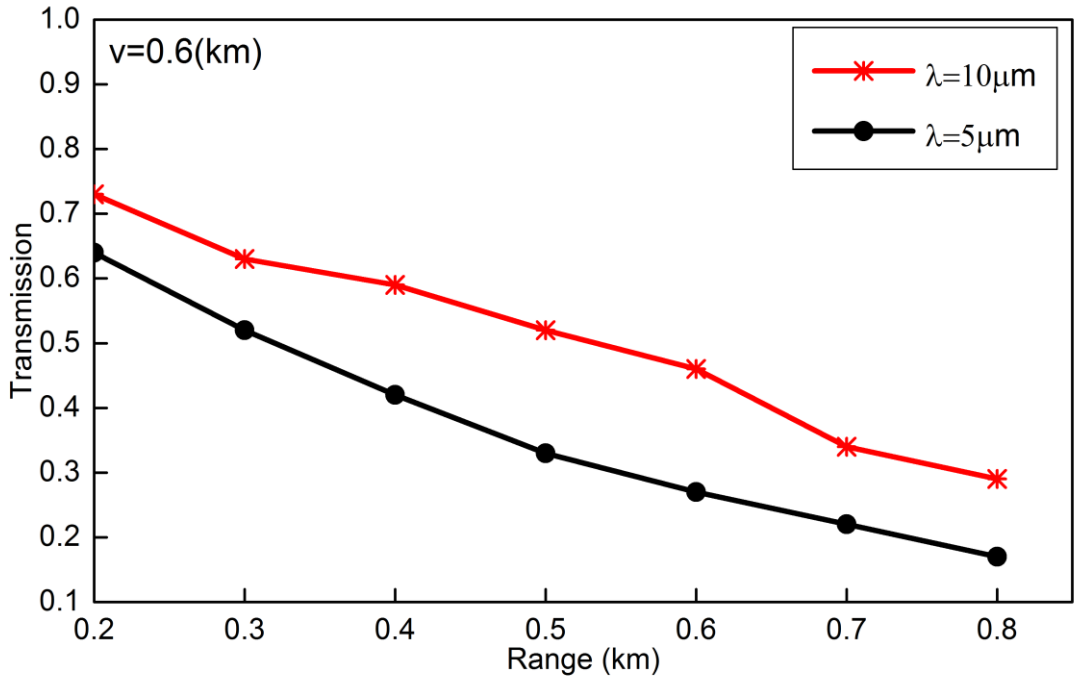

Figure 4-20: The atmosphere transition of IR radiation at V = 0.6 Km.

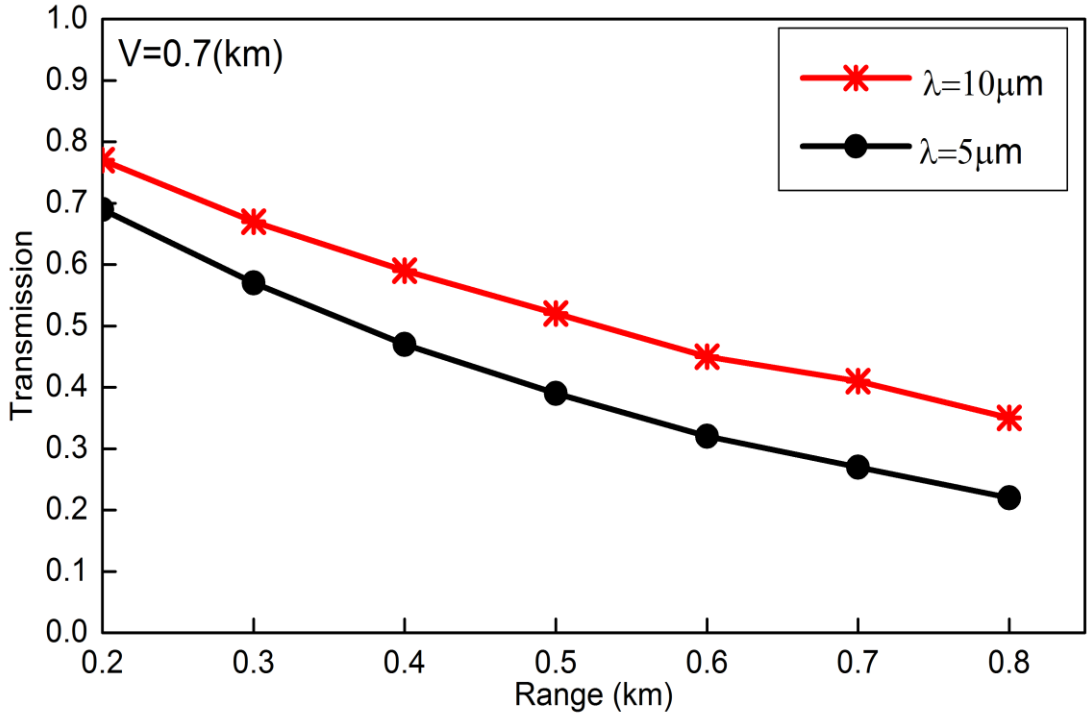

Figure 4-21: The atmosphere transition of IR radiation at V = 0.7 Km.

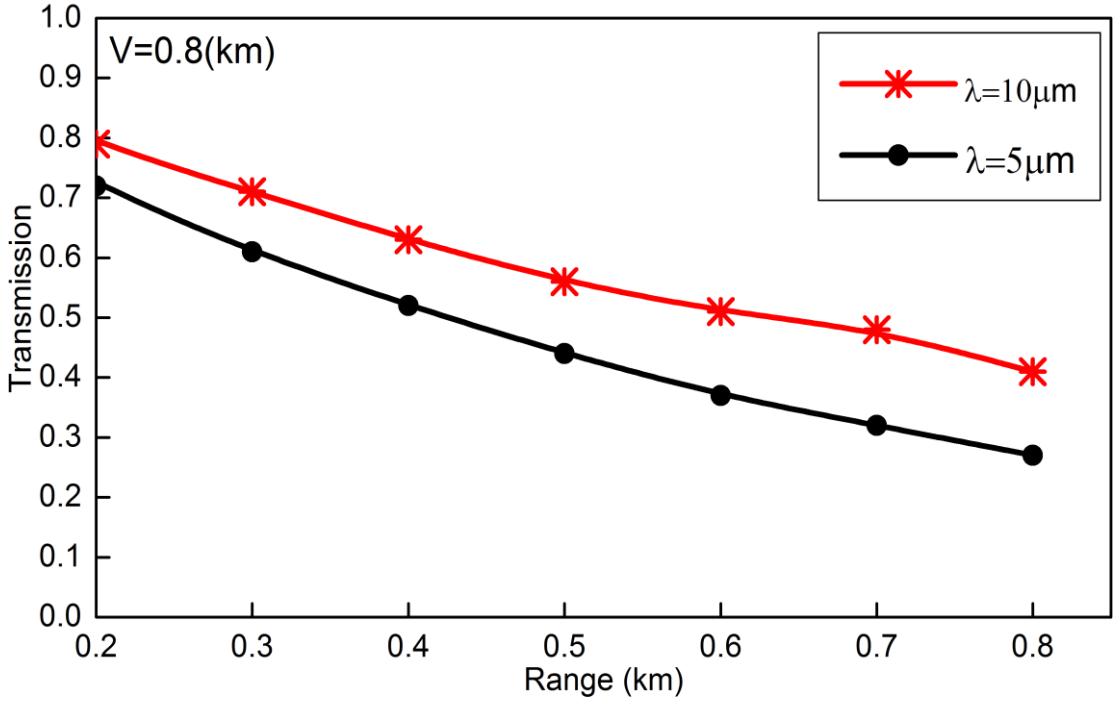

Figure 4-22: The atmosphere transition of IR radiation at V = 0.8 Km.

Figures (4-23, 4-24, 4-25, 4-26) illustrate the thermal images of the target (vehicle) captured at date (19/12/ 2020) in the Ain Al-Tamer area of the holy city of Karbala. The vehicle is considered a target at different ranges (200, 300, 400, 500) m in case the visibility is 400 m. Figure (4-23) shows the image of the target by the thermal camera ((PT-602CZ HD) at R =0.2 km and V=400 m. It is clear from the figure that the image is not completely clear (foggy image) and the target is detected only but not recognition. Images presented in figures (4-24, 4-25, 4-26) are also a blur and the target does not detect and recognition because of increasing the range to (300, 400, 500) m, respectively. The transition of IR radiation, in the last, showed three cases, decreases, and thus, thermal imaging is impossible. From all results (theoretically and experimentally), the experimental results in figures (4-23, 4-24, 4-25, and 4-26) are in good agreement with the theoretical results in figure (4-18).

Figure 4-23: Thermal image of vehicle at R =0.2 km and V=400 m.

Figure 4-24: Thermal image of vehicle at R=0.3 km and V=400m.

Figure 4-25: Thermal image of vehicle at R=0.4 Km and V=400 m.

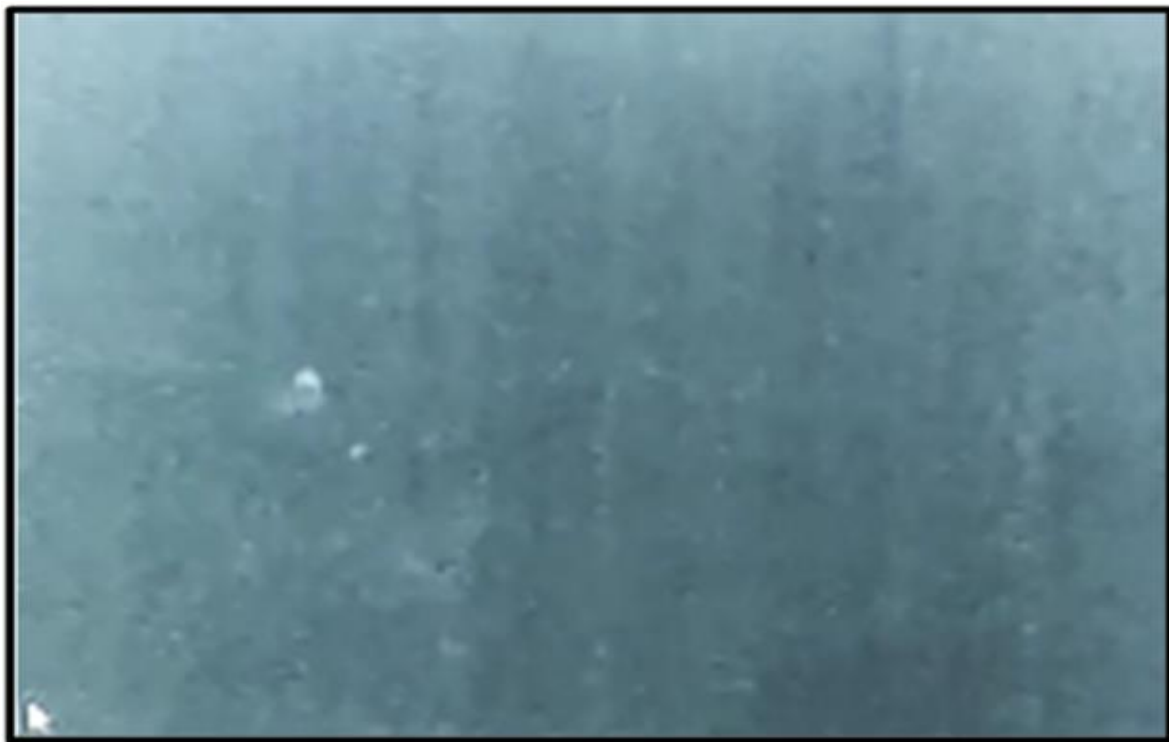

Figure 4-26: Thermal image of vehicle at R=0.5 km and V=400 m.

4-5 The Effect of Different PM_{10} Particle Concentrations on Thermal Imaging

The performance of the optical system such as the thermal imaging system is suffering from ambient particulate matter $PM_{10.}$ This problem appears on the IR atmosphere transition of the radiation where the thermal system cannot distinguish targets and sometimes cannot detect them. The study in this section aims to investigate the efficiency of thermal imaging in detecting and recognizing the target under specific conditions (different concentrations of particulate matter PM_{10}) in the Ain Al-Tamer area of Karbala city. Here, the object of the intensity distribution is calculated at different particulate matter PM_{10} concentrations by programing the BSF equation using Mathcad software. The Atmospheric Transmission of the Infrared Radiations (ATIR) with wavelengths 10 μm is also determined in different values of visibility due to various PM_{10} concentrations. This determination is performed

wavelengths of 10 μm of IR radiation are adopted in this case. The calculations were achieved by considering an empirical expression of transmittance in equation (2-38). The selection of the study area is considered according to many military operations that occur from time to time by terrorists .Therefore thermal imaging has a significant role in surveillance cameras in case of bad weather conditions such as dust storms and to update and display the information of targets in the monitor in bad weather conditions.

Figure 4-27 illustrates the visibility range due to different concentrations of particulate matter PM_{10}. The range of visibility depends strongly on the concentration values of, where its values begin from 1.1 Km at 10 $\mu g/m^3$ and become 0.35 Km at 42 $\mu g/m^3$. It is clear that the visibility is close to zero in case of a high concentration of PM_{10}, especially when the concentration exceeded the standard values 123 $\mu g/m^3$

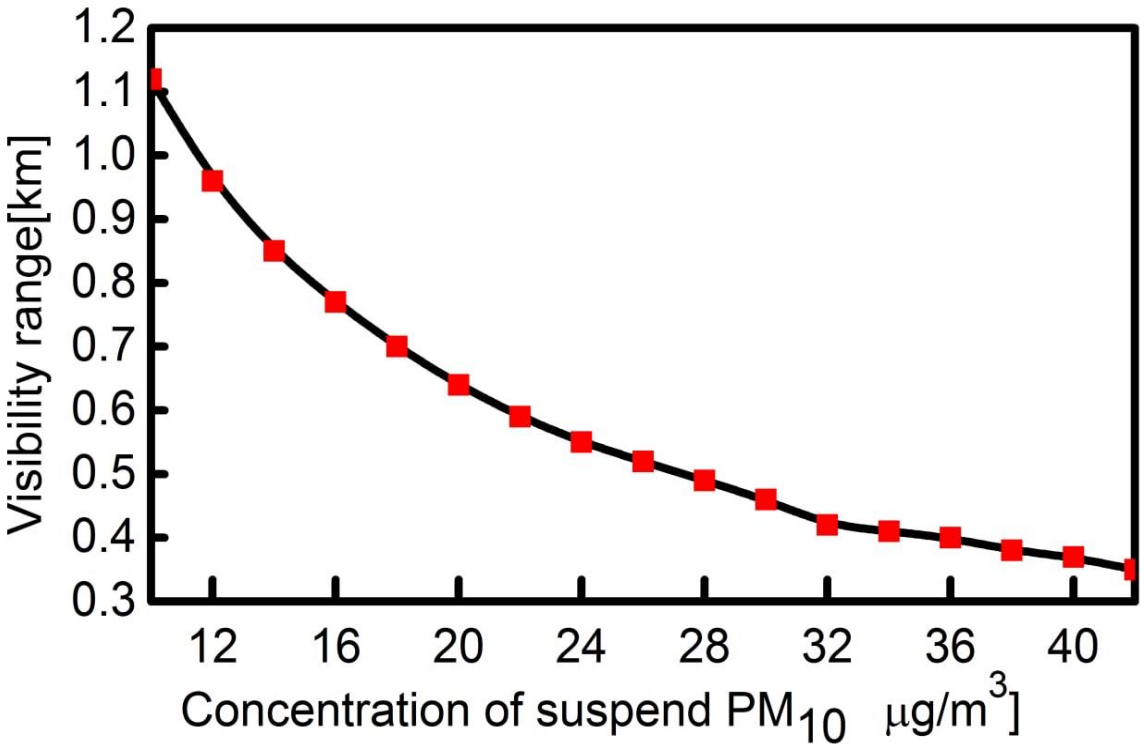

Figure 4-27: The visibility due to different concentrations of particulate matter PM_{10}.

The atmospheric transmission of the infrared radiations (ATIR) decreases along with the distance between the target and the optical system in thermal imaging due to different concentrations of particulate matter PM_{10}. Figure 4-28 (a) shows the ATIR

at different ranges and at different PM_{10} concentrations. The ATIR, presented in figure 4-28 (a), are (0.85,0.82,0.79) at (10, 12, 14) µg/m^3, respectively. The IR transmittance behavior has uniformly reduced due to a steady increase in PM_{10} concentration.

The same IR transmittance behavior appears in the case of increasing the PM_{10} concentration as shown in Figures 4-28 (b, c, d, e, and f). The ATIR reaches the minimum value at 0.49 when the PM_{10} concentration is (50 µg/m^3), as shown in figure 4-28 (f). The ATIR increased as V increased due to the reduction in PM_{10} concentration. The transition has large values at the close range of 200 m (the distance of the object from the camera). While the ATIR values decrease at the far range (800m). This is due to an increase in the concentration of particles through distance, leading to a decrease in the IR transition. Therefore, the thermal image will be clear at the near range of (200 m) but it is a blur in the far range of (800 m). From this discussion, one can consider that the object can be detected at the near ranges although there is the absorption of IR radiation that PM10 caused by concentration.

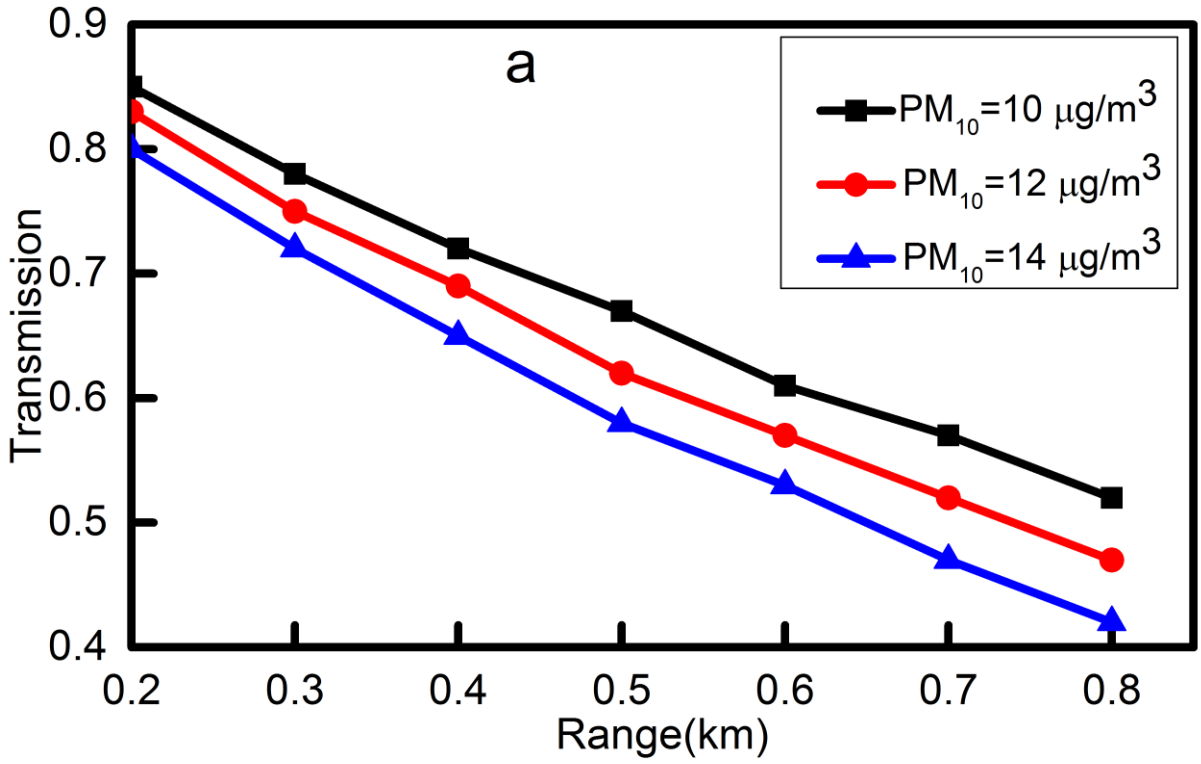

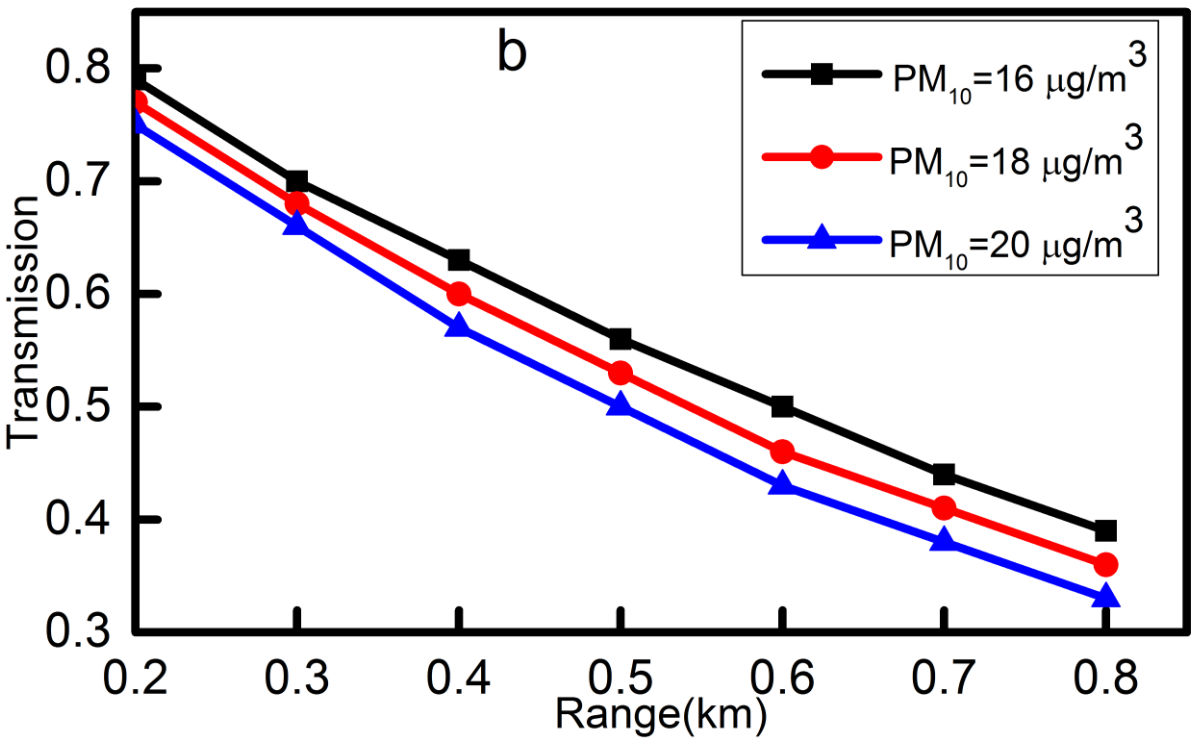
b
PM10=16 μg/m3
PM10=18 μg/m3
PM10=20 μg/m3
Transmission
Range(km)
0.8
0.7
0.6
0.5
0.4
0.3
0.2
0.3
0.4
0.5
0.6
0.7
0.8

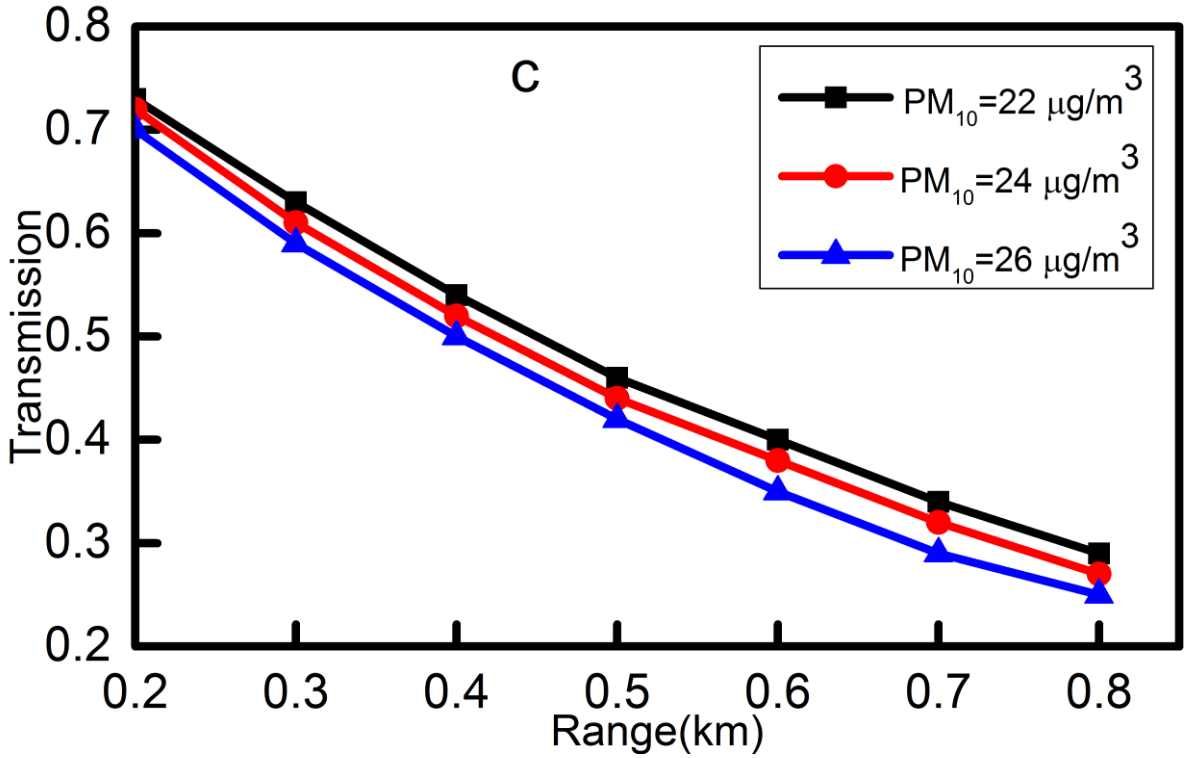
c
PM10=22 μg/m3
PM10=24 μg/m3
PM10=26 μg/m3
Transmission
Range(km)
0.8
0.7
0.6
0.5
0.4
0.3
0.2
0.3
0.4
0.5
0.6
0.7
0.8

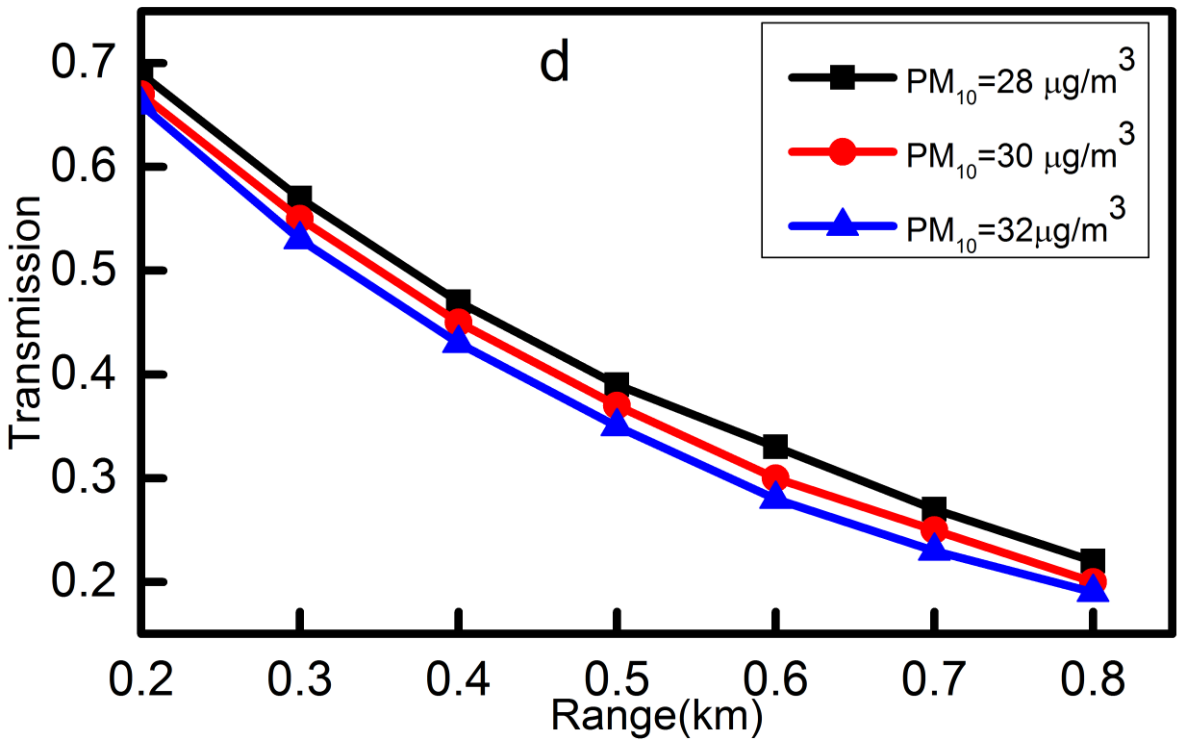
d
PM10=28 μg/m3
PM10=30 μg/m3
PM10=32μg/m3
Transmission
Range(km)
0.2
0.3
0.4
0.5
0.6
0.7
0.8

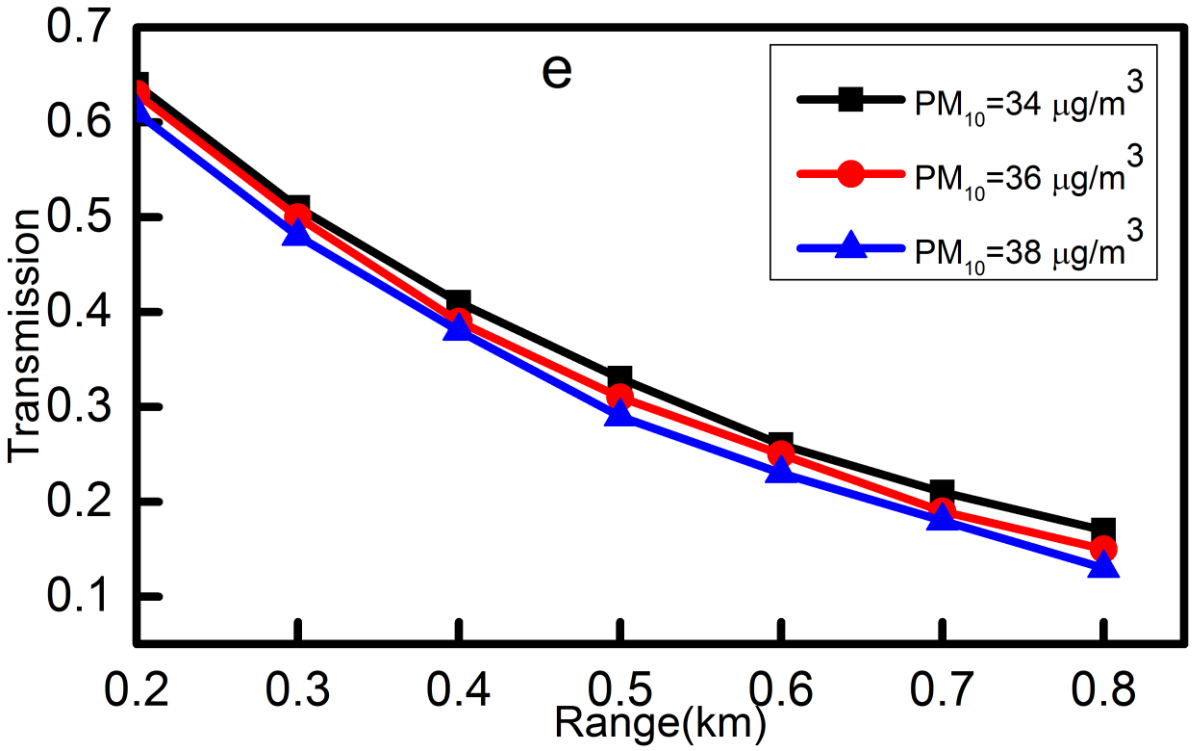
e
PM10=34 μg/m3
PM10=36 μg/m3
PM10=38 μg/m3
Transmission
Range(km)
0.1
0.2
0.3
0.4
0.5
0.6
0.7
0.8

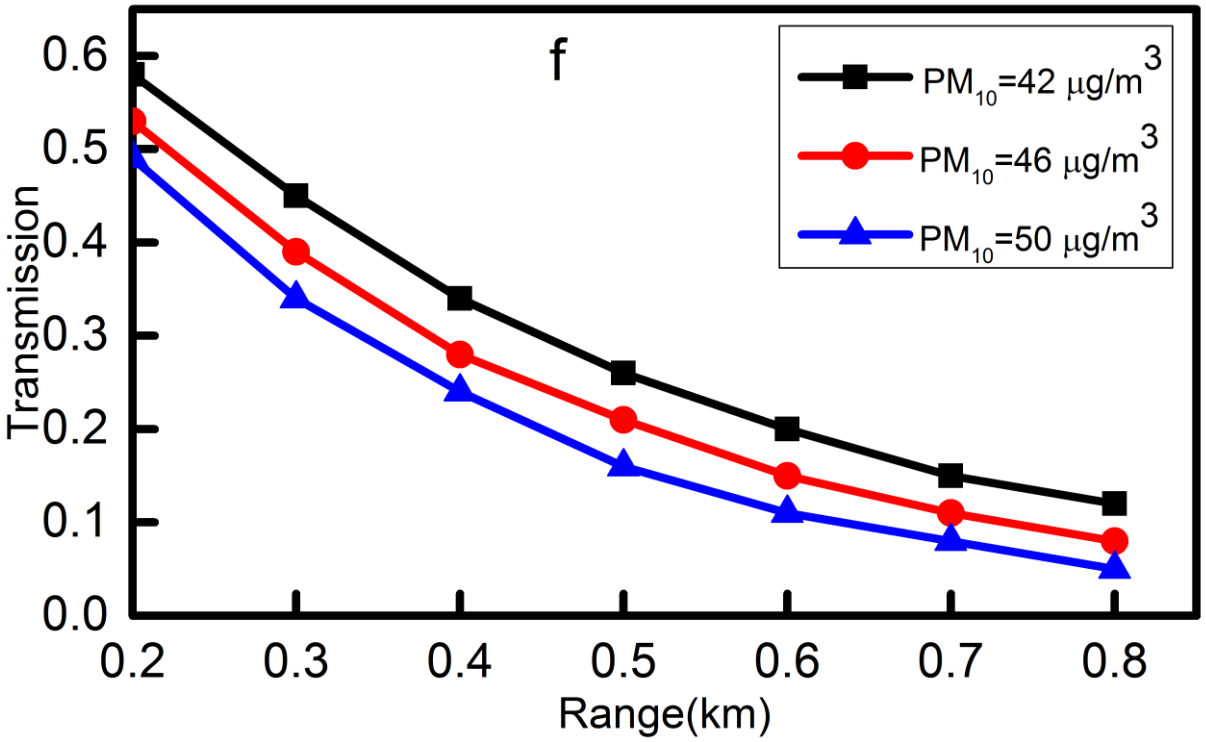

Figure 4-28 (a, b, c, d, e, and f): The IR atmospheric transmittance at different concentration of particulate matter PM_{10}.

Figures 4-29, 4-30, 4-31 illustrated the intensity distribution in the thermal images due to different concentrations of PM_{10} and different ranges (R). The PM_{10} concentration, used in these figures, is (10, 20, 30, 40, 50) $\mu g/m^3$, corresponding to the absorption of (2.35, 2.60, 2.85, 3.15, 3.69), respectively. The PM_{10} concentration strongly affects the central peak intensity values. Furthermore, the intensity distribution of the central peak is also affected. From figure 4-29, it is clear that the intensity in the thermal image at the absorption of A= 2.35 is 0.51. Moreover, the curve shape of the central peak has an intensity value that enables the thermal system only detect the object and not recognize it at the range of (0.5 Km).

The degradation of the central intensity distribution in the thermal images at higher values of the absorption (A) affects the peak shape of the thermal image, where, the values of central intensity are (0.46, 0.42, 0.38, 0.33) for the absorption of (2.60, 2.85, 3.15, 3.69), respectively. In addition, the shape of curves becomes

broadening in these cases. The concentration of PM_{10} (20,30,40,50) $\mu g/m^3$, which is corresponds to the absorption of (2.60, 2.85, 3.15, 3.69), makes the thermal imaging is impossible at the range of (0.5 Km) at the study area (Ain al-Tamer area, Karbala city).

The behavior of the intensity distribution in figures 4-30 and 4-31 is similar to the behavior of the intensity distribution in figure 4-29. The intensity degradation, in figures 4-30 and 4-31, is very similar to these in figure 4-29. The values of the central peaks are (0.50, 0.46, 0.42, 0.38, 0.33) and (0.48, 0.45, 0.42, 0.38, 0.33) for the ranges of (1, 1.5) Km, respectively. Therefore, we can judge from that, at the study area, the captured thermal images, at PM_{10} concentration of (10) $\mu g/m^3$ will have a bad resolution because of the reduction in the value of the central peak intensity of the images are strong for the ranges of (1, 1.5) Km. At a higher concentration of PM_{10} (20, 30, 40, 50) $\mu g/m^3$, the reduction in the central peak value of intensity becomes very effective on the image quality. It is clear that detection and recognizing objects is impossible in these cases because of increasing the value of the absorption because of the high concentration of PM_{10} and thus the visibility (V) will be very weak.

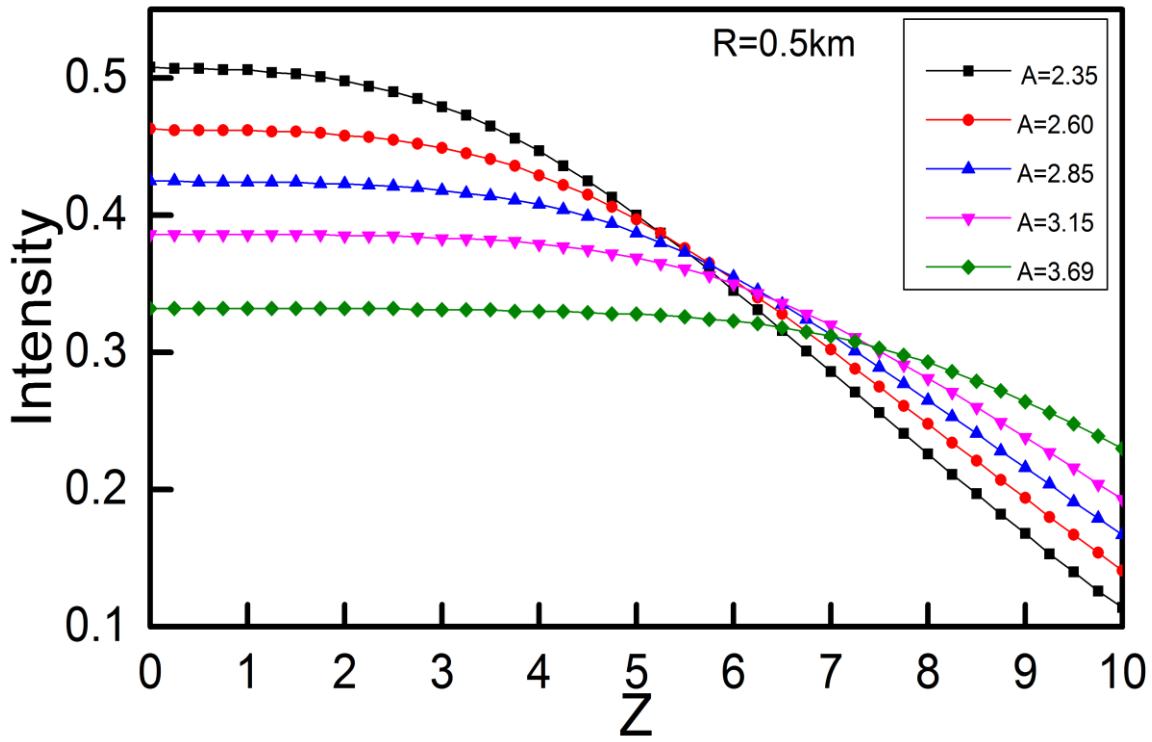

Figure 4-29: The intensity distribution in the thermal image at different absorption (A) of IR by PM_{10} at R=0.5 Km.

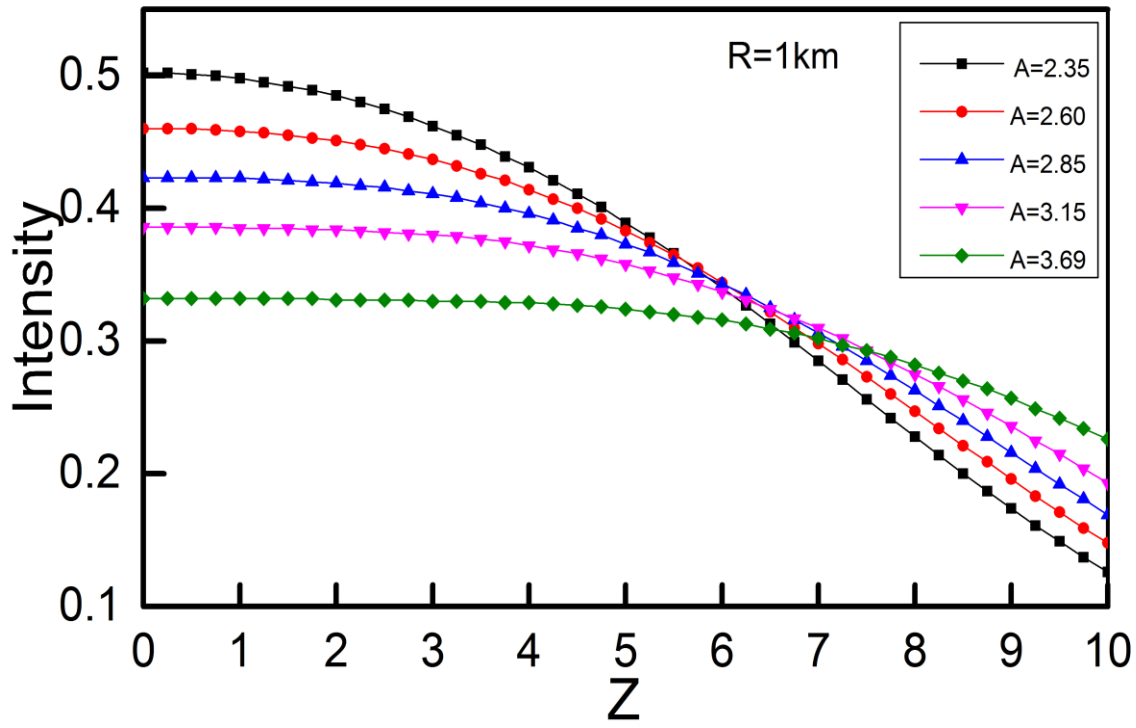

Figure 4-30: The intensity distribution in the thermal image at different absorption (A) of IR by PM_{10} at R=1 Km.

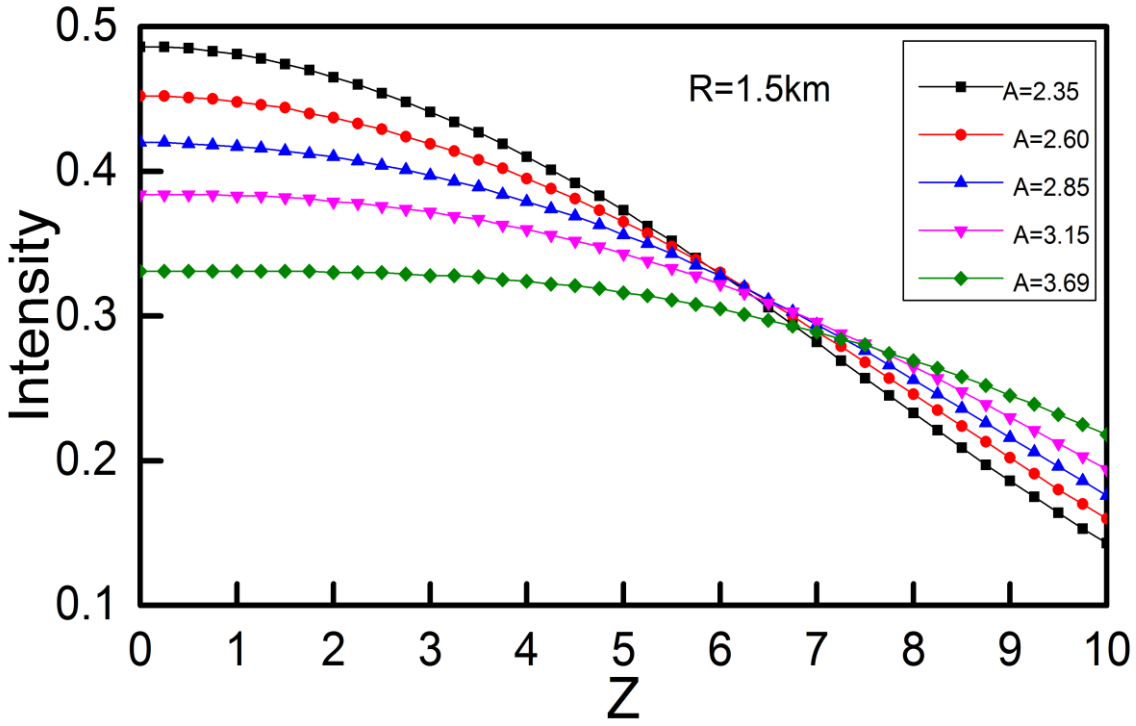

Figure 4-31: The intensity distribution in the thermal image at different absorption (A) of IR by PM_{10} at R=1.5 Km.

Chapter Five

Conclusions and future works

5-1 Conclusions

1- Transfer function such as Bar Spread Function (BSF) is a suitable tool to evaluate the efficiency of the thermal camera by determining the intensity distribution in the thermal image. Intensity distribution in thermal images plays an important role in detecting and recognizing targets.

2- The moving image (moving target) and bad weather conditions significant affect the intensity distribution of the thermal images that appears clearly at the long-range of the object. As the range increased, the effect of image motion slightly decreased and vanished at high values.

3- When the range of the target becomes more than 500 m, the values of image motion are decreased and the value of the linear motion factor becomes less than (0.5), therefore the intensity distribution in the image does not affect.

4- At the range 500m, the target is detected and recognized but when the range is 750 m the target is detected but not recognized. The detection is obtained at the range (1250-2500) m but at low resolution, above this range, thermal image becomes a blur and the target does not detect or recognize. Therefore, the thermal imaging, in this case, is impossible.

5-The thermal camera (PT-602CZ HD) has short-range detection of approximately 2500m.

6- The comparing between thermal images and intensity distribution in the image can guide technical work in this field.

7- The detection and recognition of targets in thermal imaging depend on IR emission from targets and its transmission of the IR through the atmosphere. The atmosphere transition of IR (10) μm is an important factor estimating the thermal imaging.

8-The clear and blur images of the object are affected by the state of the weather. The atmosphere transition of IR (10) μm various with the concentration of PM_{10}. The concentration of PM_{10} above 10 $\mu g/m^3$ affects the thermal imaging, at high concentration (20,30,40,50) thermal imaging is impossible for the range (1,1.5) Km.

9- The atmosphere transition of IR (5 and10) μm at various values of Visibility (0.2,0.3,0.4) Km has a small value (0.1-0.2), and this value does not present a good condition to make an image by a thermal camera, therefore the thermal imaging is impossible in this condition.

10- When the visibility increased due to the reduction in fog concentration. The transition has large values (0.7-0.8) for 10 μm at close range but the values decrease at far range. The thermal image is clear at near range (0.2-0.4) Km but it is a blur in far range (0.5-0.8) Km.

5-2 Future Works

1- Improvement of the efficiency of the thermal camera by using different filters such as Gaussian filter, Hamming filter annular filter.

2- Investigated the performance of thermal imager efficiency of objects with different emissivity, different temperatures, and different spectral radiant exitances.

3- Studying the efficiency of the thermal camera for static objects with different rotation and vibration movement factors.

4- Studying the efficiency of the thermal camera used in aerial photography.

5- Thermal imaging is used in medical applications to provide temperature measurement changes that are clinically significant.

References

[1] E. F. J. Ring, "The discovery of infrared radiation in 1800," *Imaging Sci. J.*, vol. 48, no. 1, pp. 1–8, 06 Oct 2016.

[2] A. A. Ziyed, A. Y. Qasim, R. S. Mahmod, W. A. Obaid, and M. M. Mohammed, "Investigation And Present Of The Thermal Imaging Camera." IJISET - International Journal of Innovative Science, Engineering & Technology, Vol. 2 Issue 2, February 2015.

[3] R. Gade and T. B. Moeslund, "Thermal cameras and applications: a survey," *Mach. Vis. Appl.*, vol. 25, no. 1, pp. 245–262, 2014.

[4] E. J. Koerperick, "High power mid-wave and long-wave infrared light emitting diodes: device growth and applications," *Theses Diss.*, p. 304, 2009.

[5] J. S. Browder, S. S. Ballard, and P. Klocek, *Physical properties of glass infrared optical materials*. Marcel Dekker, Inc., New York, New York, 1991.

[6] A. Akula, N. Khanna, R. Ghosh, S. Kumar, A. Das, and H. K. Sardana, "Adaptive contour-based statistical background subtraction method for moving target detection in infrared video sequences," *Infrared Phys. Technol.*, vol. 63, pp. 103–109, 2014.

[7] M. Teena and A. Manickavasagan, "Thermal infrared imaging," in *Imaging with Electromagnetic Spectrum*, Springer, pp. 147–173. , 2014.

[8] P. Timofeeva, "Object detection in thermal imagery for crowd density estimation," 56 pages 6 April 2020.

[9] Q. H. Tran, D. Han, C. Kang, A. Haldar, and J. Huh, "Effects of ambient temperature and relative humidity on subsurface defect detection in concrete structures by active thermal imaging," *Sensors*, vol. 17, no. 8, p. 1718, 2017.

[10] N. P. Avdelidis and A. Moropoulou, "Emissivity considerations in building thermography," *Energy Build.*, vol. 35, no. 7, pp. 663–667, 2003.

[11] B. Chu, H. C. McEvoy, and J. W. Andrews, "The NPL reference sources of blackbody radiation," *Meas. Sci. Technol.*, vol. 5, no. 1, p. 12, 1994.

[12] M. Vollmer and K.-P. Möllmann, *Infrared thermal imaging: fundamentals, research and applications*. John Wiley & Sons, 2017.

[13] Thomas P. Hardman, Lie Detectors, Extrajudicial Investigations and the Courts, 48 W. Va. L. Rev. (1941)

[14] L. SOFRADIR-EC, "or MWIR infrared imaging: Which is best for your application," *Infrared Imaging White Pap. Fairfield, New Jersey*, 2013.

[15] T. Jaeger, A. Nordbryhn, and P. A. Stokseth, "Detection of low contrast targets at 5 μm and 10 μm: a comparison," *Appl. Opt.*, vol. 11, no. 8, pp. 1833–1835, 1972.

[16] T. W. Tuer, "Thermal imaging systems relative performance: 3-5 micrometers vs 8-12 micrometers," *Final Rep.*, 1977.

[17] A. Goldberg, T. Fischer, S. Kennerly, W. Beck, V. Ramirez, and K. Garner, "Laboratory and field imaging test results on single-color and dual-band QWIP focal plane arrays," *Infrared Phys. Technol.*, vol. 42, no. 3–5, pp. 309–321, 2001.

[18] K. Chrzanowski, "Testing thermal imagers practical guidebook," 2010.

[19] H. Kaplan, *Practical applications of infrared thermal sensing and imaging equipment*, vol. 75. SPIE press, 2007.

[20] A. Rogalski and K. Chrzanowski, "Infrared devices and techniques," *Optoelectron. Rev.*, vol. 10, no. 2, pp. 111–136, 2002.

[21] S. B. Campana, "Passive electro-optical systems," *infrared electro-optical Syst. handbook-IR/EO Syst. Handb.*, 1993.

[22] P. W. Kruse, *Uncooled thermal imaging: arrays, systems, and applications*, vol. 51. SPIE press, 2001.

[23] F. S. Z. Al-Abedeen, "Atmosphere Effects on 3-5 μm Band Thermal Imaging Ph," *D., Al-Mustanseriyah Univ.*, 2004.

[24] S. G. BuS. G. Burnay, T. L. Williams, and C. H. Jones, Applications of thermal imaging. CRC Press, 1988.rnay

[25] T. D. Rahmlow Jr, J. E. Lazo-Wasem, S. Wilkinson, and F. Tinker, "Dual-band antireflection coatings for the infrared," in *Infrared Technology and Applications XXXIV*, 2008, vol. 6940, p. 69400T.

[26] C. C. Alexay, "Multispectral infrared imaging optics," in *Infrared Technology and Applications XXIX*, 2003, vol. 5074, pp. 830–838.

[27] S. M. Stewart, "Analysis of the relative merits of the 3-5 μm and the 8-12 μm spectral bands using detected thermal contrast," in *Thermosense: Thermal Infrared Applications XXXVII*, 2015, vol. 9485, p. 94851B.

[28] R. D. Hudson, *Infrared system engineering*, vol. 1. Wiley-Interscience New York, 1969.

[29] C. Plesa, D. Turcanu, and V. Bodoc, "The use of infrared radiation for thermal signatures determination of ground targets," *Rom. J. Phys.*, vol. 51, no. 1/2, p. 63, 2006.

[30] J. Wardlaw, M. Gryka, F. Wanner, G. Brostow, and J. Kautz, "A new approach to thermal imaging visualisation," *EngD Gr. Proj. Univ. Coll. London*, 2010.

[31] R. Vadivambal and D. S. Jayas, "Applications of thermal imaging in agriculture and food industry—a review," *Food Bioprocess Technol.*, vol. 4, no. 2, pp. 186–199, 2011.

[32] A. Berg, "Detection and Tracking in Thermal Infrared Imagery." Linköping University Electronic Press, 2016.

[33] M. Rai, T. Maity, and R. K. Yadav, "Thermal imaging system and its real time applications: a survey," *J. Eng. Technol.*, vol. 6, no. 2, pp. 290–303, 2017.

[34] J. L. Rowe, "The impact of thermal imaging camera display quality on fire fighter task performance." 2008.

[35] A. Rogalski, “Recent progress in infrared detector technologies,” *Infrared Phys. Technol.*, vol. 54, no. 3, pp. 136–154, 2011.

[36] T. Williams, *Thermal imaging cameras: characteristics and performance*. CRC Press, 2009.

[37] D. Perić, B. Livada, M. Perić, and S. Vujić, “Thermal imager range: Predictions, expectations, and reality,” *Sensors*, vol. 19, no. 15, p. 3313, 2019.

[38] A. A. Gowen, B. K. Tiwari, P. J. Cullen, K. McDonnell, and C. P. O’Donnell, “Applications of thermal imaging in food quality and safety assessment,” *Trends food Sci. Technol.*, vol. 21, no. 4, pp. 190–200, 2010.

[39] R. Paugam, M. J. Wooster, and G. Roberts, “Use of handheld thermal imager data for airborne mapping of fire radiative power and energy and flame front rate of spread,” *IEEE Trans. Geosci. Remote Sens.*, vol. 51, no. 6, pp. 3385–3399, 2012.

[40] L. Hoegner and U. Stilla, “Thermal leakage detection on building facades using infrared textures generated by mobile mapping,” in *2009 Joint Urban Remote Sensing Event*, 2009, pp. 1–6.

[41] B. B. Lahiri, S. Bagavathiappan, T. Jayakumar, and J. Philip, “Medical applications of infrared thermography: a review,” *Infrared Phys. Technol.*, vol. 55, no. 4, pp. 221–235, 2012.

[42] N. A. Diakides and J. D. Bronzino, *Medical infrared imaging*. CRC press, 2007.

[43] P. Rudol and P. Doherty, “Human body detection and geolocalization for UAV search and rescue missions using color and thermal imagery,” in *2008 IEEE aerospace conference*, 2008, pp. 1–8.

[44] A. Berg, K. Öfjäll, J. Ahlberg, and M. Felsberg, “Detecting rails and obstacles using a train-mounted thermal camera,” in *Scandinavian Conference on Image Analysis*, 2015, pp. 492–503.

[45] D. Huang12, L. Luo, M. Wen12, Z. Chen12, and C. Zhang12, “Enable scale and aspect ratio adaptability in visual tracking with detection proposals,” 2015.

[46] T. T. Zin, H. Takahashi, and H. Hama, “Robust person detection using far infrared camera for image fusion,” in *Second International Conference on Innovative Computing, Informatio and Control (ICICIC 2007)*, 2007, p. 310.

[47] A. W. M. Smeulders, D. M. Chu, R. Cucchiara, S. Calderara, A. Dehghan, and M. Shah, “Visual tracking: An experimental survey,” *IEEE Trans. Pattern Anal. Mach. Intell.*, vol. 36, no. 7, pp. 1442–1468, 2013.

[48] Y. Wu, J. Lim, and M. Yang, “Visual tracking benchmark,” *IEEE Trans. Pattern Anal. Mach. Intell*, vol. 37, no. 9, pp. 1834–1848, 2015.

[49] O. Javed, M. Shah, and A. Yilmaz, “Object tracking: A survey,” *ACM Comput. Surv.*, vol. 38, no. 4, pp. 1–45, 2006.

[50] S. Finnie, F. Zhang, and T. Rhee, “Visual Object Tracking in Spherical 360° Videos: A Bridging Approach,” in *2020 35th International Conference on Image and Vision Computing New Zealand (IVCNZ)*, 2020, pp. 1–6.

[51] A. Li, M. Lin, Y. Wu, M.-H. Yang, and S. Yan, “Nus-pro: A new visual tracking challenge,” *IEEE Trans. Pattern Anal. Mach. Intell.*, vol. 38, no. 2, pp. 335–349, 2015.

[52] N. Vaswani, A. K. Agrawal, Q. Zheng, and R. Chellappa, “Moving object detection and compression in IR sequences,” in *Computer Vision Beyond the Visible Spectrum*, Springer, 2005, pp. 141–165.

[53] F. Cremer, W. De Jong, and K. Schutte, “Infrared polarization measurements and modelling applied to surface laid anti-personnel landmines,” *Opt. Eng.*, vol. 41, no. 5, pp. 1021–1032, 2002.

[54] J. Shi, “Obstacle detection using thermal imaging sensors for large passenger airplane,” 2012.

[55] Y. Iwasaki, M. Misumi, and T. Nakamiya, “Robust vehicle detection under various environmental conditions using an infrared thermal camera and its application to road traffic flow monitoring,” *Sensors*, vol. 13, no. 6, pp. 7756–7773, 2013.

[56] E. Bernard, N. Riviere, M. Renaudat, P. Guiset, M. Pealat, and E. Zenou, “Experiments and models of active and thermal imaging under bad weather conditions,” in *Electro-Optical Remote Sensing, Photonic Technologies, and Applications VII; and Military Applications in Hyperspectral Imaging and High Spatial Resolution Sensing*, 2013, vol. 8897, p. 889703.

[57] N. Goyette, P.-M. Jodoin, F. Porikli, J. Konrad, and P. Ishwar, “A novel video dataset for change detection benchmarking,” *IEEE Trans. Image Process.*, vol. 23, no. 11, pp. 4663–4679, 2014.

[58] K. Lenac, I. Maurović, and I. Petrović, “Moving objects detection using a thermal Camera and IMU on a vehicle,” in *2015 International Conference on Electrical Drives and Power Electronics (EDPE)*, 2015, pp. 212–219.

[59] Y. Cao, G. Wang, D. Yan, and Z. Zhao, “Two algorithms for the detection and tracking of moving vehicle targets in aerial infrared image sequences,” *Remote Sens.*, vol. 8, no. 1, p. 28, 2016.

[60] R. Usamentiaga and D. F. García, “Infrared thermography sensor for temperature and speed measurement of moving material,” *Sensors*, vol. 17, no. 5, p. 1157, 2017.

[61] L. Maddalena and A. Petrosino, “Background subtraction for moving object detection in RGBD data: A survey,” *J. Imaging*, vol. 4, no. 5, p. 71, 2018.

[62] Z. Tong, C. Can, F. W. Xing, H. H. Qiao, and C. H. Yu, “Improved small moving target detection method in infrared sequences under a rotational background,” *Appl. Opt.*, vol. 57, no. 31, pp. 9279–9286, 2018.

[63] J. CORNÉ and U. H. SJÖBLOM, “Investigation of IR transmittance in different weather conditions and simulation of passive IR imaging for flight scenarios.” MS thesis, KTH Royal Institute of Technology, Stockholm, Sweden, 2019.

[64] Mate Krišto, M. Karišto, M. Ivasic-Kos, and M. Pobar, “Thermal Object Detection in Difficult Weather Conditions Using YOLO,” IEEE Access, vol. 8, pp. 125459–125476, 2020.

[65] Y. Han and D. Hu, “Multispectral Fusion Approach for Traffic Target Detection in Bad Weather,” *Algorithms*, vol. 13, no. 11, p. 271, 2020.

[66] S. Malpani, C. S. Asha, and A. V Narasimhadhan, “Thermal vision human classification and localization using bag of visual word,” in *2016 IEEE Region 10 Conference (TENCON)*, 2016, pp. 3135–3139.

[67] R. R. Shannon, *The art and science of optical design*. Cambridge University Press, 1997.

[68] T. Li and H. Feng, “Comparison of different analytical edge spread function models for MTF calculation using curve-fitting,” in *MIPPR 2009: Remote Sensing and GIS Data Processing and Other Applications*, 2009, vol. 7498, p. 74981H.

[69] S. Lu, X. Zhang, R. Guo, D. Xia, J. Yu, and J. Han, “Research on measuring optical transfer function,” in *Optical Design and Testing IV*, 2010, vol. 7849, p. 784931.

[70] G. D. Boreman, *Modulation transfer function in optical and electro-optical systems*, vol. 4. SPIE press Bellingham, WA, 2001.

[71] B. Nielsen, “Resolution, unsharpness and MTF.” Linköping University Electronic Press, 1980.

[72] G. Presenza-Pitman and J. Thywissen, “Determination of the contrast and modulation transfer functions for high resolution imaging of individual atoms,” *NSERC summer report, Univ. Toronto*, vol. 83, 2009.

[73] M. K. Devi and T. V. Reddy, “Study of Optical Transfer Function in an Optical System with Gaussian Filter.” ISSN 0974-3103 Volume 10, Number 1 (2018), pp. 13-21

[74] R. Bell, *Introductory Fourier transform spectroscopy*. Elsevier, 2012.

[75] C. da Costa, M. Kashiwagi, and M. H. Mathias, “Rotor failure detection of induction motors by wavelet transform and Fourier transform in non-stationary condition,” *Case Stud. Mech. Syst. Signal Process.*, vol. 1, pp. 15–26, 2015.

[76] R. N. Bracewell and R. N. Bracewell, *The Fourier transform and its applications*, vol. 31999. McGraw-Hill New York, 1986.

[77] I. W. Selesnick and C. S. Burrus, “Digital Signal Processing Handbook. Chapter 8" Fast convolution and filtering.” Boca Raton: CRC Press LLC, 1999.

[78] W. G. Gardner, “Efficient convolution without input/output delay,” 1994.

[79] M. J. Kidger, “Fundamental optical design,” 2001.

[80] R. Fischer, B. Tadic-Galeb, and P. Yoder, *Optical system design*. McGraw-Hill Education, 2008.

[81] J. J. M. Braat, S. van Haver, A. J. E. M. Janssen, and P. Dirksen, “Assessment of optical systems by means of point-spread functions,” *Prog. Opt.*, vol. 51, pp. 349–468, 2008.

[82] A. Mikš, J. Novák, and P. Novák, “Method of zoom lens design,” *Appl. Opt.*, vol. 47, no. 32, pp. 6088–6098, 2008.

[83] R. B. Schulz and W. Semmler, “Fundamentals of optical imaging,” *Mol. Imaging I*, pp. 3–22, 2008.

[84] G. R. Ayers and J. C. Dainty, “Iterative blind deconvolution method and its applications,” *Opt. Lett.*, vol. 13, no. 7, pp. 547–549, 1988.

[85] W. H. Tarkhan and A. Habeeb, “Study The Effect Of Lorentzian And Gaussian Illumination On Line Spread Function For Elliptical Aperture,” *J. Educ. Pure Sci.*, vol. 8, no. 3, 2018.

[86] Y. Li and E. Wolf, “Three-dimensional intensity distribution near the focus in systems of different Fresnel numbers,” *JOSA A*, vol. 1, no. 8, pp. 801–808, 1984.

[87] M. Sub barao, “Determining distance from defocused images of simple objects,” *Tech. Rep. 89-07-20*, pp. 11794–12350, 1989.

[88] K. Singh, R. Rattan, and N. K. Jain, “Diffraction Images of Truncated Sine and Square Wave Periodic Objects in the Presence of Linear Image Motion,” *Appl. Opt.*, vol. 12, no. 8, pp. 1846–1850, 1973.

[89] J. F. Silny and H. M. Reyes Jr, “Multi-band thermal imaging sensor with integrated filter array.” Google Patents, Feb. 04, 2016.

[90] J. A. Khalati, “Experimental Study of the Influence of Dust Particle on Link Range of Free Space Laser Communication System,” *J. Coll. basic Educ.*, vol. 24, no. 102/2018.

[91] J. E. Greivenkamp, *Field guide to geometrical optics*, vol. 1. SPIE press Bellingham, WA, 2004.

[92] E. Hecht, *Optics, 5e*. Pearson Education India, 2002.

[93] F. Leira Object detection, recognition, and tracking from UAVsusing a thermal camera Grant/Award Numbers: 223254, 269480, 2021

[94] S. T Monitoring Temperature-Related Hazards Using Mobile Devices and a Thermal Camera DOI: 10.1007/978-3-030-49666-1_29, 2021

الخلاصة

تستخدم كاميرات التصوير الحراري على مدى واسع في التطبيقات العسكرية لقدراتها على الرؤية الليلية في مديات المراقبة المختلفة. تعتمد كفاءة الكاميرا الحرارية على جودة الصورة أو الكشف عن الهدف والتعرف عليه. في هذا العمل ، نموذج رياضي تمت برمجته في Mathcad للتحقق من كفاءة الكاميرا الحرارية (PT-602CZ HD) عندما يتحرك الهدف بسرعات مختلفة. يتم حساب توزيع الشدة في الصور الحرارية باستخدام دالة التحول. دالة انتشار الشق (BSF) تم حلها في حالتين مع وبدون حركة خطية للهدف.تم حساب قيم عامل الحركة الخطية للهدف بسرعات مختلفة (40 ، 60 ،80 ، 100،120) كم / ساعة. تم تقييم شدة توزيع الصورة الحرارية لمديات مختلفة (150 الى 4500) م. وأظهرت النتائج أنه يمكن الكشف عن الهدف وتمييزه في مديات (150 ، 300، 500) م ولكن الهدف يكتشف فقط في مديات (750) م. إذا كان مدى الهدف المتحرك أكبر من 750 مترًا ، فسيحدث الاكتشاف أيضًا ولكن بدقة مختلفة إذا وصل المدى إلى 2500 متر وأكثر ، يكون التصوير الحراري مستحيلًا لهذا النوع من الكاميرات الحرارية. مقارنة النتائج النظرية لانحطاط شدة الصورة الحرارية مع صورة هدف متحرك تم التقاطها عمليا بواسطة كاميرا حرارية بسرعة 40 كم / ساعة من الهدف في منطقة عين التمر لمدينة كربلاء المقدسة. يتأثر اكتشاف الهدف بحالة الأحوال الجوية. يتم تقييم النفاذية في الغلاف الجوي لنطاق الأشعة تحت الحمراء عند (10،5) مايكرومتر في رؤية مختلفة (200، 300، 400، 500، 600، 700، 800) م مع وجود الضباب في مديات مختلفة (200، 300، 400، 500، 600، 700، 800) م في نفس المنطقة من الدراسة، وتم التحقق من المدى الفعال. تجريبيا ، يتم التقاط الصور الحرارية بواسطة الكاميرا الحرارية في مديات مختلفة (200، 300، 400، 500) م في الرؤية 400 م. يتأثر انتقال الأشعة تحت الحمراء بظروف الغلاف الجوي مثل الضباب وتعتمد النفاذية على تركيز الجسيمات العالقة في الغلاف الجوي. كلا المدى والضباب لهما تأثير قوي على الصور الحرارية التي تلتقطها الكاميرا الحرارية. النفاذية في الغلاف الجوي بمقدار 10ميكروميتر في ظل ظروف ضبابية أفضل من ٥ ميكرومتر. لذلك ، يعد اكتشاف الهدف والتعرف عليه بواسطة الكاميرا الحرارية بحجم ١٠ ميكرومتر هو المفضل. النتائج النظرية تتفق مع الصور الحرارية التجريبية التي تم التقاطها في هذه الحالة ونفس المنطقة. أيضًا، يتأثر اكتشاف الهدف بتلوث الهواء مثل الغبار (الجسيمات المحيطة PM_{10}). يتم حساب مدى الرؤية (V) مع الجسيمات المحيطة PM_{10}. يتم تقييم النفاذية في الغلاف الجوي للأشعة تحت الحمراء (ATIR) مع 10 مايكرومتر بتركيزات مختلفة من الجسيمات PM_{10} (10، 20، 30، 40، 50) ميكروغرام / م^{٣} التي سجلتها منظمة الأرصاد الجوية العراقية وعلم الزلازل في منطقة عين التمر مدينة كربلاء المقدسة ، العراق. أظهرت النتائج أن تركيز PM_{10} له تأثير كبير على قوة دقة الصورة في التصوير الحراري. تركيز PM_{10} في منطقة الدراسة له تأثير طفيف على الصورة الحرارية.

جمهورية العراق
وزارة التعليم العالي والبحث العلمي
جامعة كربلاء – كلية العلوم
قسم الفيزياء

كفاءة الكاميرا الحرارية تحت ظروف الطقس الرديء والهدف المتحرك في مدينة كربلاء المقدسة

رسالة مقدمة الى مجلس كلية العلوم - جامعة كربلاء
وهي جزء من متطلبات نيل درجة الماجستير في علوم الفيزياء

من قبل
احمد فاضل عبد الرحيم
بكالوريوس علوم فيزياء\ ٢٠٠٩

بإشراف
أ. د. فاضل خدام فليفل
أ.م. د. ازهر عبد الزهرة رحيم

2021 م
١٤٤٣هـ